Bending-active timber plate structures

the structural qualities of large-scale activity-bent timber plate structures with consideration of the time-dependent material behaviour

van Lier, Arthur J.

Award date:
2019

BENDING-ACTIVE TIMBER PLATE STRUCTURES

The structural qualities of large-scale actively-bent timber plate structures with consideration of the time-dependent material behaviour

A.J. Van Lier

Date: 6-12-2018

TU/e EINDHOVEN UNIVERSITY OF TECHNOLOGY

BENDING-ACTIVE TIMBER PLATE STRUCTURES

The structural qualities of large-scale actively-bent timber plate structures with consideration of the time-dependent material behaviour

WRITTEN THESIS for the final graduation project of the Master variant Structural Design of the master 'Architecture, Building and Planning' at Eindhoven University of Technology

Student details:
Arthur Johannes van Lier
0775616
Jan Luikenstraat 47
5615 JL Eindhoven

Graduation committee:
prof. dr. ir. A.J.M. (André) Jorissen
ir. A.P.H.W. (Arjan) Habraken
ir. G.J.C. (Gert-Jan) Rozemeijer

Date: 6-12-2018
Version: Final report

ABSTRACT

Form and structure are in close relation with each other. A relation that becomes especially clear in bending-active systems. These are structural systems that include curved beam or shell elements that base their geometry on the elastic deformation from an initially straight or planar configuration. The structural elements need a certain amount of slenderness to be formed into shape. At the same time, structural systems should be designed to withstand large external forces. Simply increasing member dimension does not satisfy. Stiffness and stability are found in the geometry, which ties form, structure, material and analysis into one holistic approach. The research of this graduation project focuses on the issues that come along when designing large-scale, long-lasting structures using flexible timber plates and discusses the development of a bending-active modular roof system.

A constant exchange between numerical and physical results has built confidence that the predictive models that use geometrical nonlinear finite element analysis for both the form-finding and the structural analysis, as well as the simulation of stress-relaxation were sufficiently accurate. It is evident that the highly prestressed parts lose about half their stresses in the first year of construction due to stress-relaxation in the wood. The investigated systems have shown that these stresses influence the load-carrying behaviour in either a positive or a negative way, depending on either predominant tensile or compressive stresses respectively.

A system was developed that is based on a pre-bent repeating module. The system harnesses the qualities that timber, and bending-active structures in general, have to offer. The geometric design of the units is led by the properties of the material. The orthotropic nature of the plywood panels was a leading factor for this design. It gave the preference to a primary, main, and secondary, supportive, load-carrying direction.

A full-scale prototype was constructed from 3.6 mm thick birch plywood. In this prototype, five units were linked in the longitudinal direction. The prototype has shown that the building method works without resulting in fractures or formability issues. Geometrical improvements to the system were proposed that would further increase the load-carrying capacity of the system. The research concludes with a proposition for a circular roof design that shown potential to be used in a building structure.

PREFACE

During the master's course, my interests have always been piqued by finding innovative ways in using materials. For my final project, I did not want to give up on any playful structural design interests, but I wanted it to have some relevance for applications in practice.

By playing around with plywood strips, I immediately started to appreciate the flexibility and the strength of these very thin timber elements. I was intrigued by the natural curvatures that are obtained by elastic bending. The forms looked very pleasing, as they were solely determined from the properties of the elements. My enthusiasm for this construction method was fuelled during the attendance of a masterclass on computational methods for bending-active structures, prior to the IASS symposium in Hamburg. The masterclass was given by Julian Lienhard and Riccardo La Magna among others, who are some of the leading researchers in the field of bending-active structures.

I would like to thank my supervisors André Jorissen and Arjan Habraken for their continuous support and enthusiasm during my search towards a working solution for this rather interesting construction method. I have experienced all our meetings in a very positive way. I really appreciated the right balance between space for exploration, and narrowing this space down to steer my work towards a goal.

For the connection with building practice, I would like to thank Gert-Jan Rozemeijer from Adviesbureau Lüning for his enthusiasm and interesting discussions about the project. Your belief in practical applications for my work has fuelled my enthusiasm even more.

The development of the prototype could never have been possible without the help of Verhoeven Timmerfabriek. Therefore, I am very grateful to Peter Verhoeven and the CNC team for sponsoring and milling the plywood. Thank you very much for helping me bring my project to life.

I am very grateful to my friends and family, who have not only physically helped me with the construction of the prototype, but have always supported me throughout the lengthy process of graduating. I would like to thank my parents in particular for welcoming me back into the family house throughout my graduation period and always being supportive and caring during extensive sessions of work.

Arthur van Lier
Eindhoven, December 2018

CONTENTS

1. INTRODUCTION

1.1. ACTIVE BENDING AS AN APPROACH

Curved shapes are often desired in large-span structures because of the superb structural qualities they can achieve. When properly designed, their main load-carrying behaviour is by axial or membrane forces, which utilise the element's cross-section in the most optimal way. Additionally, extra stiffness and stability can be achieved by designing double curved geometries. The manufacturing costs of these structures, however, can be astronomical. Compared to straight elements, the price of single and double curved elements are respectively about two and six times higher (Schreurer, 2011).

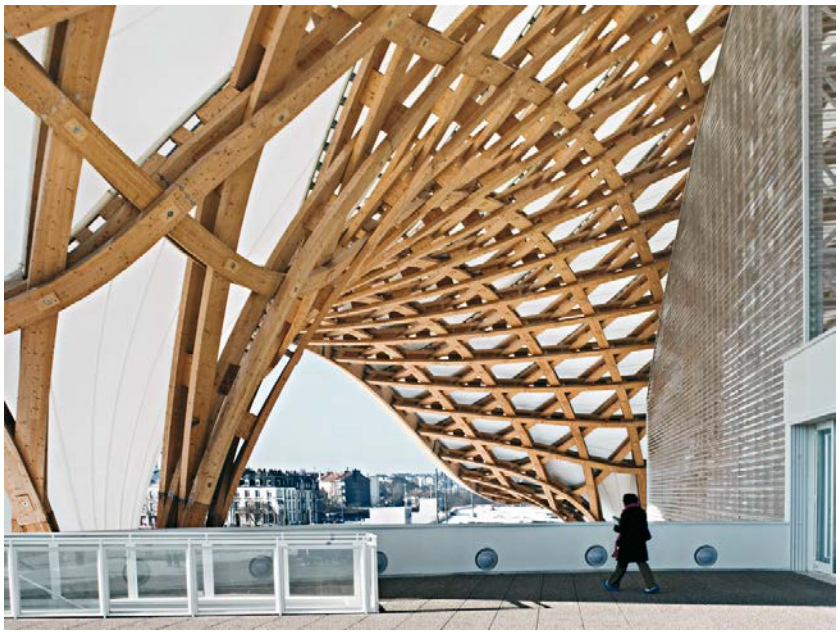

Figure 1.1. The roof structure of the Centre Pompidou in Metz. All the elements are uniquely bent into shape by lamination.

There are several ways to develop curvature in timber elements. Ideally, the wood is bent into shape to keep the fibres intact. In traditional timber construction, wood is bent by steam or lamination. Steam bending uses hot air to plasticise the wood and to bend it easily over a form or mould. The wood retains its curvature when it is cooled and dried, although a certain amount of spring back can be observed. Nowadays, lamination is mostly used in construction. Thin layers of wood are elastically bent inside a mould. The layers are glued and compressed into the desired shape and the laminated element retains its shape when the glue dries. Curved shapes can also be milled out of the elements. With computer numerical control (CNC), curves can be made with precision of 0.1 millimetres. Milling, however, destroys the fibrous structure of the wood, hence it weakens the elements.

Figure 1.2. *A d*ouble curved timber element from the Centre Pompidou in Metz.

The presented methods all rely on special machinery, a significant amount of energy or the presence of forms and moulds to develop a curved piece of wood. This all contributes to the increasing

manufacturing costs. An alternative to these rather laborious methods exists in the elastic bending and restraining of initially straight elements. This construction method provides a very time and material efficient alternative since it neither depends on the fabrication of expensive moulds nor on the auxiliary support of complicated formwork (Panagoulia and Schleicher, 2016). Lienhard (2014, p. 13) describes these structures as bending-active systems and gives the following definitions:

> *"Bending-active structures are structural systems that include curved beam or shell elements which base their geometry on the elastic deformation from an initially straight or planar configuration."*

> *"Bending-active in structural terms: constrained statically indeterminate structures with residual bending stress."*

Form and structure have a very tight relation. The geometry plays an important role in the load-carrying ability of a structure. Traditional structural design often has the aim to minimise bending moments in a system. Bending-active structures harness bending to generate complex and very lightweight designs. The geometry is determined for a large extent by the mechanical properties of the material. Elasticity and geometry become very closely related. The material defines the geometry, instead of the other way around (La Magna, 2017).

Bending-active structures have the potential to overcome practical limitations for the construction of shell structures. Applications for bending-active structures are for instance lightweight facades, roofs or freestanding canopies (Schleicher, Magna and Zabel, 2017). The structural elements need a certain amount of slenderness to be formed into shape. At the same time, structural systems should be designed to withstand large external forces. Simply increasing member dimension does not satisfy. Stiffness and stability should be found in the geometry, which ties form, structure, material and analysis into one holistic approach (La Magna, 2017).

1.2. TIMBER AND BENDING-ACTIVE STRUCTURES

The performance of bending-active structures is very closely related to the material that is facilitating the structure. Kotelnikova *et al.,* (2013) gives an assessment on some of the most popular structural materials and their performance for active bending. The materials are valued for 1) a high elastic limit strain to fit with the construction process, 2) high material stiffness to give the structure its final stiffness and stability, 3) their maximum elastic strain rate to facilitate handling on site, 4) a low price for a given performance, 5) high environmental properties and 6) high durability of the material. The combination of values 1 and 2 automatically results in the appreciation for the material's flexural

Figure 1.3. The Brazilian Oca house is a traditional bending-active structure

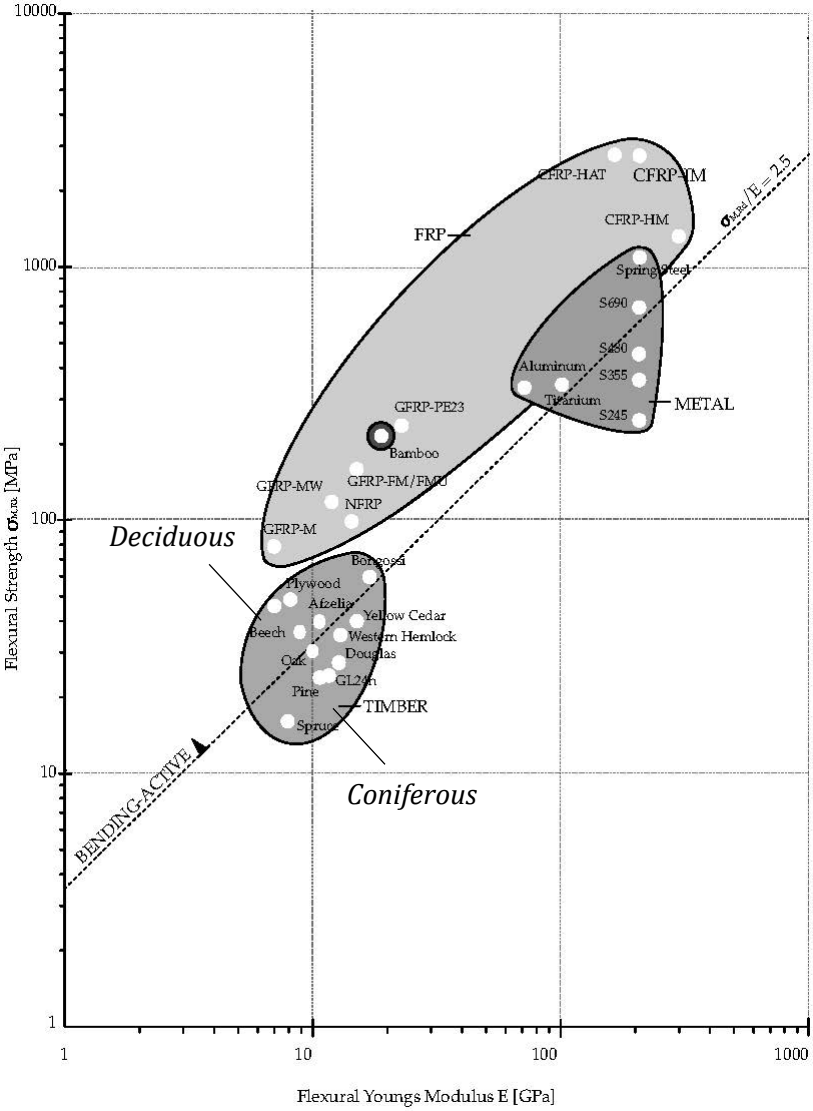

Figure 1.5. Applicable materials for bending-active structures (Lienhard, 2014).

strength. In general, it can be said that materials that have a ratio for the flexural strength (in MPa) to the flexural Young's modulus (in GPa) of $f_m/E < 2.5$ are applicable for bending-active structures (Lienhard, 2014). **Figure 1.5** gives an overview of some popular materials and their mechanical properties.

Timber, as a natural composite material, scores relatively well on most assessed parameters. Other suitable materials are fibre reinforced polymers (FRP) and some metals. These materials might perform a little bit better on mechanical properties, but, a big advantage of wood is its environmental quality and its workability. Furthermore, the high strength-to-weight ratio makes timber ideal for lightweight construction.

Bending-active systems can generally be divided into two categories, based on the element dimensions. One-dimensional elements, i.e. slender beams and rods, have been used frequently throughout the ages to build bending-active structures. Some of the applications are age-old, like the Brazilian Oca house from **Figure 1.3**. Gridshells are a more recent example of one-

Figure 1.4. Plywood dome constructed by Thomas Moore in 1957 at Washington Square in San Francisco to a design of Buckminster Fuller.

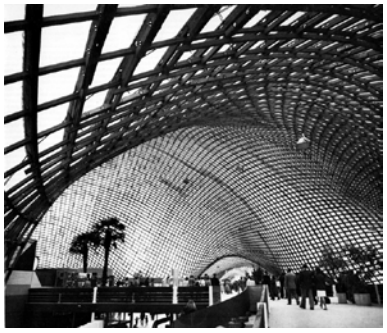

Figure 1.6. The Multihalle in Mannheim, constructed in 1975, is the most well-known example of a gridshell.

dimensional bending-active structures. These structures are built by erecting a rectangular mesh of flexible timber rods and fixing it to the foundation. Most research on bending-active systems has been focussed on this type of systems. The most well-known example is the Multihalle in Mannheim by Frei Otto (**Figure 1.6**).

Bending-active structures with two-dimensional elements, i.e. thin plates and strips, are less researched. Due to the dimensional limitation given by trees, timber plate elements have only found their way into the industry by the 20th century, with the adoption of engineered wood products, such as plywood. The plydome (**Figure 1.4**), designed by Buckminster Fuller, was the first system on record that actively used the flexibility of the plates to construct a spatial structure from a standard off-the-shelf plate element. By using plates instead of rods, the system is stable in its plane and the structural elements can immediately provide for a cover.

1.3. STATE-OF-THE-ART

Figure 1.7. The ICD/ITKE research pavilion 2010 (Fleischmann and Menges, 2011)

In the past decade, research on bending-active plate structures has received growing interest from architects and engineers. This research often goes hand-in-hand with developments in computational methods and with the construction of prototypes or pavilions. A detailed overview of these projects can be found in **Annex A**.

In the bending projects of Frei Otto and Buckminster Fuller, the flexibility of the elements was used to approximate predefined structural geometries, which were based respectively on a hanging chain model or on a geodesic dome. Recent research on bending-active structures incorporates numerical form-finding methods that accurately incorporate the bending-behaviour of structural elements into the design process. This research, therefore, integrates the behaviour based approach from traditional bending-active structures, such as the Oca house (**Figure 1.3**), where the material and structure are empirically worked to find an appropriate configuration, with the more geometrical and analytical design methods, as used by Otto and Fuller (Lienhard, 2014).

Figure 1.8. Timberfabric (Weinand and Hudert, 2010)

Some prototypes and pavilions that result from this research are the 2010 ICD/ITKE research pavilion (**Figure 1.7**), the Timberfabric project at IBOIS EPFL (**Figure 1.8**) and the Berkeley Weave (**Figure 1.9**). The form-finding methods that were developed will be discussed in **Chapter 4**.

Figure 1.9. Berkeley Weave (Schleicher and La Magna, 2016)

The research is characterised by the application of plate material in structural design and highlights interesting ways to develop innovative configurations and geometries that hold surprisingly good structural qualities in a material efficient way. This approach is often combined with computer aided manufacturing (CAM) techniques that allow for mass customisation of elements.

1.4. RESEARCH OBJECTIVE

The challenge when designing bending-active systems, lies in developing a structurally sound system from flexible elements. For small and medium scale projects, prototypes have proven that this possesses no problems. However, when the step to large-scale projects is made, problems arise regarding structural deformations and stability. These problems occur because the effects of self-weight and destabilisation by compressive stress increases with a larger scale (Lienhard and Knippers, 2013; Takahashi *et al.*, 2016).

These problems cannot simply be overcome by using thicker cross-sections, because the cross-sectional dimensions are limited to facilitate the bending. Also, the forces that are necessary to bend the elements increase with growing scale, which might result in impractical or unsafe conditions during construction.

Furthermore, the time-dependent behaviour of timber, i.e. creep and stress-relaxation, influences the structural behaviour of a system over time. Depending on the nature of the stresses (tension or compression), these effects influence the structure in a positive or a negative way (Lienhard, 2014; La Magna and Knippers, 2017).

What is certainly interesting about bending-active timber plate structures, is that they can achieve great structural qualities, are efficient in transportation and construction and poses a high aesthetic appeal. Due to its cost efficiency in designing curved forms, this construction method truly has great potential for an application in the building industry. This research provides a framework for the development of long-term large-scale bending-active structures. The work that was carried out for this graduation project can be outlined as follows.

> *Develop in-depth knowledge and understanding on the structural behaviour of fundamental bending-active systems.*
>
> *Research to the applicability of bending-active timber plate systems for large-scale long-term building structures.*

Develop insight in the time-dependent aspects of bending-active timber.

Provide a practical implementation by designing an actively bent timber roof system.

1.5. METHODOLOGY

The research encompassed both a physical, as a numerical approach. In a new field of research, it is evident that numerical simulations will not always give the designer the insight that can be achieved from working physically with the material. Early in the process, physical design explorations and simple test set-ups were made that developed the designers intuition on the elastic formability and numerical accuracy. This was coupled to the theoretical framework on bending-active structures that is available in literature. Together with the study of several reference projects, this gave a fundamental understanding about bending-active systems and the solutions and approaches that can used when design these systems.

The research has strong ties to what certain bending-active solutions will mean for timber engineering in particular. This has led to a practical design solution that has potential for the field of bending-active timber plates systems. Again, it is important that the numerical approach was sufficiently verified via prototypes to gain confidence in the numerical methods that are needed for the structural design and engineering of a large-scale bending-active structure.

The research of this thesis is divided over nine chapters. An overview of these chapters is given below.

Chapter two gives a theoretical background on the mechanical behaviour of bending-active systems.

Chapter three discusses the form defining parameters of a bending-active structure, such as the material properties, element dimensions and system configuration. It describes how previous projects have managed to acquire rigidity from flexible elements.

Chapter four focuses on the numerical form-finding of bending-active systems. Three different approaches are discussed and evaluated.

Chapter five dives deeper into the numerical approach that will be used for this research. It provides an in-depth explanation of the numerical workflow.

Chapter six discusses fundamental bending-active systems. The numerical approach is validated and basic insight on the nature of bending-active systems, including the time-dependent effects is developed.

Chapter seven gives a design proposition for a bending-active roof system. A detailed overview of the parameters that describe the geometrical and structural behaviour of the system is provided.

Chapter eight describes the development of a bending-active prototype that has been built by the author. It focuses on the design considerations that need to be taken into account when developing bending-active timber structures and dives deeper into the structural behaviour of the system. Different design solutions are discussed that can further enhance the qualities of the system. The chapter concludes with large-scale applications using thicker plates.

2. MECHANICAL BEHAVIOUR OF BENDING-ACTIVE TIMBER

2.1. INTRODUCTION

A theoretical background on the mechanical behaviour of bending-active systems will be given according to beam theory. Although, this approach may not be completely correct for all systems where plates are actively bent, bending-active systems can, as a rule, only be formed by bending around a single axis. This decreases the application field to conical and cylindrical element orientations. This somewhat justifies this simplification. Multi-directional bending is, of course, possible when the topology of the plate allows for this. also discretised systems can be formed which harness possibilities to achieve double curvature. We will see more on this in **Chapter 3.**

2.2. RESIDUAL STRESS

All bending-active systems are formed through elastic deformation of initially straight or planar elements. **Figure 2.1** shows the internal forces that are present when a single strip is bent and restrained by a horizontal force. A certain amount of prestress is developed as a result of these internal forces. This stress influences the structural behaviour and is commonly referred to as residual stress (Lienhard, 2014). This term will be adopted in this report.

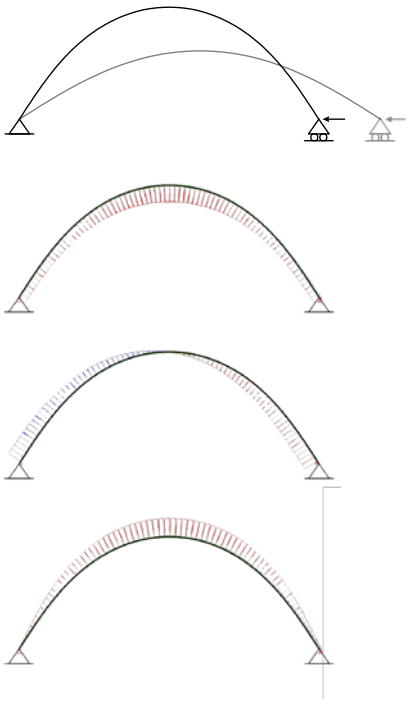

Figure 2.1. Normal force, shear force and moment diagram of a single bent strip.
Blue = positive; red = negative

The residual stress remains constant when the structure is not subjected to any loading and material relaxation is not considered. The bending-active system should be designed in a way that the residual stress never reaches the elastic limit stress of the used materials, hence, Hook's law for linear elastic materials can always be applied (Lienhard, 2014). The amount of residual stress is primarily determined by the flexural stresses that result from bending, and secondarily, by membrane – or axial – stresses introduced by restraining forces.

The Euler-Bernoulli (2.1) law states that the bending moment M_y is proportional to the change in curvature κ, which is the inverse of the radius r. Using the moment-stress relation (2.2), where σ_M is the flexural stress, and W_y is the flexural resistance, it can be derived that the residual stress is only influenced by the Young's modulus E, the cross-sectional height h and the curvature (2.3).

$$\frac{1}{r} = \kappa = \frac{M_y}{E \cdot I_y} \tag{2.1}$$

$$\sigma_M = \frac{M_y}{W_y} \tag{2.2}$$

$$\sigma_M = \frac{E \cdot I_y}{r \cdot W_y} = \frac{E \cdot h}{2 \cdot r} \tag{2.3}$$

From (2.3) it can be deduced that, when retaining the same curvature, the flexural stress increases linearly with the cross-sectional height. The flexural stress cannot surpass the elastic limit of a material, and, therefore the cross-sectional height should be kept to a minimum to facilitate the bending. Hence, the second moment of area should be as high as possible to fortify the stiffness of a structure. This means that solid and wider cross-sections are generally preferred over hollow or double-symmetric sections (Lienhard, 2014). The influence of the residual stress on the behaviour of a system will be elaborated in **Section 2.5**.

2.3. THE SHAPE OF A BENT CURVE

From equation (2.1), it is clear that the curvature of a bent element varies proportional to the bending moment and in inverse proportion to the element stiffness *EI*. The elastic energy as a result of bending for a thin plate with a constant stiffness is equal to:

$$U = \frac{1}{2} EI \int_0^L \kappa^2 dx \qquad (2.4)$$

According to the principle of minimum total potential energy, the plate deforms to the shape that minimises the internal strain energy (D'Acunto and Kotnik, 2013). This shape is commonly known as the elastica. For a rise *f* to span *L* ratio of below 0.3, the elastica is very similar to the catenary **(Figure 2.2)**.

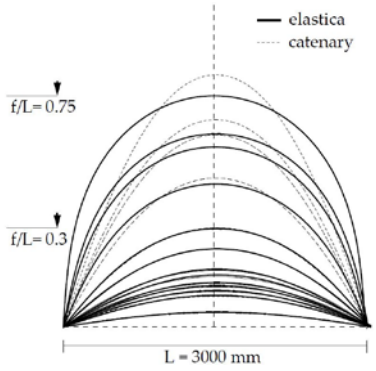

Figure 2.2. Parametric study of elastica and catenary based on FEM form-finding results to show the similarity of the elastica and the catenary (Lienhard, 2014, p. 113).

2.4. NONLINEARITY

Bending-active systems exceed the field of linear structural analysis. Three different forms of nonlinearity can be described in structural mechanics, i.e. material nonlinearity, nonlinearity of boundary conditions and geometrical nonlinearity (Lienhard, 2014). Material nonlinearity occurs when the material behaviour takes plasticity into account. Bending-active structures are designed to remain within the linear elastic region of the material. Material nonlinearity will therefore not be considered. Nonlinear boundary conditions occur when large deformations lead to change in the structures supports. This could be the case for some bending-active structures, where large deformations might lead to additional supporting points and contacts between initially separate elements. Geometrical nonlinearity occurs when there is a nonlinear relation between the external forces and the structure's deformation. This means that, in contrast to linear theory, an increase in load with a factor *n* will not result in an increase in deformations by *n*. All bending-active structures behave geometrically nonlinear. First, during the formation process, where large deformations are imposed to bend the elements into shape, and secondly, in the final structure, which often behaves quite flexible compared to traditional structures and where buckling often is the governing failure mechanism.

This section explains the fundamentals of nonlinear structural analysis for beam elements, reproduced from Crisfield (1997). The principle will be explained by analysing the system of **Figure 2.3**. When θ is assumed to be small, vertical equilibrium gives us

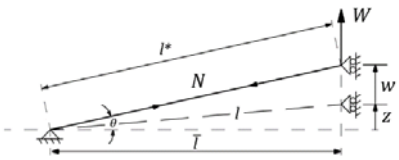

Figure 2.3. Mechanical system.

$$W = N\sin\theta = \frac{N(z+w)}{l^*} \cong \frac{N(z+w)}{l} \tag{2.5}$$

The strain in the bar can be derived by Pythagoras' theorem

$$\begin{aligned}\varepsilon &= \frac{l^*-l}{l} \\ &= \frac{\left((z+w)^2+\bar{l}^2\right)^{1/2}-\left(z^2+\bar{l}^2\right)^{1/2}}{\left(z^2+\bar{l}^2\right)^{1/2}} \\ &\cong \left(\frac{z}{l}\right)\left(\frac{w}{l}\right)+\frac{1}{2}\left(\frac{w}{l}\right)^2\end{aligned} \tag{2.6}$$

The force in the bar is given by

$$N = AE\varepsilon = AE\left(\left(\frac{z}{l}\right)\left(\frac{w}{l}\right)+\frac{1}{2}\left(\frac{w}{l}\right)^2\right) \tag{2.7}$$

The relation between the force and the displacement follows

$$W = \frac{EA}{l^3}\left(z^2w+\frac{3}{2}zw^2+\frac{1}{2}w^3\right) \tag{2.8}$$

The system's stiffness can be defined by a spring constant K_T

$$\begin{aligned}K_T &= \frac{\mathrm{d}W}{\mathrm{d}w} = \frac{(z+w)}{l}\frac{dN}{dw}+\frac{N}{l} \\ &= \frac{EA}{l}\left(\frac{z+w}{l}\right)^2+\frac{N}{l} \\ &= \frac{EA}{l}\left(\frac{z}{l}\right)^2+\frac{EA}{l}\left(\frac{2zw+w^2}{l^2}\right)+\frac{N}{l}\end{aligned} \tag{2.9}$$

Which can also be written as

$$K_T = K_E + K_U + K_G \tag{2.10}$$

The terms that occur in this formula can be explained as 1) the tangential stiffness K_T that describes the stiffness of a system; 2) the elastic stiffness K_E, which directly relates to the elastic material stiffness and is constant for all bending-active structures; 3) the initial displacement stiffness K_U, that is related to the deformation of the system; 4) the geometric stiffness K_G, which is related to the stabilising and destabilising effect caused by the normal forces in the structure. This geometric stiffness plays an important role when designing bending-active structures and can best be explained by investigating the simple system of **Figure 2.4**, in which a clamped mast is subjected to a horizontal force *H*. When a compressive normal force is present in the element, this force results in an increase of the deformation caused by *H*. On the other hand, the presence of a tension force decreases the lateral deformation. This phenomenon is known as the second order effect. In general it can be said that an internal tension force stabilises, and an internal compression force destabilises a structural system.

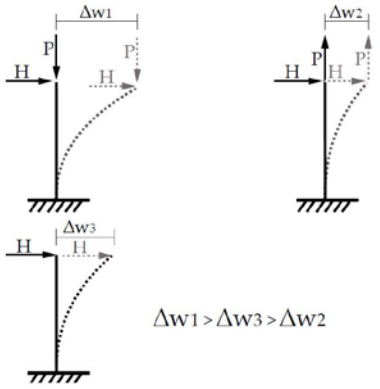

Figure 2.4. Clamped mast for visualisation of 2nd order effects (Lienhard, 2014).

2.5. STIFFNESS AND STABILITY

Lienhard (2014) gives an explanation on how the different terms in equation (2.10) can be related to bending-active systems. In **Figure 2.5**, the contribution of each of the stiffness terms is differentiated for an elastica arch with an applied central point load *F*. The figure shows how the stiffness changes for a completely flat to a fully bent configuration. The different arches are specified by the inward movement of the support w_x. K_E remains constant because the material is assumed linear elastic. K_U increases after bending, because the curvature adds stiffness to the system. Once the strip starts moving inwards, K_U slightly decreases. K_G is negative because the restraining force in the supports introduces a compressive normal force into the system. This compression force increases second order deformations, hence decreases the stiffness of the system.

For an elastica arch with a rise-to-span ratio of 0.15 the difference in buckling behaviour with and without residual stresses was investigated by Lienhard for a variable line-load. The snap-through analysis from **Figure 2.6** shows that for the geometrical nonlinear case, where all stresses resulting from bending and restraining are taken into consideration, the critical load factor λ is about 25% lower.

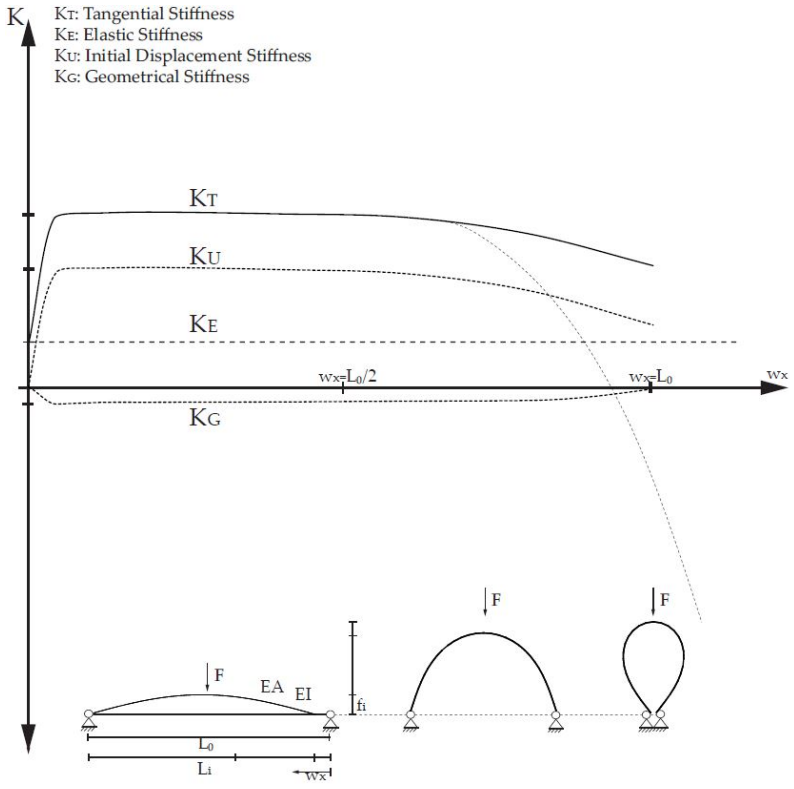

Figure 2.5. Differentiation of the stiffness matrix for an elastica arc with constant stiffness and beam length under different support locations. Modified from (Lienhard, 2014, p. 143).

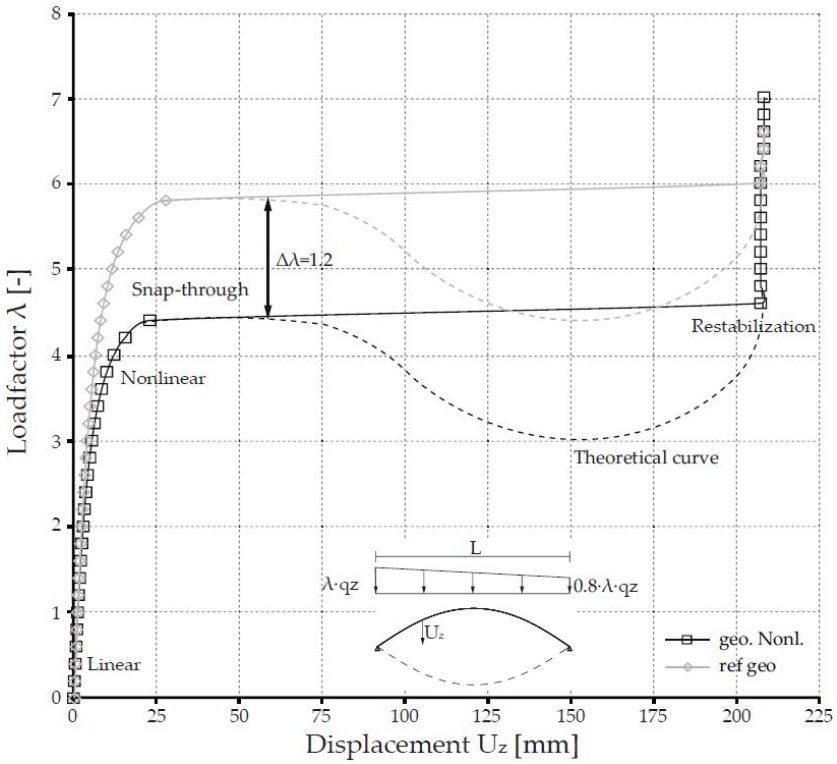

Figure 2.6. Influence of residual stress on stiffness for the geometric nonlinear case including all residual stresses and the reference geometry without pre-stress. Modified from (Lienhard, 2014, p. 143).

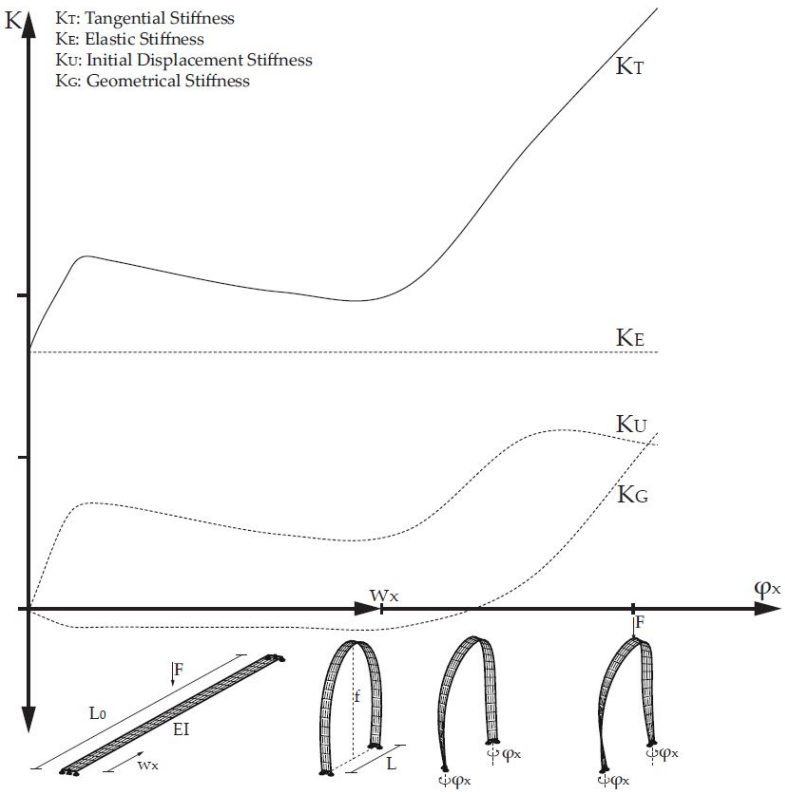

Figure 2.7. Differentiation of the tangential stiffness when a beam is first bent and then twisted. Modified from (Lienhard, 2014, p. 157)
$w_{x,max} = \pm 0.5\ L_0$
$\varphi_{x,max} = \pm 0.5\ \pi$

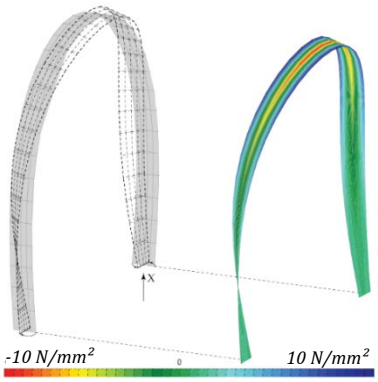

Figure 2.8. Membrane stresses in the longitudinal direction in the centre of the cross-section. (Lienhard, 2014, p. 157)

Figure 2.8 gives the differentiation of the tangential stiffness for an element that is bent and twisted. The strip is first bent by moving the supports inwards (w_x) to about half its length, and then twisted by rotating the strip at the supports (φ_x) about half way around its longitudinal axis. The figure shows how the stiffness under an applied point load in the centre is altered under these different configurations. A large increase in stiffness is obtained as a result of the twist. This rise is primarily caused by the increasing geometric stiffness, resulting from a tension stiffening effect. **Figure 2.7** shows that there is a large presence of tension stresses in the centre of the cross-section as a result of the twist.

2.6. TIME-DEPENDENT MATERIAL BEHAVIOUR OF TIMBER

Timber, as a viscoelastic material, is susceptible to time-dependent material behaviour.

2.6.1. CREEP AND STRESS-RELAXATION

A structure creeps when a constant long-term loading, such as self-weight, acts on it, resulting in increasing deformations over time. On the other hand, when an element is elastically deformed, the load that is necessary to maintain a constant deformation decreases over time due to stress-relaxation. This means that the residual stresses that are present in bending-active systems reduce over time, which has consequences for the structural behaviour of the system. Where creep directly causes plastic deformations, the plastic deformations from stress-relaxation only become visible when the structure is dismantled **(Figure 2.9)**. This deformation can best be explained by the lower spring-back force that is present in the elements after a structure's lifetime.

Figure 2.9. Plastic deformation as a result of stress-relaxation in the elements of the dismantled AA/ETH pavilion (top) and 2010 ICD/ITKE pavilion (bottom).

So far, the only research to stress-relaxation in relation to bending-active timber plate structures has been carried out by Lienhard (2014) during the erection of the 2010 ICD/ITKE pavilion. This test shows the amount of relaxation in birch plywood for three different rise to span ratio's **(Figure 2.10)**. Although, exact information of the stress-levels in the elements is absent, the graph clearly shows that a large part of the relaxation occurs in the first few days, and furthermore, that the elements that are deformed to a larger curvature relax to a greater extend, with a highest measured relaxation value of about 55%.

The designer should pay attention to the changing stress states. In the design of the Multihalle, stress-relaxation was seen as a positive event, because the members were stressed to a great extent, and, by the time that external loads were applied, the stress levels had already reduced to acceptable levels (Happold and Liddell, 1975). Furthermore, due to the retaining forces at the foundation, compressive stresses were present in the elements, that, as explained in the previous section, had a lower destabilising effect after relaxation. When tension stresses relax, on the other hand, a large part of the additional geometric stiffness acquired by

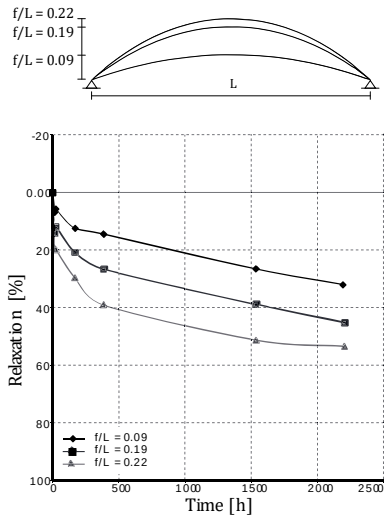

Figure 2.10. Relaxation tests of birch plywood bent to various rise to span ratios. Modified from (Lienhard, 2014, p. 68)

these stresses fades away over time. It can therefore questionable if twisted elements, which hold a lot of tension stresses, would be a viable solution for bending-active timber.

Creep as a result of dead-load causes the structure to sag. It can therefore be argued that a funicular shape, that is based on axially loaded elements is advantageous for timber shell structures. Creep is assumed to be proportional to the initial deformation. Therefore the creep in axially loaded elements is limited. As we have seen in **Section 2.3**, the elastica shows great resemblance with the catenary.

2.6.2. LOAD DURATION

Long-term loading on timber structures can result in failure over time. The strength of timber under a long-term load is approximated with the Madison curve (Jorissen, 2016). The Eurocode takes this effect into account with the k_{mod} factor. For plywood in climate class 1, for instance, the mechanical strength must be multiplied by a factor of 0.6 for permanent loading.

For actively bent timer, it can be argued that a permanent load is applied to the system when an element is bent. However, as we have seen in the previous section, a part of this stress also relaxes over time. **Figure 2.11** shows the Madison curve, together with a fast and a slow relaxation process according to **Figure 2.10**. When the amount of induced flexural stress is set to 0.86 of the ultimate strength, both the slow, as the fast relaxation curve remains below the ultimate strength during the structure's lifetime. It should, however, be noted that when an element is highly stressed, it is more likely that the fast relaxation curve is followed. Therefore, when all other conditions remain the same, it is not likely that a highly stressed element fails as a result of the prestress induced by bending over time.

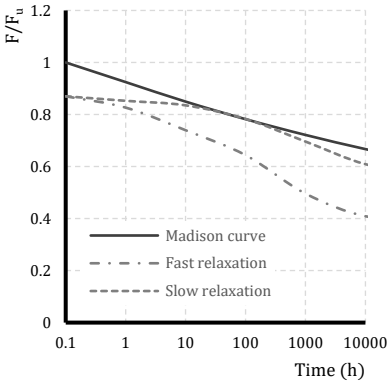

Figure 2.11. Madison curve and fast and slow relaxation curves from Figure 2.10, for an element that is stressed to 0.86 of the ultimate strength.

3. FORM AND RIGIDITY

3.1. INTRODUCTION

In bending-active systems, material and form are very closely related. The shape of actively bent timber comes from a minimisation of the elastic energy. This results in natural forms in which the shape follows the element's properties. This chapter gives an overview on the parameters that define the bending behaviour of timber elements. Furthermore, it will be explained how these elements work together to form spatial geometries. A large part of this chapter is related to the bending-active projects that are discussed in **Annex A**.

3.2. MATERIAL PROPERTIES

Wood is a natural material that is subjected to constantly changing weather conditions during growth of the tree. Other variables are more constant but location specific, such as varying soil conditions and growing space. All these factors have an influence on the material composition, making timber elements heterogeneous with a highly differentiated composition and properties. Mean values for the elastic- and shear moduli are used to describe the bending and twisting behaviour, and, it is therefore inevitable that these theoretical values will always result in an approximation of the real bent shape.

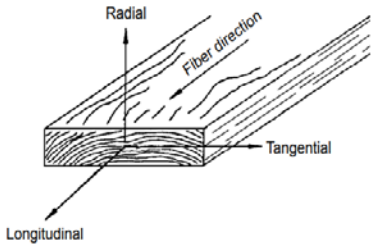

Figure 3.1. The longitudinal *L,* tangential *T,* and radial *R* axes of wood (Green et al., 1999, p. 2).

Furthermore, wood is an orthotropic material. A sawn timber element has different mechanical properties in three directions that are perpendicular to each other (**Figure 3.1**)**.** Wood behaves the strongest and stiffest along the fibre direction which is parallel to the longitudinal axis *L*. The radial axis *R* is normal to the growth rings and the tangential axis *T* is perpendicular to the fibre direction and tangent to the growth rings. The changing mechanical properties for each direction lead to anisotropic elastic behaviour in all timber elements, where twelve constants are needed to describe the material behaviour. A Young's modulus *E* for each of the three axes, a Shear modulus *G* for each of the three shear planes and six Poisson's constants ρ to indicate the ratio of the transverse to axial strain. These anisotropic material properties influence how the elements deform when they are subjected to bending and twisting moments. It is therefore of interest to have a clear idea of the ratio's between these material constants. **Table 3.1** gives an overview of the relation between Young's and shear moduli of various wood species that have been examined and charted by Green *et al.* (1999).

Species	E_T/E_L	E_R/E_L	G_{LR}/E_L	G_{LT}/E_L	G_{RT}/E_L
Hardwoods					
Ash, white	0.080	0.125	0.109	0.077	—
Balsa	0.015	0.046	0.054	0.037	0.005
Basswood	0.027	0.066	0.056	0.046	—
Birch, yellow	0.050	0.078	0.074	0.068	0.017
Cherry, black	0.086	0.197	0.147	0.097	—
Cottonwood, eastern	0.047	0.083	0.076	0.052	—
Mahogany, African	0.050	0.111	0.088	0.059	0.021
Mahogany, Honduras	0.064	0.107	0.066	0.086	0.028
Maple, sugar	0.065	0.132	0.111	0.063	—
Maple, red	0.067	0.140	0.133	0.074	—
Oak, red	0.082	0.154	0.089	0.081	—
Oak, white	0.072	0.163	0.086	—	—
Sweet gum	0.050	0.115	0.089	0.061	0.021
Walnut, black	0.056	0.106	0.085	0.062	0.021
Yellow-poplar	0.043	0.092	0.075	0.069	0.011
Softwoods					
Baldcypress	0.039	0.084	0.063	0.054	0.007
Cedar, northern white	0.081	0.183	0.210	0.187	0.015
Cedar, western red	0.055	0.081	0.087	0.086	0.005
Douglas-fir	0.050	0.068	0.064	0.078	0.007
Fir, subalpine	0.039	0.102	0.070	0.058	0.006
Hemlock, western	0.031	0.058	0.038	0.032	0.003
Larch, western	0.065	0.079	0.063	0.069	0.007
Pine					
Loblolly	0.078	0.113	0.082	0.081	0.013
Lodgepole	0.068	0.102	0.049	0.046	0.005
Longleaf	0.055	0.102	0.071	0.060	0.012
Pond	0.041	0.071	0.050	0.045	0.009
Ponderosa	0.083	0.122	0.138	0.115	0.017
Red	0.044	0.088	0.096	0.081	0.011
Slash	0.045	0.074	0.055	0.053	0.010
Sugar	0.087	0.131	0.124	0.113	0.019
Western white	0.038	0.078	0.052	0.048	0.005
Redwood	0.089	0.087	0.066	0.077	0.011
Spruce, Sitka	0.043	0.078	0.064	0.061	0.003
Spruce, Engelmann	0.059	0.128	0.124	0.120	0.010

Table 3.1. Elastic ratios for various species at approximately 12% moisture content (Green *et al.*, 1999, p. 2). The shear modulus is given by G. For example, G_{LR} is the shear modulus based on shear strain in the LR plane and shear stresses in the LT and RT planes (**Figure 3.1**).

Large plates, however, cannot be sawn from a single tree. When thin plates are needed, the obvious choice is plywood. This type of engineered wood keeps the grain intact, and therefore preserves the natural strength of timber. Plywood is made from thin layers of veneer that are laminated in a cross-wise fashion. This greatly improves the lateral strength of these elements. Compared to solid timber, plywood has some other advantageous qualities. It has less variable mechanical properties, better dimensional stability and a greater utilisation of raw timber (Gerrard, 1987). Plywood consists of at least three layers. When extra layers are added, the plate increases in homogeneity. The ratio between the Young's modulus parallel to the grain and the Young's modulus perpendicular to the grain E_0/E_{90} decreases. Also the impact of natural flaws, such as knotholes, is reduced. From the models of **Figure 3.2**, the impact

Figure 3.2. Two models constructed by the author with two sets of strips with the fibre direction oriented parallel (left) and perpendicular (right) to the longitudinal axis. The left model behaves significantly stiffer.

of the grain direction in thin plywood strips on the shape and stiffness of a bent and twisted system, is observed.

When it is desired to deviate from this cross-wise orthotropic fashion, a custom lamination procedure can be chosen, where, for instance, consecutive layers of veneer are placed in the same direction to increase the stiffness in the longitudinal plate direction. Custom lamination can also be used to alter the stiffness along the length of a plate. This procedure was used in the 2015 ICD/ITKE pavilion, where the grain direction in small parts of veneer was placed under a varying angle with the longitudinal axis (**Figure 3.3**). By varying the stiffness over the plate length, the bending behaviour of a plate can be manipulated (Bechert *et al.*, 2016). However, the manufacturing costs of these customised elements are, of course, a lot higher than the costs for off-the-shelf plywood plates. The equivalent flexural modulus of a plywood plate can be computed by

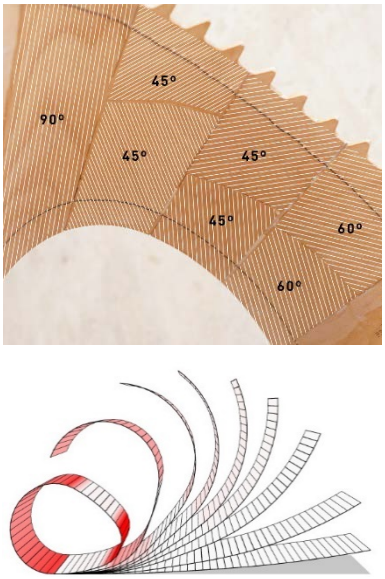

Figure 3.3. Veneer can be custom laminated (top) to vary the stiffness along the plate. This influences the bending behaviour (bottom) (Bechert *et al.,* 2016).

$$E_m = \frac{1}{I}\sum_{i=1}^{n} E_{m,i} \cdot I_i \qquad (3.1)$$

In which:

E_m is the flexural Young's modulus around the longitudinal or tangential axis
I is the moment of inertia around the longitudinal or tangential axis
t is the thickness of the plate
i indicates the veneer layer

3.3. ELEMENT TOPOLOGY

Together with the material properties, the element's cross section determines the resistance of the element to bending and torsion. Resistance to bending is expressed through the second moment of area over an axis. This value is also known as the moment of inertia. For simplification, it is assumed that a plate behaves like a thin beam. Hence, for a rectangular cross section, this value is

$$I_y = \frac{1}{12} b h^3 \qquad (3.2)$$

In which b and h describe the cross-sectional width and height. Locally decreasing the stiffness in a cross-section facilitates bending at a specific location. This can for instance be achieved by gradually altering the element's width or thickness, as can be seen in the segmented timber shells from Brütting *et al.* (2017), or by introducing cuts in the elements, which was demonstrated in the AA/ETH-Pavilion (**Figure 3.4**). Cut-outs in plates can also be made to facilitate bending in multiple directions. The 2015 ICD/ITKE pavilion and the bend9 are an example of this (see **Annex A**).

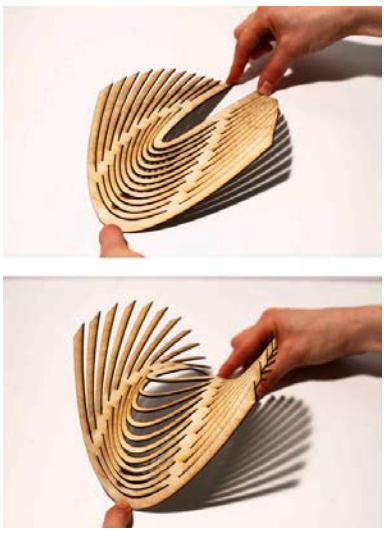

Figure 3.4. Cuts in the elements regulate the bending behaviour (D'Acunto and Kotnik, 2013).

3.4. CONNECTING AND ARRANGING ELEMENTS

In the previous paragraphs, we have seen how the element's material and topological properties determine the bending behaviour. The neutral axis of an element is constantly changing over its surface. At the same time, every element is held in place by, or imposes a force on another element. A great extent of the geometry of a structure is determined by how different elements are put together. At a connection, the element's axis is either transferred or changed. Parallelly aligned connections (**Figure 3.5**) can be achieved by gluing elements directly to each other, or by clamping them with mechanical fasteners. The connection can also be made with rotational freedom around one or more axes. Rotations might be partly blocked due to overlapping elements or can be completely fixed with an intermediate wedge, giving more dimensional stability to a system.

Figure 3.5. Systems with parallel connections (Lienhard, 2014)

Elements can be arranged by simply letting them collide with each other. These connections only partly restrain translational degrees of freedom. These systems show resemblance with the properties of woven systems, as can be found in textiles or fabrics. Research to substituting these properties to timber has led to the development of the Timberfabric module (**Figure 3.7**). In addition to following a weaving pattern, the strips are also twisted like yarn, which adds friction to the system. **Figure 3.6** shows the evolution of the weaving pattern towards a system of interlocking strips.

Figure 3.6. Difference in warp and weft direction in Timberfabric (Weinand and Hudert, 2010).

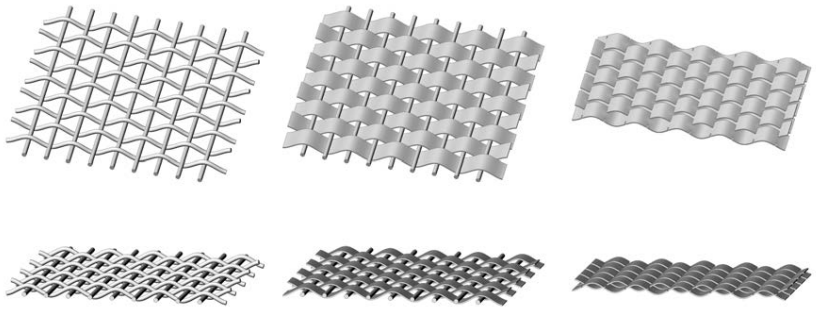

Figure 3.7. Evolution of a weaving pattern to a system of interlocking strips (Hudert, 2013).

A similar pattern is observed in the 2010 ICD/ITKE pavilion (**Figure 3.9**). These patterns, however, tent to easily rotate around the connection points. This can be prevented by introducing irregularities that alter the locations of these weak spots, or by the addition of an extra layer. This layer could be used to further shape the system according to the principle shown in **Figure 3.8.**

Figure 3.8. A third layer locks the system (Schönbrunner *et al.*, 2015).

3.5. CONFIGURATION AND ASSEMBLY

Figure 3.9. Assembly of the ICD/ITKE 2010 research pavilion (Fleischmann and Menges, 2011).

Previous bending-active projects have shown that there can be numerous ways to combine structural elements. The chosen approach will have a large impact on the internal forces, structural behaviour, assembly and shape of a system. To develop an understanding of these structures, a distinction can be made in configurations in which these systems primarily find their force equilibrium, which can be globally or locally.

Figure 3.10. A bending-active segmented shell (Brütting et al., 2017).

Global systems show a continuous bending shape. They can either be externally or internally restrained. Global systems find their equilibrium by the presence of restraining forces from exterior sources, such as foundations or tension rings and bars. Gridshells, like the Multihalle, and segmented shells (**Figure 3.10**) are good examples of these systems. Forces that are needed to assemble these structures can become quite high. Internally restrained global systems are assembled from discrete elements that restrain themselves. With the addition of each element, the final shape is further approached (**Figure 3.11**). The Plydome and the Berkeley Weave are examples of internally restrained global systems.

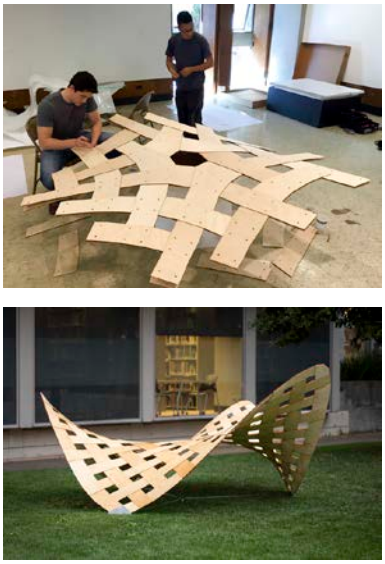

Figure 3.11. Assembly of the Berkeley Weave (Schleicher and La Magna, 2016).

Bending-active systems that find their force equilibrium locally are characterised by a multiplication of closed bending systems. The 2010 ICD/ITKE pavilion (**Figure 3.9**) and the Timberfabric project are good examples of these systems. This improves handling during construction, since forces are kept to a minimum and the form of an assembled part is close to the final shape. This is especially the case, when separate bending-active units are pre-bent into a closed equilibrium system prior to assembly, as demonstrated in the 2015 ICD/ITKE pavilion (**Figure 3.12**).

This categorisation does not endeavours to be completely inclusive for all types of bending-active structures. In reality, these structures do not tend to be easily categorised. Often a combination of configurations is present in a structure. This can clearly be observed in the 2010 ICD/ITKE pavilion. Although, the largest part of the force equilibrium is obtained locally, some restraining forces are present at the supports to fix the strips to the exact location. Furthermore, the global geometry slightly changes when adding additional strips, which indicates that the internal forces are partly distributed globally as well.

Figure 3.12. Assembly of the ICD/ITKE 2015 research pavilion which uses units that are in closed equilibrium (Bechert *et al.,* 2016).

3.6. ACHIEVING RIGIDITY

Figure 3.13. Bend9 project harnesses multi-directional bending to generate a double curved surface (Schleicher and Magna, 2016).

The structural elements need a certain amount of slenderness to be formed into shape. At the same time, structural systems should be designed to withstand large external forces. Simply increasing member dimensions does not satisfy. Stiffness and stability should therefore be found elsewhere.

Figure 3.14. The Bend9 uses multiple layers to increase rigidity (Schleicher and Magna, 2016)

Often this rigidity is found in the geometry (La Magna, 2017). Various ways have been explored to develop double curved systems by using successively bent single curved plates. The Bend9 (**Figure 3.13**) and Berkeley Weave (**Figure 3.11**) projects nicely show how a target surface can be approached by using actively bent elements. Both structures acquire double curvature by a strategical element topology that allows for multi-directional bending.

Another way of finding rigidity, is by adding pre-stressed tensile elements to the structural system, i.e. cables or membranes. These systems are referred to as bending-active tensile hybrids (BATH) (Slabbinck *et al.*, 2017). The addition of tensile elements can greatly increase the structural qualities of a system, as has been shown in the AA/ETH pavilion (**Figure 3.15**) or in the models presented by Slabbinck, Körner and Knippers (2017). However, a large issue when designing for long-term structures is the time-dependent material behaviour. Creep and stress-relaxation in the

Figure 3.15. Tension elements in the AA/ETH pavilion (D'Acunto and Kotnik, 2013).

wood result in loss of pre-stress in the tensile elements. This was experienced in the AA/ETH pavilion, where the tension elements were tightened a few times over the year the pavilion was standing to retain its structural rigidity (D'Acunto, 2017). Therefore, it is very unlikely that tensile hybrid structures with actively bent timber elements are a viable option for long-term building structures. Rigid elements that can take both compression and tension and do not rely on prestress for their stability, on the other hand, could form a better solution for strengthening bending-active timber.

At last, additional layers can be added to achieve rigidity whilst remaining the elements flexibility during construction. The layers can either be directly placed on top of the previous layer, or connected by using connector pieces in between the layers (**Figure 3.14**).

4. NUMERICAL COMPUTATION OF BENDING-ACTIVE STRUCTURES

4.1. INTRODUCTION

In general, form-finding methods are used in the computational design of form-active structures, i.e. tensile membranes and catenary arch and shell structures. The geometrical form is an outcome of given boundary restraints and a target stress field. It is an erection process that is based on the optimization of the structural behaviour of the geometry.

Where in general form-finding element characteristics are not considered, form-finding of bending-active structures uses the elements dimensions and material properties as input to describe the element's behaviour during elastic bending (Lienhard, 2014). Opposite to general form-finding, form-finding of bending-active systems does not include an optimization of the structural behaviour. The process can rather be seen as a form-development process, where numerical tools are used to develop the shape in which the bending-active system is in equilibrium. The stresses that occur in the elements during the formation are known throughout the process. **Table 4.1** describes the difference in variables involved in the form-finding process of bending-active and form-active structures.

	Bending-active	**Form-active**
Geometric		
Boundary points and edges	Input	Input
Length and surface dimension	Input	Output
Sectional dimensions	Input	Not considered
Surface/element curvature	Output	Output
Mechanic		
Material stiffness	Input	Not considered
Stress	Output	Input
Sum of input variables	4	2
Sum of output variables	2	2

Table 4.1. *Input and output variables for bending-active and form-active form-finding (Lienhard, 2014, p. 105)*

This chapter briefly explains three different numerical approaches that can be used in the form-finding of bending-active systems. Although, all these methods use contracting cable elements to simulate the bending, their calculation methods, and hence, the used software, differs. The first method uses the finite element method (FEM), the second method uses isogeometric analysis (IGA) and the third method is based on a particle spring system with dynamic relaxation. All these methods use the 3D modelling software Rhino as the basic modelling environment, sometimes

combined with the Grasshopper plug-in for parametric input. The methods were explored by the author while visiting the masterclass on software approaches for simulating bending-active systems prior to 2017's IASS symposium in Hamburg.

4.2. FORM-FINDING WITH FEA

The elastic behaviour of structures can be accurately simulated using a finite element analysis (FEA). A structural element, e.g. a plate or a beam, is discretised by a set of elements. The corner points of these elements are the degrees of freedom (DOF) to which the equilibrium formulation from equation (4.1) applies.

$$F = K_T\, u \qquad (4.1)$$

This results in a large system of equations that can be solved numerically. In this formula, F is the force vector, K_T is the tangential stiffness matrix and u is the unknown displacement vector. A finer mesh, i.e. more finite elements, generally results in more accurate computations and smoother surfaces, however, it does increase the calculation time.

As we have seen in **Section 2.5,** bending-active systems behave in a geometrically nonlinear fashion. The stiffness of the system changes with increasing displacements. K_T therefore becomes a function of u. The equilibrium equation should now be written as

$$F = K_T(u)\, u \qquad (4.2)$$

In this computation, the force vector F is applied incrementally. The equilibrium path of a structure is commonly approached by the Newton-Raphson method, which minimises the residual force in an iterative search (**Figure 4.1**). The stiffness matrix is updated after each load increment, which drastically increases the computational time of a nonlinear analysis, compared to a linear analysis.

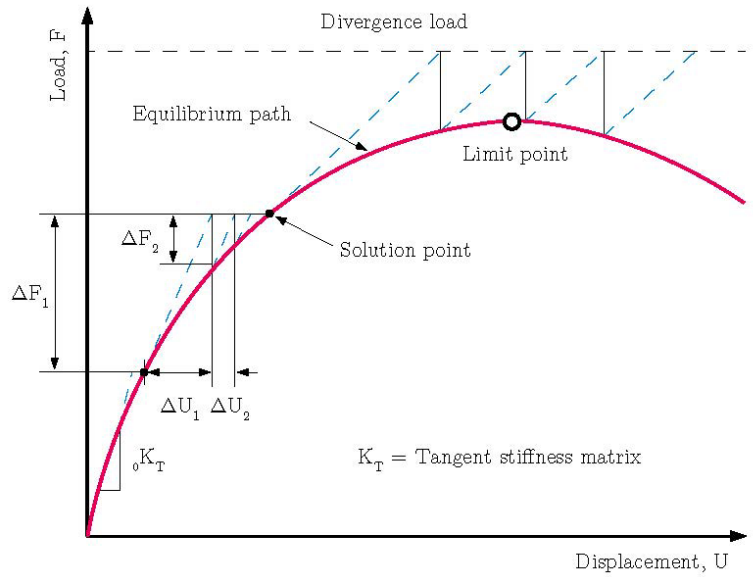

Figure 4.1. Nonlinear finite element analysis (La Magna, 2017, p. 64)

The simulations are performed in the commercial FEM software package SOFiSTiK. This commercial FE package has a stable solver that runs smoothly when large deformations, complex geometries and geometrically nonlinear effects are incorporated in the simulation (Bauer *et al.*, 2018).

Bending-active systems can be build using the elastic cable method that was developed by Lienhard (2014) during the design phase of the 2010 ICD/ITKE research pavilion (**Figure 4.2**). This is an approach that has been programmed into SOFiSTiK to increase computational time of bending-active systems. It uses contracting cables with an adaptive step-size control to gradually increase elastic strain in cables, which simulates the elastic bending. SOFiSTiK offers stable nonlinear solvers that can accurately describe the large deformations that occur during the form-finding steps. All the information on internal element stresses and strains can be used as a starting point for a next form-finding step.

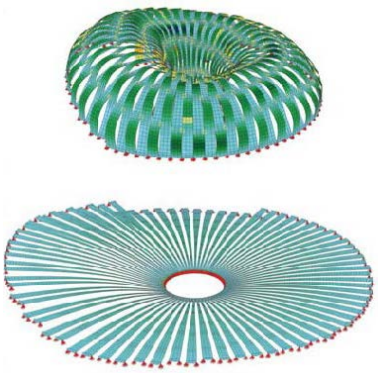

Figure 4.2. Contracting cables simulate the bending in the computation of the 2010 ICD/ITKE research pavilion (Lienhard, 2014, p. 69).

4.3. FORM-FINDING WITH IGA

An interesting new field in structural analysis is isogeometric analysis (IGA). IGA has the aim to merge computer aided design (CAD) of structures and computer aided engineering (CAE) into one single environment. Bauer *et al.,* (2017) developed a software tool Kiwi3d, that incorporates IGA into Grasshopper. The biggest difference with FEM, is that it describes the geometry through NURBS patches and trim curves, which is also used in popular 3D CAD packages, such as Rhino. The degrees of freedom (DOF) are the control points of these curves (**Figure 4.3**). In traditional FEM, a curved surface must always be described by a discretization in multiple finite elements. Hence, IGA results in a more accurate representation of the curved surface, and additionally, in less DOF's to describe the surface, which reduces the computation time. (A. M. Bauer *et al.*, 2017) (Längst, Michalski and Lienhard, 2016). However, it should be noted that the accuracy of the bending shape is still largely depending on the amount of control points used to describe the plate. This can be seen in **Figure 4.4**, where the elastica shape is approached more accurately with the addition of control points.

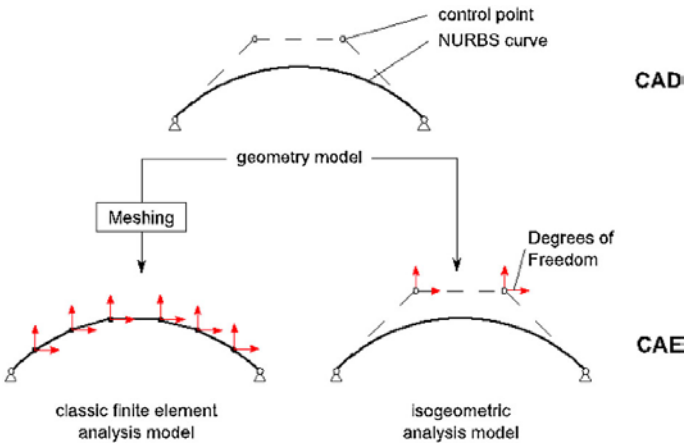

Figure 4.3. Difference between DOF's in FEM and IGA (Längst, Michalski and Lienhard, 2016)

IGA shows great potential for the computation and analysis of bending-active structures. This analysis method offers the possibility to have the same design freedom in an element before and after simulation, however, the theory behind IGA is very broad and it differs quite a bit from the standard structural design curriculum. Also, at the time of writing, the tools are still in developing phase, making it hard to offer a stable modelling approach for bending-active structures. Furthermore, only isotropic materials can currently be used in the analysis (A. M. Bauer *et al.*, 2017).

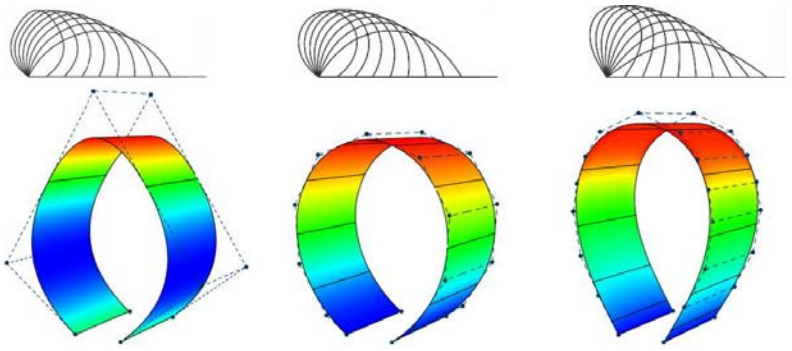

Figure 4.4. The accuracy of the elastica shape is approached more accurately with more control points (Bauer *et al.*, 2017)

4.4. FORM-FINDING WITH PHYSICS BASED MODELLING

Another way to simulate bending in CAD environments, is with the use of physics engines that simulate physical behaviour. Although, these tools have been developed for the simulation of visual effects in computer graphics, they have also found their way of application in architecture and structural design. Where form-finding using FEM software needs detailed material and geometric input from the user, such as material properties and cross-sectional dimensions, most of these physics engines are based on a particle spring system that consists of particles that are connected by springs with a certain stiffness (Nicholas and Tamke, 2013). This results in the lack of precise material data that are of interest to the structural engineer, such as stresses and deformations. However, this method does give accurate physical behaviour in the same sense as how a hanging chain accurately describes a catenary in the real word (Fleischmann and Menges, 2012).

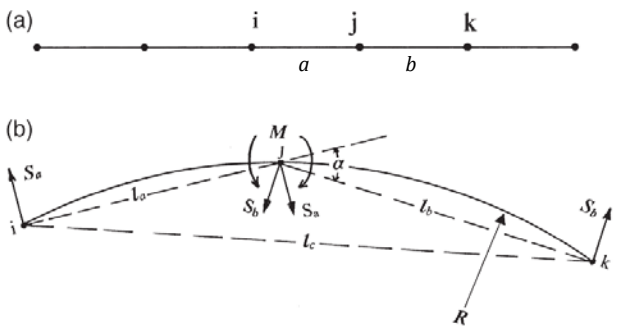

Figure 4.5. a) Segments of an initially straight beam. b) The 3DOF nodes cannot take the bending moment *M*. Bending the infinitely stiff segments results in shear forces *S* in the nodes that account for bending-stiffness (Adriaenssens and Barnes, 2001).

Particle spring systems generally have three DOF's and use dynamic relaxation (DR) to find the equilibrium shape. Without going too much into detail, this method can be explained as follows. DR adopts a step-wise approach, where small time increments are used to trace the motion of each node (with a fictitious mass) that is imposed by a force, and uses artificial damping to find a static equilibrium (Adriaenssens and Barnes, 2001). Although, these systems only have translational DOF's, flexural behaviour can be simulated in two different ways. Firstly, through a system of one-dimensional rods that acquire rotational stiffness through shear forces *S* (**Figure 4.5**). These shear forces are differentiated from the moment curvature relation for continuous beams (Adriaenssens and Barnes, 2001). Secondly, by transcribing this rotational stiffness to the hinging edges of a mesh (Tachi, 2013), enabling the simulation of the elastic behaviour of sheets (**Figure 4.6**). Similar to the previous methods, the elements are bent by contracting a rod between two nodes. However, a slightly different approach is adopted. Here, the length of the cables is directly altered, contrary to using increasing strain.

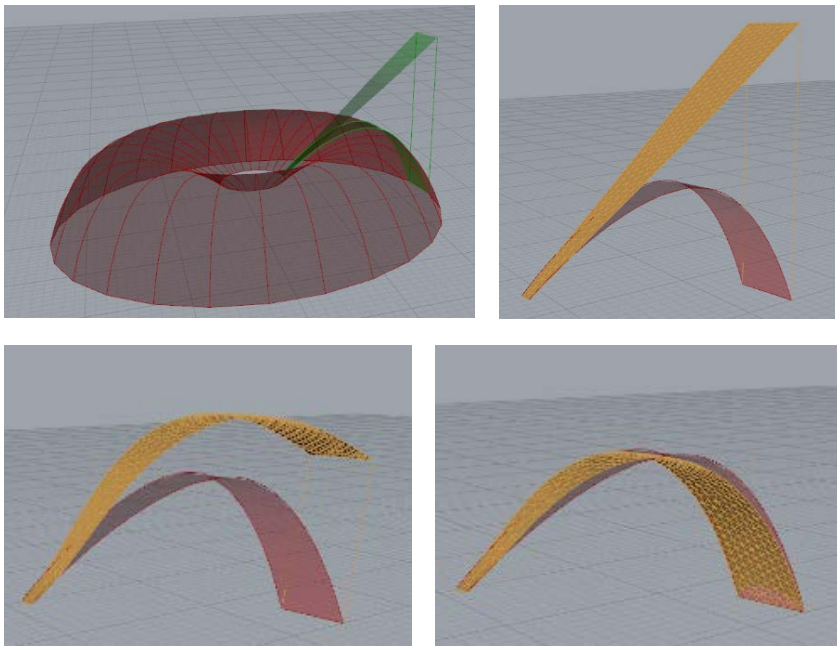

Figure 4.6. Software exploration by the author. A segment of half a torus is approached by bending, using the Kangaroo physics engine.

Physics based modelling can be done in Rhino via Kangaroo, which is a very popular physics-based tool that has been developed by Piker (2013) as a plugin for Grasshopper. The tool works fast and almost immediate feedback is felt while changing parameters. The tools can be used for design exploration, however, physics based modelling for exact engineering purposes remains very limited. The implementation of mechanical properties and geometric parameters is difficult (Nabaei, 2014). Furthermore, plate behaviour, especially for orthotropic materials such as timber, can hardly be simulated.

4.5. CONCLUDING REMARKS

Each of the discussed methods have their best application for specific tasks and stages in the design phase. An overview of these methods, together with their strengths and weaknesses can be found in **Table 4.2**. The beauty in IGA and particle spring systems, lies in the fact that they integrate design and analysis into the same software environment. Although, research is moving closer to one holistic approach for CAD and CAE, at the time of writing, this utopia for structural designers still remains out of reach. For the purpose of this research, the first method has been chosen to be most suiting. FEA is the common standard in engineering practice. It is most reliable in terms of accuracy. Since this research tries to tighten the gap for an application of bending-active structures into common building practice, it is important to deviate as little as possible from methods that are commonly accepted and trusted. Form-finding using FEM is therefore chosen as the most appropriate method for the research described in this report.

METHOD	STRENGTH	WEAKNESS
FEM (SOFiSTiK) ***(Chosen method for this research)***	+ Known to most engineers + Very accurate simulation + Good interaction with Rhino and Grasshopper + No problems with simulating orthotropic material behaviour	- Needs fine discretisation to describe curved surfaces - Large models need a lot of computation time - Solvers are very susceptible to instabilities
IGA (Kiwi3d)	+ Modelling and analysis in same environment + Quick calculation + Accurate representation of the geometry + Elements collide with each other	- New tool needs further development - Currently less accurate then FEM - Not yet possible to use anisotropic material - Difficult theory
Particle spring with DR (Kangaroo)	+ Modelling and analysis in same environment + Immediate response + Good for design exploration	- Less suited for plates - Not very accurate results - Computational time increases quickly with heavier models

Table 4.2. Assessment of the form-finding methods.

5. NUMERICAL APPROACH

5.1. INTRODUCTION

The numerical simulations will follow the elastic cable method from Lienhard (2014), where contracting cables are used to bent the planar elements. There are several ways to build these models. For a stable simulation, it is essential that the system is sufficiently restrained. Large deformations should only be allowed in the desired direction. Some different ways to come to a basic bending-active system are given in **Figure 5.1.** This chapter will further describe the software approach for the form-finding and analysis of bending-active systems.

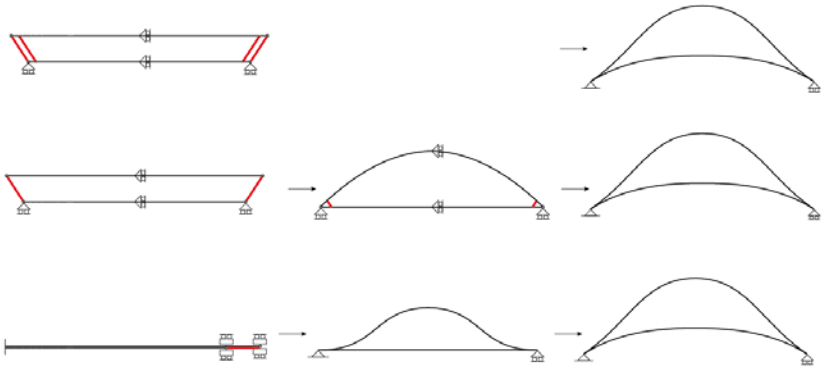

Figure 5.1. Three different ways to come to a bending-active system by contracting cables.

5.2. WORKFLOW FOR THE COMPUTATION AND ANALYSIS OF BENDING-ACTIVE SYSTEMS

The software approach for the numerical computation and analysis of bending-active structures will be carried out in Rhino for geometric modelling and SOFiSTiK for FEA. Both programs are seamlessly linked together through a Rhino SOFiSTiK interface. Both software packages have access to parametric environments. For Rhino, this is the well-known plug-in Grasshopper. Grasshopper gives a programming approach to CAD. Additionally, it offers plug-ins, such as STiKbug or GeometryGym, that have the same purpose of linking CAD and FEM. SOFiStiK has its own parametric environment called Teddy, which is based on a text based input called CADINP. Within the Teddy environment, different programs can be run for the pre-processing, analysis and post-processing of the FE model. The programs that are used for the simulation are elaborated in **Table 5.1**. The computation and analysis of bending-active structures can generally be divided into three phases, which are further described below. The full Teddy script for the form-finding of a bending-active system is given in **Annex B.**

AQUA	Define materials and cross-sections
SOFIMSHA	Parametric input of geometry
SOFIMSHC	Geometric input of geometry
TEMPLATE	Define variables
SOFILOAD	Define loads
ASE	Finite element solver

Table 5.1. Used programs within SOFiSTiK.

5.2.1. *PHASE I*

The first phase is the model preparation phase. In this phase, material and section libraries are set-up in *AQUA*. The 'flat' geometry is drawn in Rhino and is imported into Teddy with either *SOFIMSHA* for parametric input, or *SOFIMSHC* for geometric input.

5.2.2. *PHASE II*

The second phase covers of the numerical form-finding by elastic bending. The bending is driven by incrementally converging the length of a cable that ties two nodes to zero. During a simulation, the number of required iterations for an increment indicates the level of nonlinearity. Adaptive step size control is manually programmed into the solver by scaling the step size based on the number of iterations that were necessary in the previous load increment. This method has proven to greatly reduce the computational time compared to a linear progression of load increments (Lienhard, 2014).

The step size is controlled using formula (5.1), in which n is the load factor of step i, I_1 is the desired number of iterations and I_t is the number of iterations needed for the previous step. The root k can be altered to speed up the analysis, but normally varies between 0.1 and 0.3.

$$n_i = n_{i-1}\left(\frac{I_1}{I_t}\right)^k \qquad (5.1)$$

The *TEMPLATE* program defines variables that will be used in the adaptive increments loop. *SOFILOAD* describes the load case that controls the bending by predefining strain levels for a group of cables to -99.9 %. *ASE* runs a step-wise solver where this strain level is gradually applied through a loop with adaptive increments. After every step, a new primary load case 'PLC' is saved that contains all the information on node deformations and stress levels present in the elements. The latest PLC is loaded at the start of each new calculation step, which means the most up-to-date bent shape, together with all its internal stresses, is used as a starting point in each new calculation. A copy of the database is made via *SYS COPY*, and the final PLC is updated as the new starting system in *ASE*. Boundary conditions are updated to restrain the new system using *SOFIMSHA*. The steps in this phase can be repeated when an additional bending job should be carried out.

5.2.3. PHASE III

In the third phase, the bent geometry can be exported to Rhino via STiKbug. A Grasshopper script is written for efficient geometrical analysis and manipulation. Optionally, bent elements can be copied and coupled, and the new geometry is imported to Teddy via *SOFIMSHA* or *SOFIMSCHC*. However, when this additional step is blended into the framework, the stress state of the elements is lost in the process. The load cases for external loading are set-up in *SOFILOAD*. The nonlinear solver in *ASE* is used to calculate these load cases. When available, data on stress levels can be recollected by recalling the previous PLC.

5.3. SIMULATING STRESS-RELAXATION

Stress-relaxation can be numerically simulated in SOFiSTiK by giving a load factor to the internal stresses of an element. A separate relaxation program is set up in *ASE* that runs prior to the structural calculations. In this program, the 'FACL' command is used to give a load factor to the internal stresses of a group (GRP) of elements within a certain PLC. *ASE* then calculates the new equilibrium state according to the new internal stresses. The following commands can for instance be used to specify the amount of relaxation in the model:

'GRP no 1 FACL 0.8' *(=20% stress-relaxation in the elements of group 1)*
'GRP no 2 FACL 0.6' *(=40% stress-relaxation in the elements of group 2)*
'GRP no 1,2 FACL 0.2' *(=80% stress-relaxation in the elements of group 1 & 2)*

The next chapter will further describe the phenomenon of stress-relaxation in bending-active timber systems.

6. INVESTIGATING BASIC BENDING-ACTIVE SYSTEMS

6.1. INTRODUCTION

The behaviour of bending-active structures was investigated according to the analysis of two different basic systems, which are the basic hinged, and the basic clamped system. Form-finding was done using the elastic cable method, discussed in **Chapter 5** in SOFiSTiK (**Figure 6.2**). The numerical toolkit was tested and validated by comparison with simple experimental load tests (**Figure 6.1**). These tests are, by no means, following an exact experimental method, however, they are sufficiently accurate to study the general behaviour. This preliminary investigation had the aim to develop confidence in the numerical toolkit and insight into the fundamental behaviour of simple bending-active systems, which also includes the time-dependent behaviour of timber.

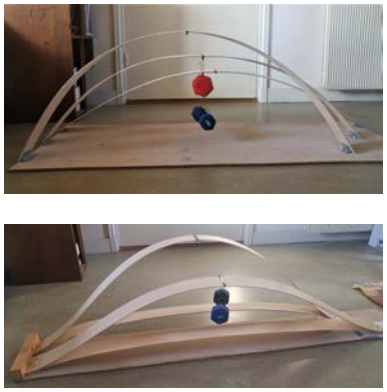

Figure 6.1. Simple load tests on the hinged (top) and clamped (bottom) system.

The tests are performed with three-layered 3mm birch plywood. No material properties were available for this thickness, however, the material properties for a 4 mm plate are given by the supplier and are shown in **Table 6.1**. For the 3mm plate, the two outer veneer layers are somewhat thinner compared to the inner layer. This results in a relatively smaller flexural Young's modulus in the longitudinal direction $E_{m,0}$. For the 3mm plate, $E_{m,0}$ was computed by a three-point flexural test and is 11,500 N/mm^2. Note that $E_{m,0}$ for a 4mm plate is equal to 16,471 N/mm^2. This value from literature was verified to be correct by means of a similar test.

Table 6.1. *Material properties for 4mm birch 3-layered plywood (UPM, 2007).*

Characteristic strength						Mean modulus of elasticity			
Bending		Compression		Tension		Bending		Tension and compression	
$f_{m,0}$ [N/mm^2]	$f_{m,90}$ [N/mm^2]	$f_{c,0}$ [N/mm^2]	$f_{c,90}$ [N/mm^2]	$f_{t,0}$ [N/mm^2]	$f_{t,90}$ [N/mm^2]	$E_{m,0}$ [N/mm^2]	$E_{m,90}$ [N/mm^2]	$E_{t/c,0}$ [N/mm^2]	$E_{t/c,90}$ [N/mm^2]
65.9	**10.6**	**31.8**	**20.2**	**45.8**	**29.2**	**16471**	**1029**	**10694**	**6806**

By bending and restraining the plates, forces are introduced into the elements. **Figure 6.3** shows the force diagrams of both systems. The internal axial forces that are induced by the boundary conditions affect the structural behaviour due to second order effects. The following sections explain what this means for the systems with reference to several design variants.

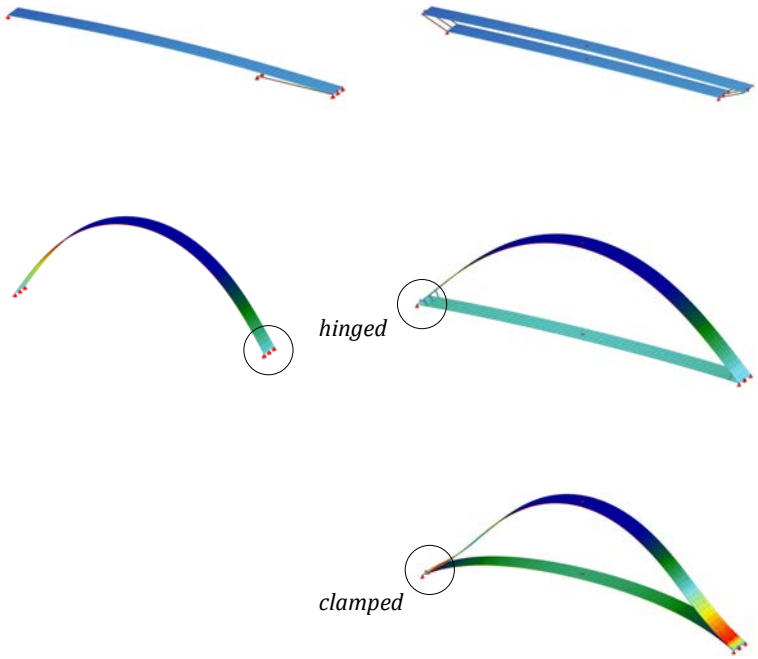

Flat geometry

Contract first set of cables to form the hinged system.

Contract second set of cables to form the clamped system

Figure 6.2. The systems were form-found using the elastic cable method. The colours show the development of stresses is the outer layer.

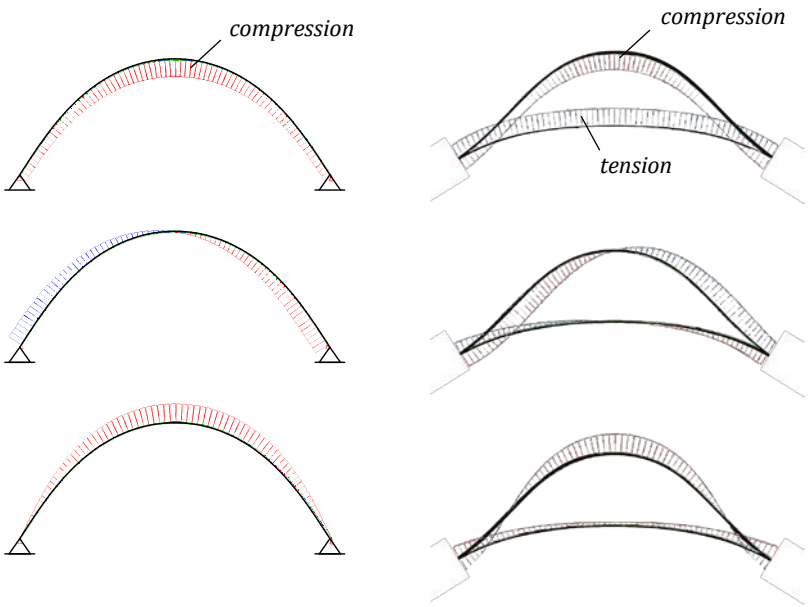

Normal force diagram

Shear force diagram

Moment diagram

Figure 6.3. Force diagrams of the basic hinged (left) and clamped (right) system.
Blue=positive; red=negative

6.2. PHYSICAL AND NUMERICAL COMPARISON OF TWO BASIC SYSTEMS

6.2.1. *HINGED SYSTEM*

Three different variants of the hinged system were built and analysed (**Figure 6.5**). Form-finding was done by using a set of contracting cables that moved the sliding support inwards (**Figure 6.2**), after which the sliding support was updated to a hinge. A compressive normal force is present in the system due to the restraining horizontal force at the supports. The models were subjected to a point load in the centre of the system. **Figure 6.4** shows both the load-displacement curve from the geometrically nonlinear FE simulation in which all the residual stresses resulting from bending were taken into account (annotated with RS=100%), as the physical test values that were recorded immediately after the system was bent. From these graphs it is seen that the geometrically nonlinear calculation describes the physical behaviour quite accurately.

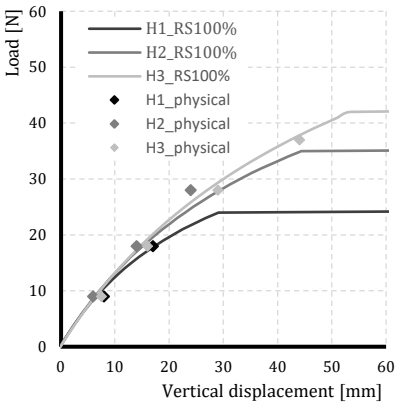

Figure 6.4. Physical and numerical results of models H1, H2 and H3. The displacement is measured for a central point load.
E_0 = 11,500 N/mm^2; t = 3mm

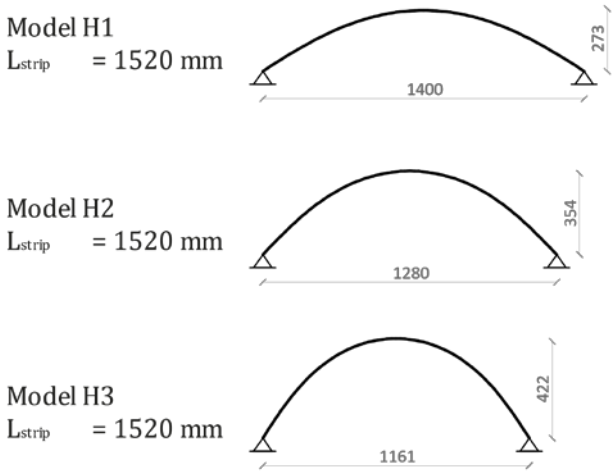

Figure 6.5. Different test setups of the hinged system

The stresses in the system have an effect on the load-carrying behaviour. **Figure 6.6** gives a comparison between the numerical models of the hinged systems including all residual stresses (RS=100%) and the stress-free geometries (RS=0%). The system becomes stiffer and the critical buckling load increases when the stresses perish. The absence of destabilising stresses resulting from the internal compression force explains this stiffening behaviour. The same effect was observed in the physical test set-up, when the load test was repeated after the system was bent for approximately 7500 hours. Since the amount of stress-relaxation is dependent on the time, the load-displacement curve will tend to move from the RS100% graph to the RS0% graph during the system's lifetime.

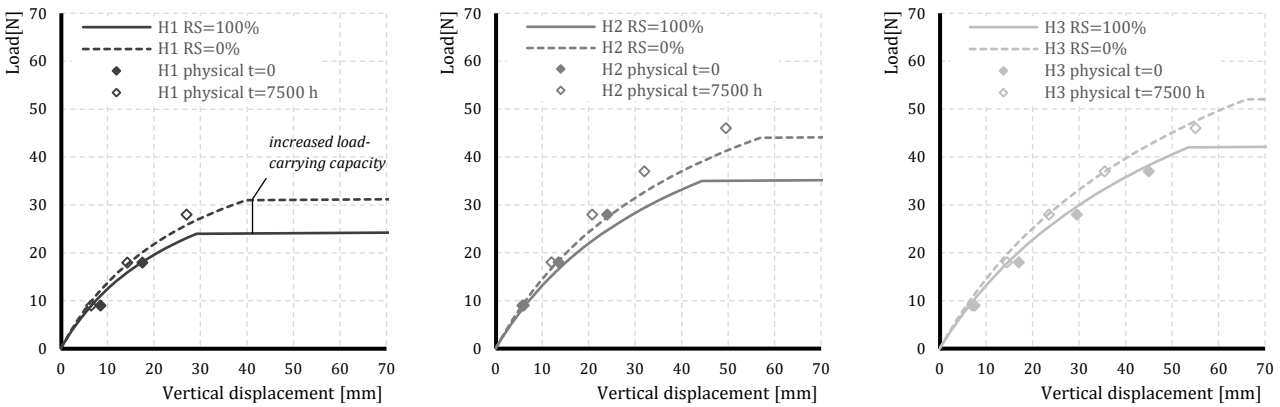

Figure 6.6. Load-displacement curves of the full stress and stress free systems H1-2-3, combined with physical measurements prior to and after relaxation. The figures show how the load-carrying capacity is increased over time.

6.2.2. *CLAMPED SYSTEM*

Two variants of the clamed system were analysed (**Figure 6.7**). The numerical form-finding consists of two bending steps. In the first step, the outer sets of cables are contracted. The second step contracts the inner sets of cables. This results in a parallel alignment of the strips. The two strips are tied with a kinematic constraint for both translation and rotation (**Figure 6.2**). The system is supported with a hinge and a roller support. Again, both the physical as the numerical system are loaded with a central point load. The results of both variants are shown in **Figure 6.8**. The physical and numerical test results show quite some resemblance with each other. However, model C2 has a slightly larger error than model C1. An explanation for this error might be the relatively larger contribution of the ground friction at the roller support in model C2. Although, friction was minimised by placing the timber on a smooth surface.

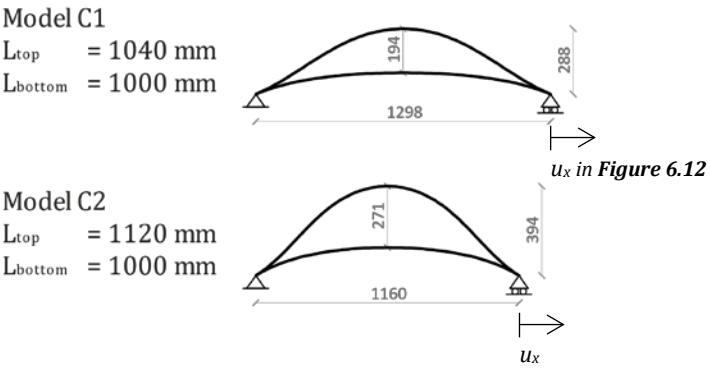

Figure 6.7. Test setups of the clamped system.

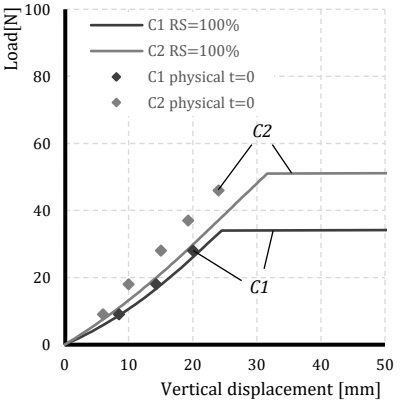

Figure 6.8. Physical and numerical calculation of models C1 and C2. The figure shows the measured displacement for a central point load.
E_0 = 11,500 N/mm^2; t = 3mm.

Contrary to the hinged system, the clamped system decreases in stiffness when the residual stresses are not taken into account in the numerical analysis (**Figure 6.10**). This can be explained by looking at the average stresses in the longitudinal direction in the centre plane of the cross-section over the full length of the strips. This value is -0.08 N/mm^2 and +0.10 N/mm^2 for the top and bottom strip respectively (**Figure 6.9**). Because the surplus of tension stresses in the bottom strip is about 20% higher than the surplus of compression stresses in the bottom strip, this results in

a positive stiffening effect in the stressed state (RS=100%). At the same time, because the compression stresses in the top strip perish, the buckling load of the system increases in the stress free state (RS=0%). This was also observed in the physical systems, which also showed an increase in maximum load after 7500 hours. Furthermore, the physical models also show a slight increase in stiffness. This is due to a more complex relaxation behaviour, which is further elaborated in the following section.

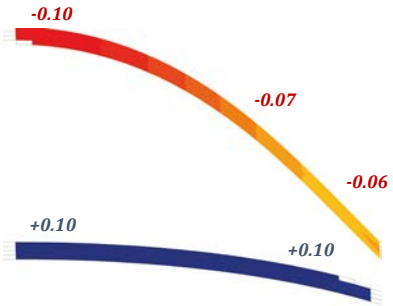

Figure 6.9. Section of system C2 that shows the stresses in the longitudinal direction in the centre plane of the cross-section. The values are given in N/mm^2.

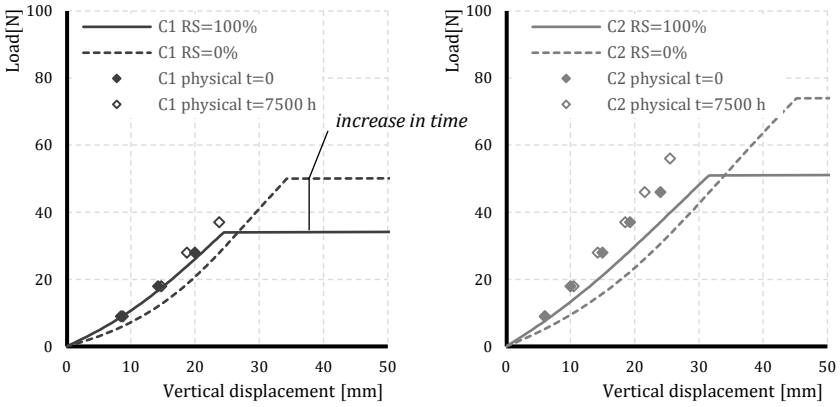

Figure 6.10. Load-displacement curves of the full stress (RS=100%) and stress free (RS=0%) systems C1-2, combined with physical measurements prior to (t=0) and after relaxation (t=7500h).

6.3. STRESS-RELAXATION IN BENDING-ACTIVE SYSTEMS

6.3.1. RELAXATION RATE

The previous tests show that a changing stress state influences the structural behaviour of actively bent systems. When timber is used, it is important to take into account that the effects of stress-relaxation can be significant. For a clear understanding of the structural behaviour of a system, the speed and magnitude of the relaxation should be known. This will be referred to as the relaxation rate. Relaxation tests, however, take a lot of time to carry out. Luckily, some information on relaxation can be obtained and reproduced from literature.

The relaxation tests from Lienhard (2014) (**Figure 2.10**) were carried out on the hinged system. Although, exact information on stress levels is missing, some general conclusions can be reproduced from these graphs. If we assume that the rise to length ratios are translated to a strip with a 1 m length, the absolute value of the average stress levels over the length of the strip can be computed (**Table 6.2**). If the stress for f/L=0.09 is then normalised to be 1.00, one observes that the relation between the relaxation after 2000 hours and the average stress levels in the element after bending is somewhat linear (**Figure 6.11**).

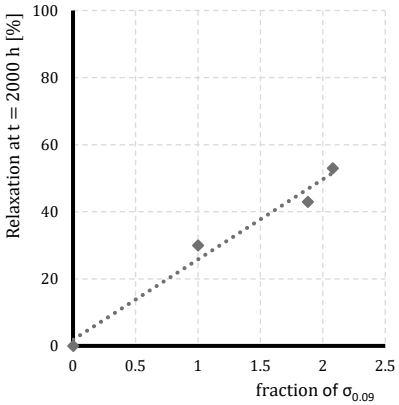

Figure 6.11. Approximated curve drawn from of the average stress levels and relaxation rates from ***Table 6.2***.

f/L	Relaxation (t = 2000 h)	$\lvert\sigma_{avg}\rvert$ [N/mm^2]	Fraction of f/L=0.09
0.09	30 %	9.8	1.00 $\sigma_{0.09}$
0.19	43 %	18.4	1.88 $\sigma_{0.09}$
0.22	53 %	20.4	2.08 $\sigma_{0.09}$

Table 6.2. Average stress values linked to the relaxation graph of **Figure 2.10.**
L = 1 m; t = 3 mm; E = 11500 N/mm^2

In the clamped system, two elements are stressed simultaneously. Their bent shape is a direct result of the internal force equilibrium. Due to the differences in curvature, the bending moment, and therefore the stress, is larger in the top strip. As previously stated, the relaxation rate depends on the amount of stress that is present in an element. The top strip loses relatively more stress in a shorter time span than the bottom strip, resulting in a change in internal force equilibrium. This leads to small changes in the system's shape. In the physical test setup, it was observed that the system elongated over time in the unloaded configuration (**Figure 6.12**). The horizontal elongation u_x was no longer significantly increasing after approximately 2500 hours.

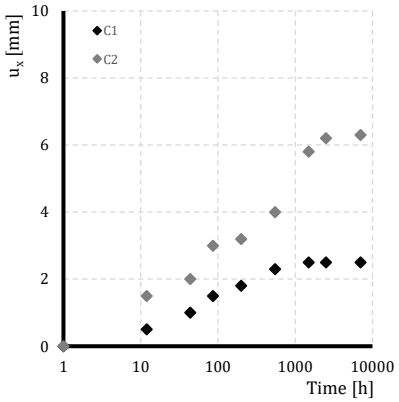

Figure 6.12. Measurements of the horizontal elongation u_x of the unloaded systems C1 and C2 over time

The question that comes to mind is if this unequal relaxation can be simulated numerically. Since the magnitude of the stresses in an element can be controlled with the 'FACL' (= factor of loading) command in SOFiSTiK, it is possible to give different relaxation values to the top and bottom strip. Continuing from the assumption that the relaxation rate is related to the extent of the stresses in the strip, the relaxation values can for instance be chosen with respect to the ratio between the average stresses in both strips (**Table 6.3**). **Table 6.4** shows the elongation for both systems under a constant relaxation value of 50% for one of the strips, and varying values for the other strip. The same kind of horizontal elongation is clearly observed in this simulation, however, since the extension under a given relaxation ratio does not coincide with the stress ratio, a predictive model cannot be made by using this approach.

System	$\lvert\sigma_{avg,bottom}\rvert$ [N/mm²]	$\lvert\sigma_{avg,top}\rvert$ [N/mm²]	*Stress ratio top/bottom*	u_x t=2500h [mm]
C1	9.8	17.0	*1.7*	2.5
C2	15.2	24.3	*1.6*	6.3

Table 6.3. Stress levels and horizontal deformation in time of system C1 and C2

FACL bottom (GRP1)	FACL top (GRP2)	Relaxation bottom	Relaxation top	*Relaxation ratio*	C1 u_x [mm]	C2 u_x [mm]
0.50	0.5	50%	50%	*1.00*	0.0	0.0
0.60	0.5	40%	50%	*1.25*	0.9	2.0
0.70	0.5	30%	50%	*1.67*	1.8	3.9
0.80	0.5	20%	50%	*2.50*	2.7	5.7
0.90	0.5	10%	50%	*5.00*	3.6	7.5
1.00	0.5	0%	50%	∞	4.4	9.3

Table 6.4. Horizontal elongation under different relaxation ratio's

FACL bottom (GRP1)	FACL top (GRP2)	Relaxation bottom	Relaxation top	*Relaxation ratio*	C1 u_x [mm]	C2 u_x [mm]
0.50	0.50	50%	50%	*1.00*	0.0	0.0
0.50	0.40	50%	60%	*1.20*	2.3	2.0
0.50	0.30	50%	70%	*1.40*	4.5	4.0
0.50	0.20	50%	80%	*1.60*	6.6	6.0
0.50	0.10	50%	90%	*1.80*	8.7	7.9
0.50	0.00	50%	100%	*2.00*	10.7	9.9

6.3.2. ITERATIVE APPROACH

The relaxation curves from **Figure 2.10** show that stress-relaxation was most severe in the early stages of the test. This can be explained by the iterative nature of the phenomenon. As soon as the test started, stress starts to fade away. Since the relaxation rate is related to the amount of stress that is present, it can be concluded that the relaxation process slows down due to the lower stress levels in the elements. Furthermore, since changing stress levels have a constant effect on the internal force equilibrium in the clamped model, the relaxation rate is constantly changing. Hence, an iterative relaxation process should be carried out for an accurate simulation. In this process, the stress-relaxation in the bottom layer is set to a constant value. The relaxation in the top layer is given by the ratio between the average stress in the top and bottom layer. The magnitude of stress-relaxation in the top layer at a given time-step becomes:

$$SR_{2,i} = SR_1 \left(\frac{s_{2,i-1}}{s_{1,i-1}}\right), with\ i > 0 \qquad (6.1)$$

In which:

SR_1 Stress-relaxation in the bottom layer
$SR_{2,i}$ Stress-relaxation in the top layer at time-step i
$S_{1,i-1}$ Average stresses in the bottom layer at time-step i-1
$S_{2,i-1}$ Average stresses in the top layer at time-step i-1

After each calculation, s_1 and s_2 should be computed for the newly found equilibrium condition. For both the system C1 as C2, the iterative procedure was carried out, using a constant relaxation in the bottom strip of 10% per time step (**Table 6.5**). In the graphs of **Figure 6.14**, the relaxation behaviour of system C2 is visualised. The horizontal elongation has the same tendency of converging towards a steady state.

The amount of stress relaxation that occurred in the physical systems can be approximated by using the plastically deformed strips (**Figure 6.13**) as the starting geometry in a new form-finding simulation. Comparing the average stress values with the stress values at t = 0, gives an approximation of the amount of stress-relaxation after 7500 hours. From **Table 6.6**, it follows that the total amount of relaxation was approximately equal in systems

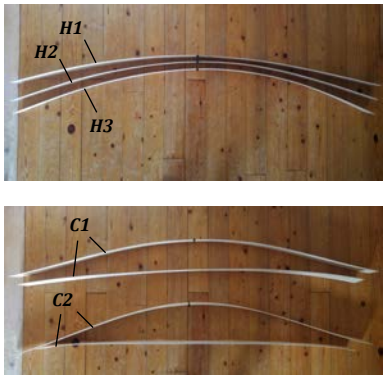

Figure 6.13. The top picture shows the shape of the strips from systems H1-2-3 after 7500 hours of relaxation.
The bottom picture shows the systems C1-2 after 7500 hours of relaxation.

H1-2-3. Furthermore, the relaxation in systems C1-2 have a value that roughly correlates with time step 3 in the iterative process. To visualise the effect of the stress-relaxation on the stiffness, the load-displacement graph at this time step is given in **Figure 6.15**.

Table 6.5. *Iterative relaxation process*

System C1

Time Step	**0**	**1**	**2**	**3**	**4**	**5**	**6**	**7**	**8**	**9**	**10**	**11**	**12**	**13**	**14**	**15**
s_1 [N/mm^2]	9.6	8.5	7.4	6.6	5.8	5.2	4.6	4.1	3.6	3.2	2.9	2.6	2.3	2.0	1.8	1.6
s_2 [N/mm^2]	17.0	14.2	11.9	10.1	8.7	7.4	6.4	5.6	4.9	4.2	3.7	3.2	2.9	2.5	2.2	2.0
s_2/s_1	1.77	1.67	1.61	1.53	1.50	1.42	1.39	1.37	1.36	1.31	1.28	1.23	1.26	1.25	1.22	1.25
SR_1 [%]	0.0	10.0	10.0	10.0	10.0	10.0	10.0	10.0	10.0	10.0	10.0	10.0	10.0	10.0	10.0	10.0
SR_2 [%]	0.0	17.7	16.7	16.1	15.3	15.0	14.2	13.9	13.7	13.6	13.1	12.8	12.3	12.6	12.5	12.2
$SR_{1,total}$ [%]	0	11	23	31	40	46	52	57	63	67	70	73	76	79	81	83
$SR_{2,total}$ [%]	0	16	30	41	49	56	62	67	71	75	78	81	83	85	87	88
u_x [mm]	***0.0***	***0.7***	***1.3***	***1.7***	***2.1***	***2.4***	***2.6***	***2.8***	***3.0***	***3.1***	***3.2***	***3.3***	***3.4***	***3.5***	***3.5***	***3.6***

System C2

Time Step	**0**	**1**	**2**	**3**	**4**	**5**	**6**	**7**	**8**	**9**	**10**	**11**	**12**	**13**	**14**	**15**
s_1 [N/mm^2]	15.2	13.4	11.8	10.4	9.3	8.2	7.3	6.5	5.8	5.1	4.6	4.1	3.6	3.3	2.9	2.6
s_2 [N/mm^2]	24.3	20.6	17.6	15.1	13.0	11.3	9.8	8.6	7.5	6.6	5.8	5.1	4.5	3.9	3.5	3.1
s_2/s_1	1.60	1.54	1.49	1.45	1.40	1.38	1.34	1.32	1.29	1.29	1.26	1.24	1.25	1.18	1.21	1.19
SR_1 [%]	0.0	10.0	10.0	10.0	10.0	10.0	10.0	10.0	10.0	10.0	10.0	10.0	10.0	10.0	10.0	10.0
SR_2 [%]	0.0	16.0	15.4	14.9	14.5	14.0	13.8	13.4	13.2	12.9	12.9	12.6	12.4	12.5	11.8	12.1
$SR_{1,total}$ [%]	0	12	22	32	39	46	52	57	62	66	70	73	76	78	81	83
$SR_{2,total}$ [%]	0	15	28	38	47	53	60	65	69	73	76	79	81	84	86	87
u_x [mm]	***0***	***1.2***	***2.1***	***2.8***	***3.5***	***4***	***4.4***	***4.8***	***5.1***	***5.3***	***5.5***	***5.7***	***5.8***	***6***	***6.1***	***6.2***

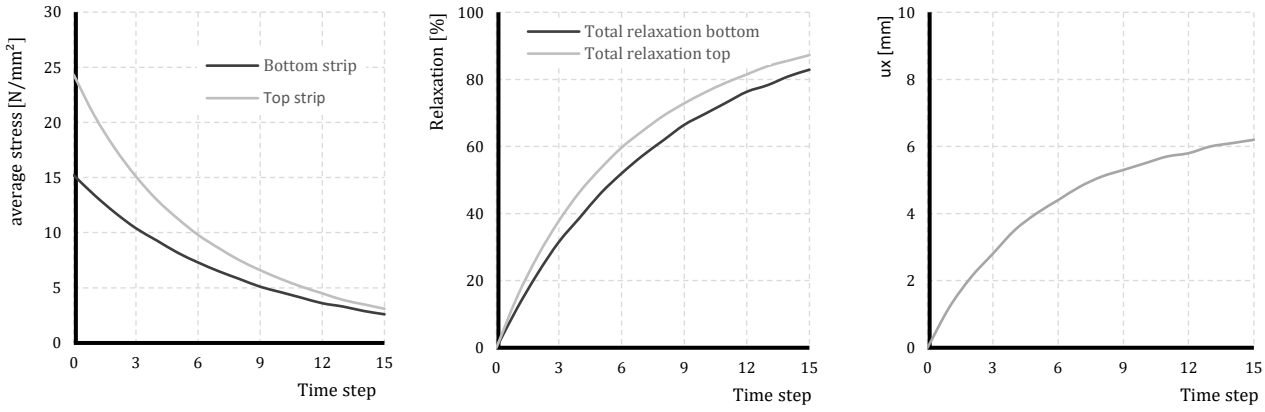

Figure 6.14. Relaxation behaviour of system C2

System		$\|\sigma_{avg}\|$ t=0 [N/mm²]	$\|\sigma_{avg}\|$ t=7500 h [N/mm²]	Relaxation t=7500 h [%]
H1		12.6	7.6	40
H2		18.2	10.6	42
H3		22.5	13.5	40
C1	bottom	9.6	6.2	35
	top	17	10	41
C2	bottom	15.2	11.2	26
	top	24.3	14.6	40

Table 6.6. Stress relaxation in the physical models after 7500 hours.

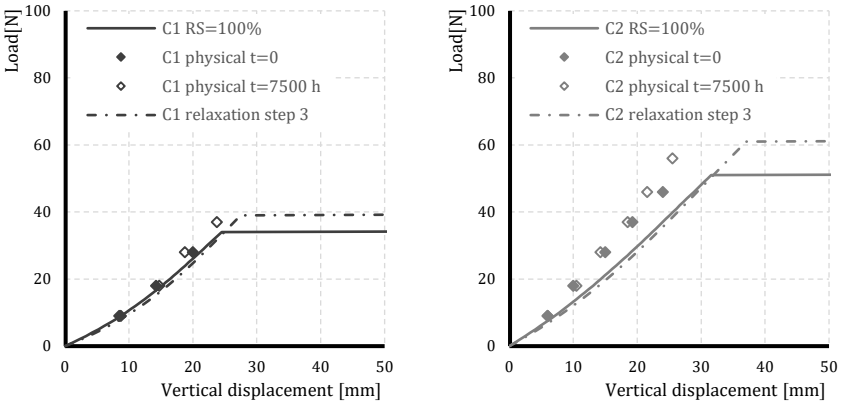

Figure 6.15. Load displacement curves of system C1 (left) and C2 (right), compared with the iterative relaxation step 3. The numerical simulations show the same behaviour as the physical tests. Iteration step 3 therefore roughly correlates with relaxation after 7500 hours.

6.3.3. CONCLUDING REMARKS

The main purpose of these simple load tests was to gain confidence in the numerical simulation method. The tests show that the structural behaviour of the systems can be approached fairly accurately. Also stress-relaxation can be simulated to a certain extent, although the simulated elongation did not yet match the physical measurements. The elongation does, however, show the same tendency of converging towards a steady state. The error might be explained by two assumptions that were made in the iterative process.

First, it was assumed that the stress-relaxation is the same over the entire length of the element. In reality, however, the stresses in an element vary greatly, resulting in different relaxation rates throughout the element. To be precise, an iterative process for this local stress-relaxation should also be adopted.

The second assumption was that the relation between the relaxation rate and the stresses in the element is linear. This assumption was made from an interpretation of the relaxation tests from Lienhard (2014). Further experimental research is needed that would give a better understanding about the speed and severity of stress-relaxation in bending-active timber structures.

Furthermore, a smaller step size for the relaxation increments might increase the accuracy of the analysis. At this point, the iterative relaxation simulation is quite labour intensive. Stress levels have to be read and processed manually for each time-step and the relaxation values are computed accordingly. A numerical loop could be used to automate the process. This asks for an automated interpretation of the calculation results and a variable input for the 'FACL' command, what might be possible in SOFiSTiK with the right set of programming skills. This research, however, only aimed to highlight this phenomenon and will not go deeper into developing such a automated relaxation program.

7. A MODULAR SYSTEM

7.1. INTRODUCTION

It is still a large step to get from these simple basic systems to a fully working large scale bending-active solution. Although, all the case-study projects presented in the reference section (**Annex A**) show very innovative, and sometimes ground-breaking principles, most of them are still far away from an application in a 'real' structure. However, a lot can be learned from studying the principles on which they are designed and built. This reference study has resulted in the following design principles, which will be further elaborated in the next section.

- Simplicity of design
- 3D configuration to improve stability
- Closed modules for better handling on site
- Use orthotropic timber properties
- Vertical connection to improve structural qualities
- Adequate structural behaviour through time

This chapter proposes the design of an actively-bent timber roof system that shows potential to be used as a long-span solution in a building structure.

7.2. DESIGN CONSIDERATIONS

When bending timber for the design of a long-lasting load-carrying structure, the effect of stress-relaxation should always be taken into account. In an ideal scenario, the structural qualities would improve when the stresses perish. The advantageous stress-stiffening effects caused by the tension stresses should be neglected, because this stiffening effect will fade away over time. The principle of active bending is therefore primarily used to develop a curved system that finds its structural qualities from the geometry.

In the previous chapter, the effect of the relaxation on the simple systems was discussed. From this, we have seen that the predominant compressive stresses in the hinged system improve the structural qualities over time. The clamped system retains roughly the same stiffness, but increases in ultimate load after relaxation. These simple systems can be used as a starting point when designing an actively bent structure. The ICD/ITKE 2010 research pavilion, for instance, is based on a multiplication of the basic hinged system. As explained in **Chapter 3**, the integrity of these structures is often determined by the geometry. Strategic positioning of weak points (**Figure 7.1**) and the use of (double) curvature are crucial to obtain sufficient stiffness.

This research focuses on the clamped system as a starting point for the design of a roof structure. The system is stable by itself and does not rely on an auxiliary structure to retain its bent shape. This

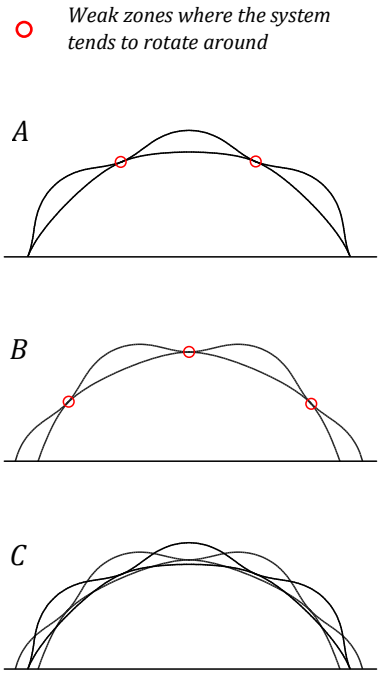

Figure 7.1. The weak links at the coupling between two clamped systems can altered in the adjacent section (A & B). Together they form a stable system (C).

offers the possibility for a unit based system, what improves the handling of the forces necessary for bending during construction since the units can be pre-bent prior to assembly. The structural qualities of these bending-active units, by themselves, can be greatly improved with simple enhancements (**Figure 7.2**).

First of all, the plate thickness is restricted by the desired amount of curvature. The thickness should, however, be as high as possible to gain the maximum amount of rigidity. Secondly, struts can be added to create a coupling between the plates. The length of these struts can be increased to develop structural height in the system, resulting in increased prestress. Thirdly, a shear connection can be made that makes the system behave as a truss. In the clamped system, a shear connection is already present where the plates are joined. Contrary to using diagonals, a shear connection in the middle can for instance be made through lateral couplings. At last, an additional layer can be added on top of the previous layer. Again, shear connections between these layers should be present to fully utilise the newly attained plate thickness. This last option, however, should only be used as a last resort, since it doubles the amount of material and asks for a lot of additional fasteners. **Figure 7.4** shows the improvements in load-carrying behaviour that can be made to system C2 by adding bar elements.

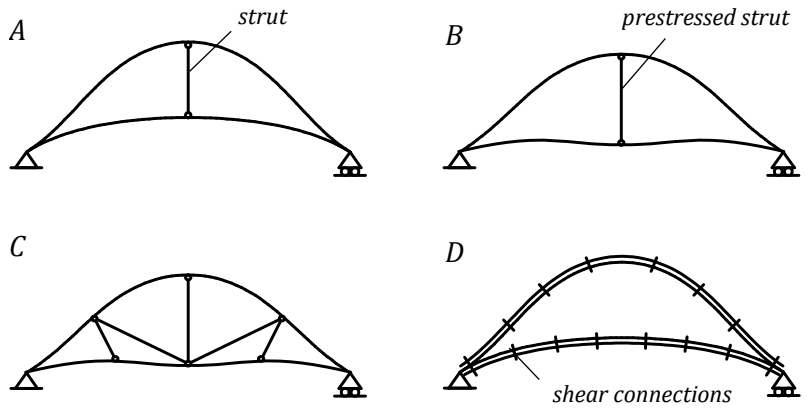

Figure 7.2. *Methods to strengthen the basic clamped system: A) with a single strut; B) with a single prestressed strut; C) by creating a truss; D) by adding an extra layer.*

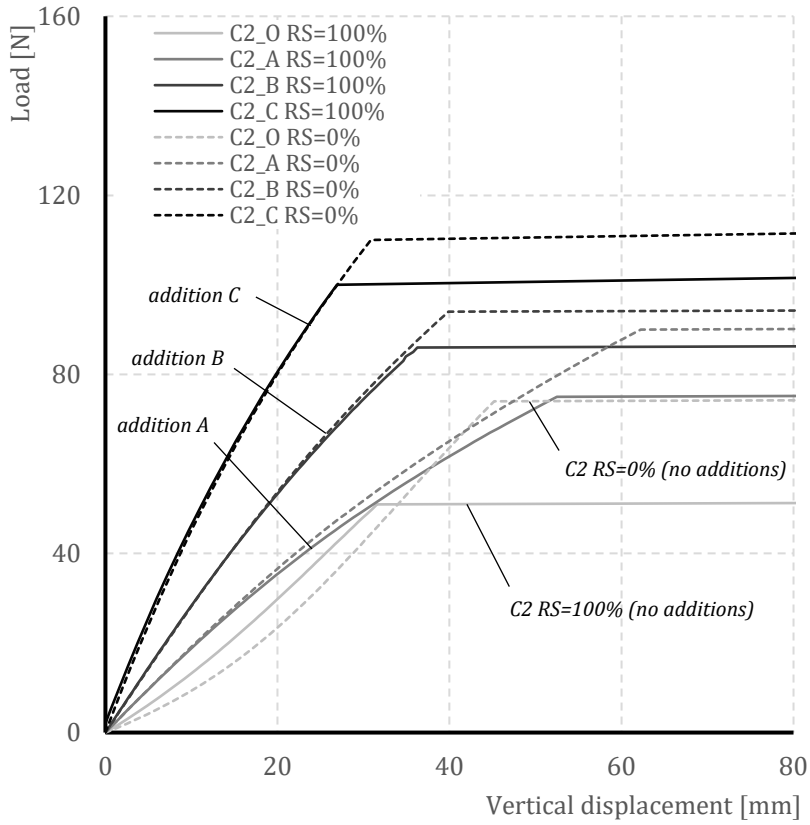

Figure 7.4. Load-displacement graphs of the original system C2 with no additions (O) compared to the enhancements (A, B & C) from ***Figure 7.2*** for a central point load.

7.3.A 3D MODULE

Following the design principles outlined in the previous paragraph, a unit based system has been developed. The unit shows similarity with the simple clamped system. However, a connection is made in two directions. This results in an extra shear connection halfway through the unit. The difference in Young's moduli for the longitudinal and lateral plate directions result in different allowable curvatures. The stiffness in the lateral direction is lower and the plate length can therefore be smaller. The height of the system is determined by struts that connect both plates and drastically increase the stiffness. **Figure 7.5** shows both the flat as the bent geometry. Some of the most important input and output parameters are given in the drawing.

The units are combined to form an arched structure (**Figure 7.8**), where every end-point is supported by the midpoint of a neighbouring unit. This stabilises the weak connections in the longitudinal cross-section. The design of the unit defines the shape of the arch. **Figure 7.6** gives the relation between the unit's angle with the ground plane α, the unit length L_0 and the length of the connection $L_{c,0}$ with the arches radius R. The modular approach maximises efficiency in fabrication, ease of construction and simplicity in the design phase. Structural detailing can be kept to one standard.

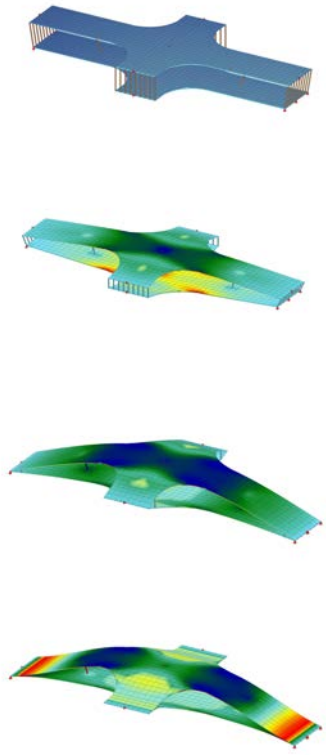

Figure 7.3. Form-finding of the unit, from flat to bent, and stress build-up. The red and blue zones indicate the locations with the highest amount of stress.

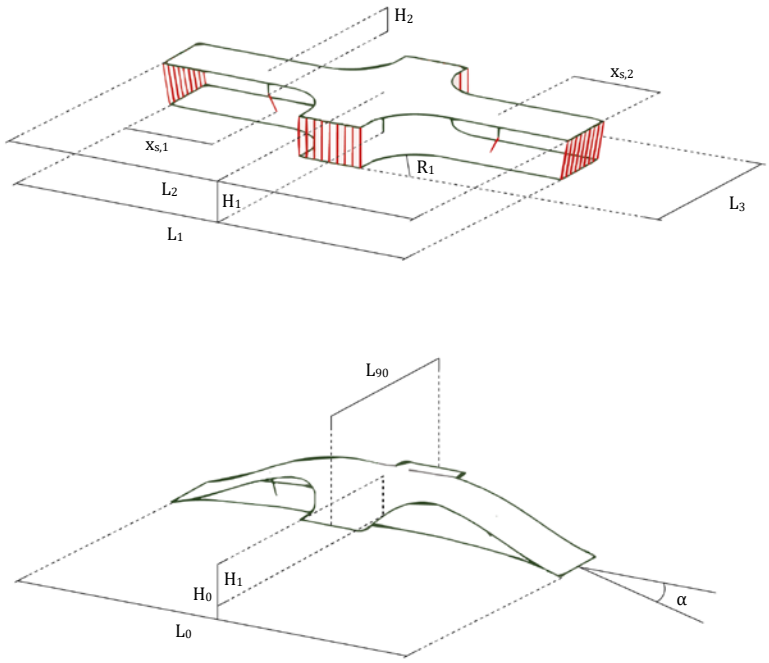

Figure 7.5. Input and output parameters of the unit

The form-finding process of the unit is similar to the form-finding of the two-dimensional clamped system (**Figure 7.3**). Two form-finding jobs are programmed into SOFiSTiK, where the first job contract the outer set of cables, and the second job contracts the inner set of cables, resulting in a parallel plate alignment. The accuracy of the form-finding is tested with an image overlay. **Figure 7.7** shows a picture of a physical model of the bending-active unit. The blue lines represent the form-found geometry. The virtual geometry follows the same curvature as the physical model. It can therefore be assumed that the simulations give an accurate representation of the real bent shape.

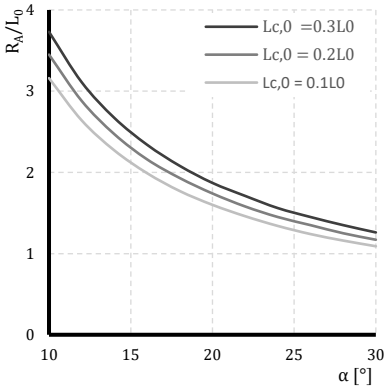

Figure 7.6. The radius of the arch depends on the angle α, the unit length L_0 and the length of the connection $L_{c,0}$.

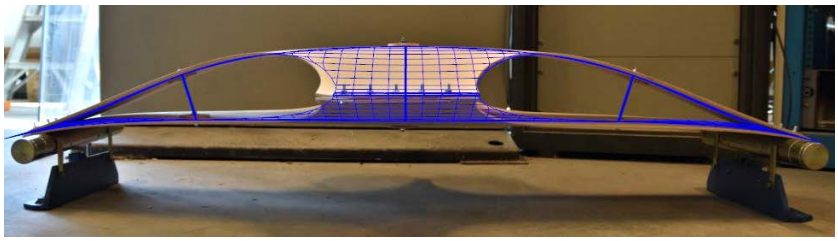

Figure 7.7. The form found geometry gives an accurate representation of the real bent shape

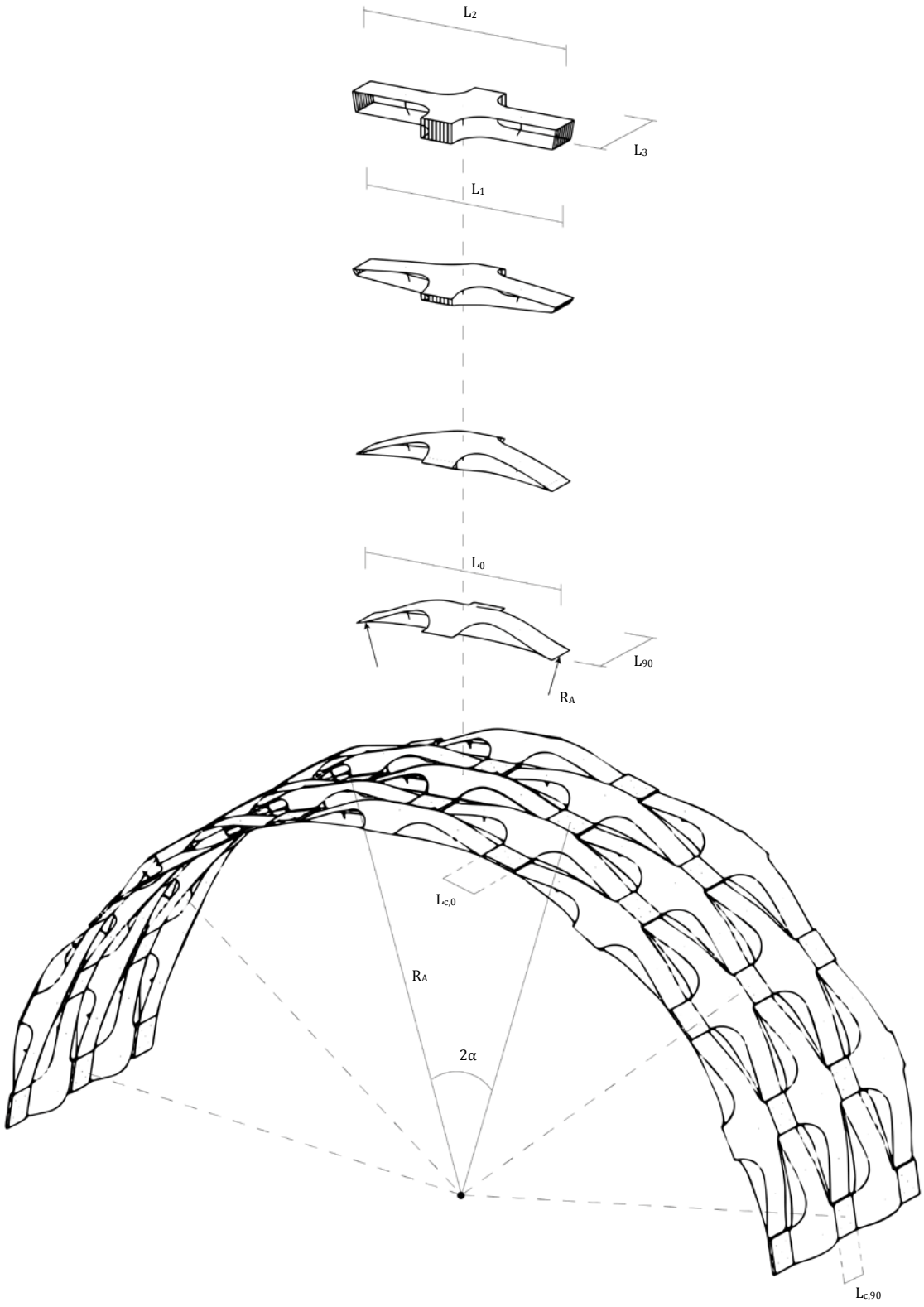

Figure 7.8. Multiple units form an arch

7.4. PARAMETER STUDY

Small alterations in the dimensions of an element can already have a huge impact on the geometry and the behaviour of the structure. This paragraph focuses solely on the influence of the dimensional parameters on the geometry. It is assumed that the material will not fail under the imposed curvatures. The structural behaviour will be discussed in the next section. The parameters are described as *input* and *output parameters*. The input parameters contain all the dimensions of the initial flat geometry prior to bending. The output parameters describe the dimensions of the unit in its bend state. All the parameters are listed in **Table 7.1**.

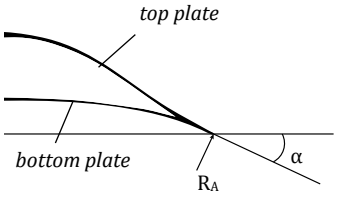

Figure 7.9. The angle of the unit with the ground plane is indicated by α, which determines the arch radius R_A.

Table 7.1. Input and output parameters. See **Figure 7.5** and **Figure 7.8** for a visual representation.

INPUT PARAMETERS		OUTPUT PARAMETERS	
$E_{m,0}/E_{m,90}$	Ratio between the orthogonal flexural moduli	L_0	Length of the unit in longitudinal direction
t	Plate thickness	L_{90}	Length of the unit in lateral direction
L_1	Longitudinal length of the bottom plate	α	Angle between the strips and the ground plane
L_2	Longitudinal length of the top plate	H_0	Height of the unit from the ground plane
L_3	Lateral length of the top and bottom plate	H_1	Height of the central strut
$R_{1/2}$	Radii of the corner	H_2	Height of the side struts
H_1	Height of the central strut	R_A	Arch radius
H_2	Height of the side struts	t_{con}	Thickness of the connection
$x_{S,1}$	Strut distance from centre on bottom plate		
$x_{S,2}$	Strut distance from centre on top plate		
$L_{c,0}$	Connection length in longitudinal direction		
$L_{c,90}$	Connection length in lateral direction		

Table 7.2. Parameter domain and coding method, e.g. an L_2/L_1 ratio of 1.04 is described as A104.

PARAMETER	DOMAIN	CODE
Longitudinal plate length ratio (L_2/L_1)	1.02 – 1.10	A102 - A110
Lateral plate length ratio (L_3/L_1)	0.45 – 0.55	B45 – B55
Elongation of the central strut	0% – 80%	M0 – M80

7.4.1. INFLUENCE OF THE PARAMETERS ON FINAL GEOMETRY

The dimensions of the arch are determined by the parameters L_0, $L_{c,0}$ and α, which are indicated in **Figure 7.8**. The unit length L_0 only fluctuates very little if L_1 is held constant and other parameters are varied. For $\alpha < 30°$, this parameter is assumed to be constant. **Figure 7.6** shows the relation between α and the arch radius R_A. The connection length $L_{c,0}$ is held constant during the analysis. This means that the angle α will almost solely determine the form of the geometry. In the following paragraphs, the effect of the different input parameters on α will be elaborated. The units were build-up step by step, starting with the influence of the longitudinal plate lengths, following with the lateral plate lengths, then the central struts and finally the struts at the side. The parameters that were varied for this analysis are listed in **Table 7.2**. This table also shows the coding method that will be used to describe the systems.

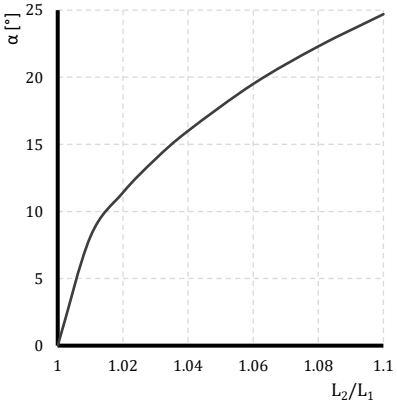

Figure 7.10. Influence of the longitudinal plate length ratio L_2/L_1 on α.

7.4.2. *INFLUENCE OF THE LONGITUDINAL PLATE LENGTHS*

By increasing the ratio between the lengths of the top and the bottom plate (L_2/L_1), the curvature in the plates increases. Consequently, the height and the angle of the system both increase. **Figure 7.10** shows how α is related to difference in plate lengths.

7.4.3. *INFLUENCE OF THE LATERAL PLATE CONNECTION*

The connection of the lateral plates account for stability of the system. The central shear connection also increases the angle α. For a longitudinal plate length ratio between 1.03 and 1.08, which a very common ratio's for this system, the change in α is very accurately related to the ratio between the lateral plate length L_3/L_1 and the longitudinal plate length ratio L_2/L_1, which is the ratio L_3/L_2. The increase in α can therefore accurately be predicted using **Figure 7.11**. For this analysis, the E_0/E_{90} ratio was chosen to be 10. If this ratio is lowered, stiffness in the lateral direction increases, what further increases α.

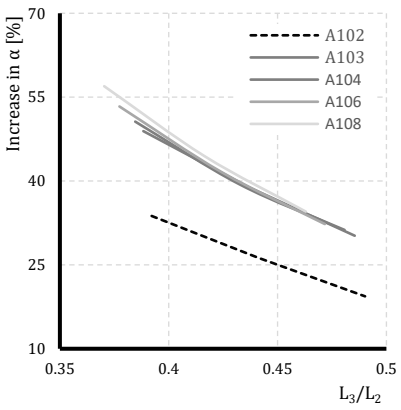

Figure 7.11. Influence of the lateral plate length on the increase in α.

$$\frac{L_3/L_1}{L_2/L_1} = L_3/L_2$$

7.4.4. *INFLUENCE OF THE CENTRAL STRUT*

For a lateral plate length ratio of 0.45, **Figure 7.12** shows how the longitudinal plate length ratio influences the structural height of the unit. The stiffness of the system can be improved significantly by the addition of a strut to connect the midpoint of the top and bottom plates. When the strut length is increased, it pushes both plates outwards. The bottom plate is the least resistant to this load and deforms the most. **Figure 7.14** shows how the systems A103 and A105 deform when the strut length is increased by a percentage of 20 and 40. The total height of the system slightly decreases and α becomes smaller (**Figure 7.13).** The addition of the strut gives more dimensional control over the system because it gives a fixed distance between the two plates. By altering this distance, small changes in curvature can be made to the arch.

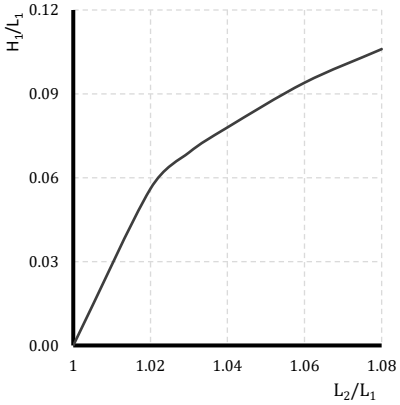

Figure 7.12. Influence of the longitudinal plate length ratio on the structural height for B45

7.4.5. *INFLUENCE OF THE SIDE STRUTS*

Although some minor geometric alterations can be made by altering the length of the side struts, their main contribution comes to the stability of the system. They prevent the top plate from buckling under an external load, while at the same time, they improve the stiffness near the support. Their location should be

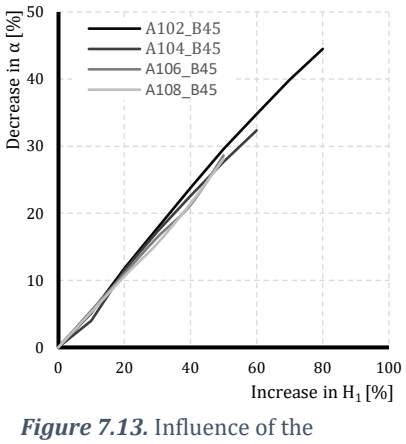

Figure 7.13. Influence of the increase in central strut length on the decrease in α for $L_3/L_1 = 0.45$

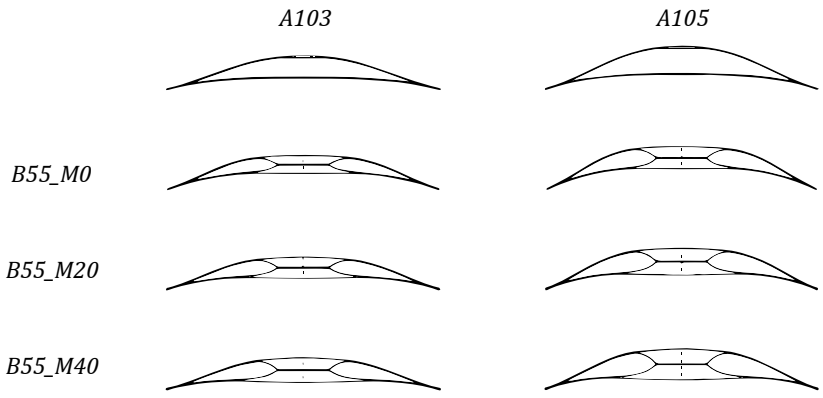

Figure 7.14. Systems A103 (left) and A105 (right) with varying central strut lengths

chosen, so it sufficiently stabilises the system at both sides of the strut. This will be discussed in the next section.

7.4.6. STRUCTURAL ANALYSIS

In addition to the direct effect that the parameters have on the geometry, they also have a large effect on the structural behaviour of the system. The influence of the geometrical parameters on the stiffness and strength was analysed for the systems of **Figure 7.14**. The position and length of the struts were altered according to **Figure 7.15**. **Table 7.3** gives an overview of all the parameters that were varied for the analysis. The combination of the variables led to the analysis of 54 different models in total, that could be modelled fairly quickly due to the parametric input in SOFiSTiK. Every model is named by a code, e.g. A103_M20_S03-20.

PARAMETER	VALUES	CODE
Length of the bottom plate (L_1)	1.0 m	-
Longitudinal plate length ratio (L_2/L_1)	1.03; 1.05	A103; A105
Lateral plate length ratio (L_3/L_1)	0.45	B45 (excluded from model name)
Elongation of the mid strut	0%; 20%; 40%	M0; M20; M40
Position of side struts from support	0.3 * $L_1/2$ 0.4 * $L_1/2$ 0.5 * $L_1/2$	S03 S04 S05
Elongation of side struts	*For A103:* 0%; 20%; -20% *For A105:* 0%; 10%; -10%	*For A103:* S…-0; S…+20; S…-20 *For A105:* S…-0; S…+10; S…-10

Table 7.3. Varying parameters for stiffness analysis. For the analysis a constant value of 1.0m is chosen for L_1.

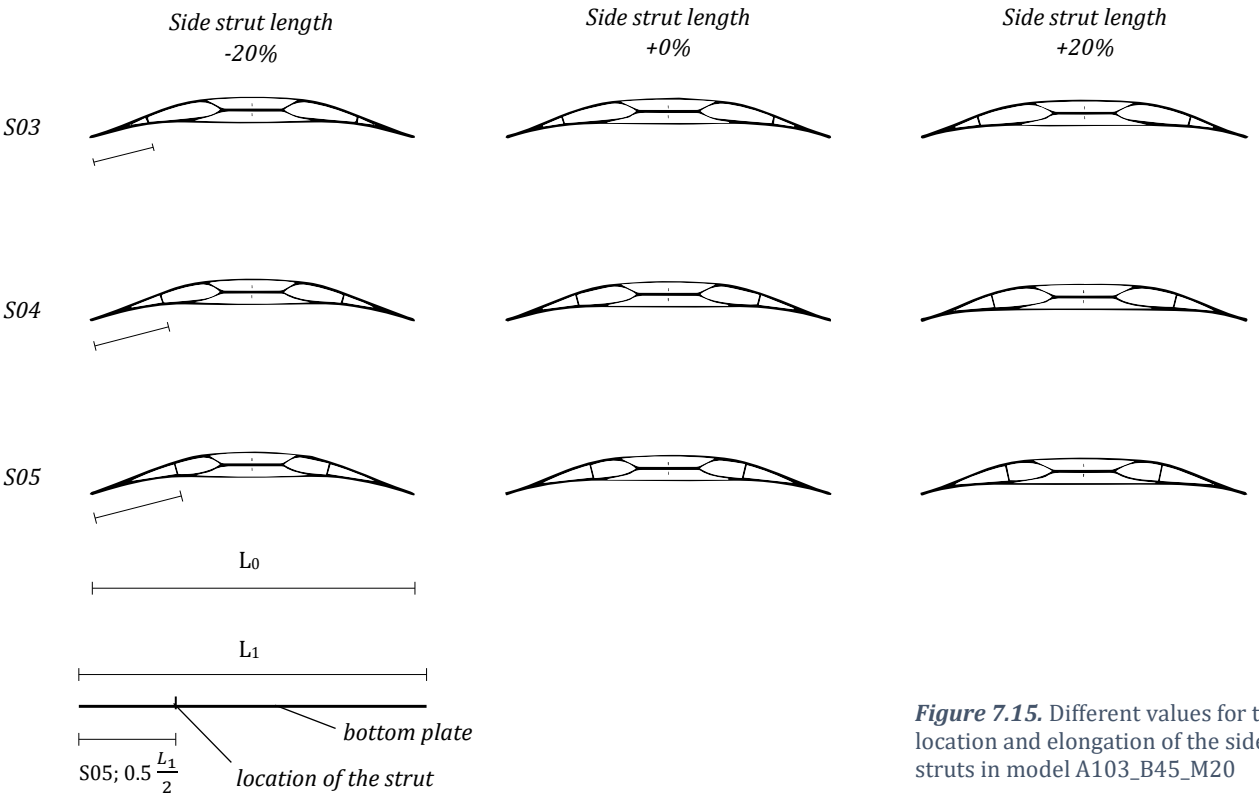

Figure 7.15. Different values for the location and elongation of the side struts in model A103_B45_M20

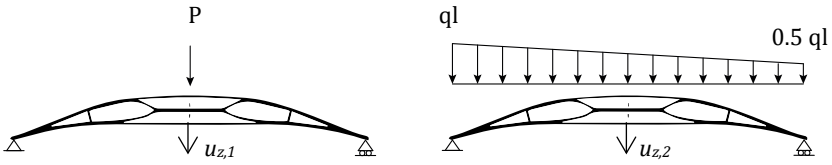

Load case 1 *Load case 2*

Figure 7.16. Load cases for stiffness analysis

The systems are tested for two different load cases (LC) (**Figure 7.16**). LC 1 is a central point and LC 2 a variable line load, where the largest part of the load is applied to the weakest part of the system near the support. A hinged and a roller support are modelled as boundary conditions. Further properties of the model are given below:

- E_0 = 10,000 N/mm^2
- E_{90} = 1,000 N/mm^2
- t = 3mm
- Step size LC1 is 0.1 kN
- Step size LC2 is 0.2 kN/m

For each load case, the maximum load and the displacement at the centre ($L_0/2$) were measured. A stiffness factor k is calculated for both load cases from the load and vertical displacement u_z in the first load step by:

$$k_1 = \frac{P}{u_{z,1}}; k_2 = \frac{0.75ql}{u_{z,2}} \quad (7.1)$$

The mean values of the results are given in **Table 7.4**. The deviation from this mean value is calculated and averaged for both load cases and is indicated with a maximum load factor F_{max} and a stiffness factor K. The results are given in **Table 7.5**. A value of 1.0 means that the factor correlates with the average results from **Table 7.4**. Higher values are therefore preferred. For every system n, the values for F_{max} and K are computed using:

$$F_{max} = \frac{1}{2}\left(\frac{P_{max,n}}{P_{max,mean}} + \frac{ql_{max,n}}{ql_{max,mean}}\right) \quad (7.2)$$

$$K = \frac{1}{2}\left(\frac{k_{1,n}}{k_{1,mean}} + \frac{k_{2,n}}{k_{2,mean}}\right) \quad (7.3)$$

A full overview of the results is given in the **Annex C.** The main conclusions of the analysis are stated below:

- The systems with a longitudinal plate length ratio of 1.05 all behave stiffer and have significantly higher failure loads than their 1.03 equivalents.
- By increasing the length of the central strut, the stiffness is greatly increased. The stiffness can be more than doubled when the length is increased by 40%.
- Moving the side struts to the supports creates a more favourable system for a divided load. The system is better

Table 7.4. Mean values of the results from **Annex C**.

		Mean value
LC1	P_{max} [kN]	0.5
	k_1 [N/mm]	24.9
LC2	ql_{max} [kN/m]	0.7
	k_2 [N/mm]	36.5

in resisting the part of the load that covers the plates near the support.

- By moving the side struts to the centre, the moment resistance of the system around the centre is increased and the system becomes more favourable to resist a central point load.
- The most optimal strut location for both load cases is therefore halfway through the plate.
- Decreasing the lengths of the side struts always results in less favourable geometries to resist divided loads. For some cases, however, the system's geometry becomes better in resisting a central point load (A103_M0_S03 – A105_M(0-20)_S05)
- Increasing the lengths of the side struts always resulted in more favourable geometries to resist divided loads. This is explained by the stiffening of the plates near the supports.

A103		S03			S04			S05		
		-20	0	+20	-20	0	+20	-20	0	+20
M0	F_{max}	0.70	0.84	0.75	0.56	0.56	0.70	0.70	0.75	0.79
	K	0.45	0.36	0.35	0.37	0.58	0.68	0.56	0.82	0.69
M20	F_{max}	0.79	0.93	1.07	0.65	0.75	0.93	0.42	1.02	0.89
	K	0.46	0.63	0.82	0.56	0.97	1.13	0.80	1.15	1.07
M40	F_{max}	0.89	1.12	1.40	0.65	0.89	1.12	0.42	0.75	1.07
	K	0.71	0.95	1.29	0.77	1.27	1.53	0.90	1.43	1.76
A105		S03			S04			S05		
		-10	0	+10	-10	0	+10	-10	0	+10
M0	F_{max}	0.98	0.98	0.98	0.79	0.93	0.93	1.16	1.07	1.12
	K	0.35	0.40	0.45	0.58	0.68	0.73	0.83	0.95	0.89
M20	F_{max}	1.17	1.31	1.45	0.98	1.12	1.12	1.35	1.35	1.30
	K	0.61	0.73	0.83	0.97	1.23	1.37	1.30	1.40	1.23
M40	F_{max}	1.35	1.35	1.49	0.98	1.35	1.45	0.98	1.35	1.49
	K	0.90	1.10	1.33	1.20	1.58	1.73	1.56	1.72	1.78

Table 7.5. Deviation from the average result. A value of 1.00 means that the response to LC1 and LC2 for the system is corresponding with the average results.

7.4.7. INFLUENCE OF THE MATERIAL AND THICKNESS

In general, it was noticed that the systems where the plates were stressed to the largest extend, often possessed the most favourable structural qualities. The additional structural height and curvature increase the stiffness of these systems. The material should, however, allow these levels of curvature to exist without developing fractures. At the same time, the used material should always be sufficiently stressed to improve the structural height and reach the highest possible structural qualities that can be achieved with a certain plate thickness. Relatively thicker plates can therefore be used for units with a smaller curvature. **Figure 7.17** gives the relation between the stress development in a unit

when the longitudinal plate length ratio increases. This relation is almost linear. Equation (2.2-2.4) explain that the bending stress has a linear relation with the cross-sectional height h, which is restated in equation (7.4). The stress build-up in the units can therefore be predicted with some accuracy. Increasing the central strut length did not result in higher average stresses, however, peak stresses were increased that should be taken into consideration.

$$\sigma_M = \frac{E \cdot h}{2 \cdot r} \qquad (7.4)$$

When designing an arch that has a certain radius, it is the question if either more structural height, or a thicker plate is favourable. A comparison was made between two models with different longitudinal plate length ratio's, resulting in different curvatures and heights. The models that were compared are given in **Figure 7.18**. They have approximately equal values for α, so they result in the same arch radius. The average and peak stresses in the 3mm and 4mm model are roughly the same, so a fair comparison can be made. **Figure 7.19** shows that the A103_..._4mm model had a better load-carrying ability than the A105_..._3mm model.

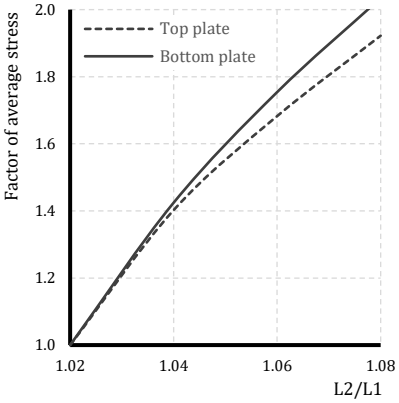

Figure 7.17. Development of average stresses with increasing longitudinal plate ratio's. The lateral plate length ratio is 0.45. The average stresses for L_2/L_1 are normalised to be 1.0.

A103_M20_S03-0
α = 17°
t = 4mm

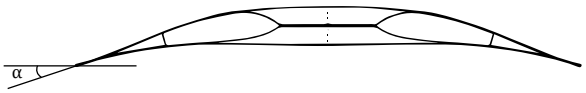

A105_M40_S03+10
α = 18°
t = 3mm

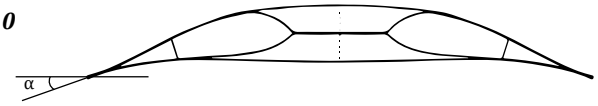

Figure 7.18. Two models with different plate thickness for comparison.

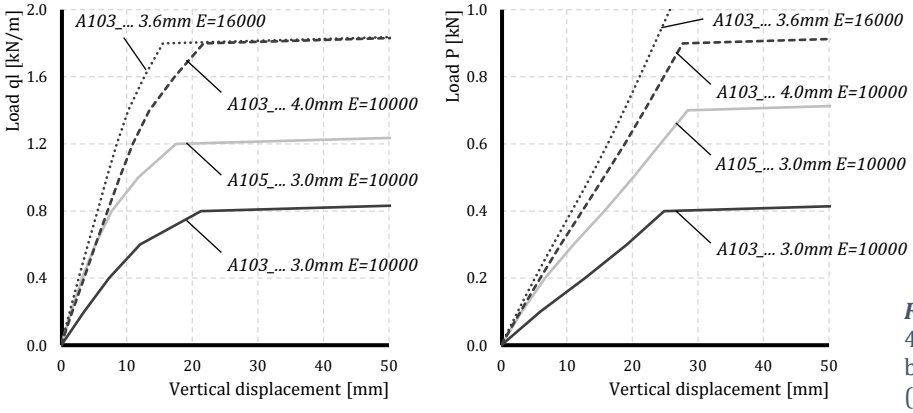

Figure 7.19. The models where 4mm plates were used show better performance for both LC1 (left) as LC2 (right).

In this example, however, it was assumed that the mechanical properties remained constant with increasing plate thicknesses. In reality, finding the right balance between plate thickness and the chosen dimensional parameters can be quite tricky. For off-the shelf plywood plates, the mechanical properties differ quite a lot

when the thickness increases, because the E_0/E_{90} ratio changes with the addition of layers. In the case of the 4 mm plate, the additional thickness is provided for by using thicker veneers for the two outer layers. These outer layers have the main contribution to the longitudinal bending stiffness. E_0 is therefore higher, i.e. 16,000 N/mm^2. When the plate thickness is increased further, additional veneer layers are added in a cross-wise fashion, what increases the contribution to the bending stiffness perpendicular to the grain direction. The mean thickness of these plates is 3.6 mm. The load-carrying behaviour for these material properties is also given in **Figure 7.19**.

The previous sections show that the geometrical and structural design of the system are very closely related to each other. The material properties are exhausted by stressing the plywood to its limits to find geometrically efficient shapes, where small dimensional alterations to the flat plate configurations can have a significant effect on the geometry and load-carrying behaviour.

7.5. COMBINING THE MODULES

The numerical form-finding of a single unit can be done in a rather fast and controlled manner. However, when multiple units are bent simultaneously, some problems occur in the simulation. Undesired movements of the plates can no longer be sufficiently restricted during bending. This results in kinetic mechanisms that cannot be solved in a finite element analysis. Although, the form-finding of an arch where two units are linked in the longitudinal direction was accomplished after a painful and slow modelling process (**Figure 7.21**). Analysis of this arch for three different load cases, shows that the system behaves somewhat stiffer in the fully stressed configuration compared to the fully relaxed model (**Figure 7.22**). Taking into account that the system is based on a repeating unit, the question arises if it is really necessary to form-find the whole system. Perhaps a simplification of the system can be made that would give an accurate lower-bound calculation of the stiffness of the arch with several combined units. This section briefly describes two methods.

The system can be simplified as a line model with one-dimensional beam elements. Rhino uses NURBS curves that accurately describe the shape of a bent curve with only a few control points. In this way, a single unit can be drawn according to **Figure 7.20**, that can easily be multiplicated to form a barrel vault. In this way, a completely automated optimisation process could be developed using Karamba for FEA. From an in-depth investigation it was concluded that this simplification by 1D beam elements did not result in satisfying results for varying dimensional parameters, what made the tool not very reliable.

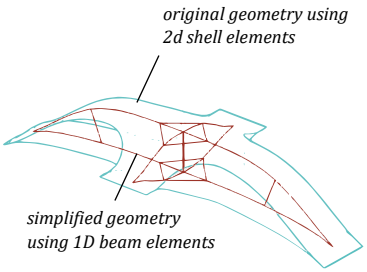

Figure 7.20. Simplification of the geometry by 1D beam elements.

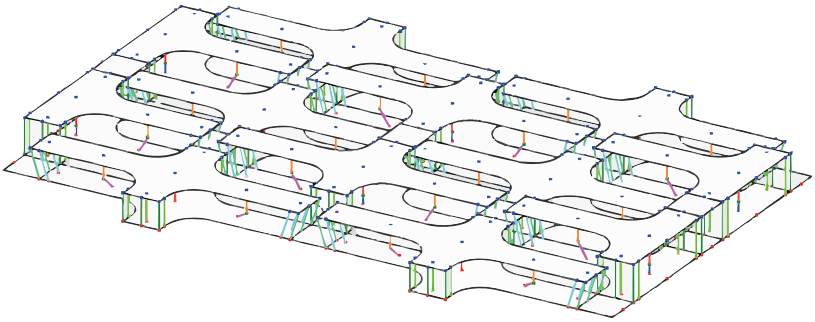

Flat geometry is drawn in Rhino. The contracting cables are blue, green and purple coloured.

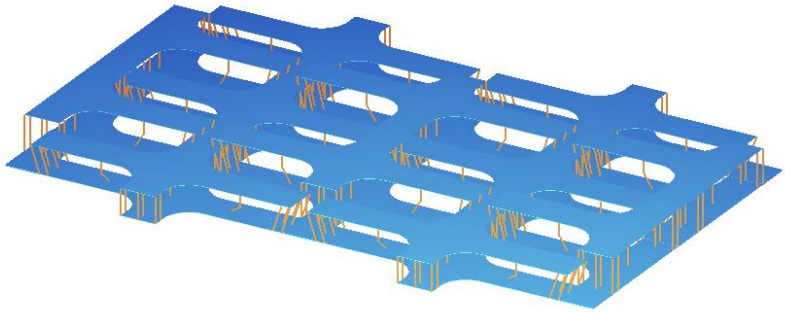

The geometry is imported to SOFiSTiK.

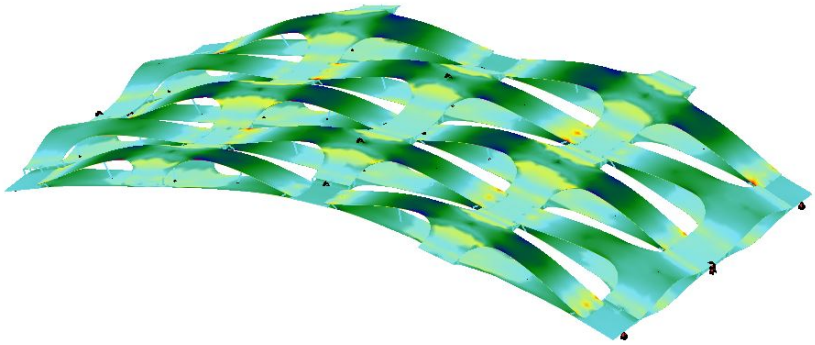

The cables are all contracted at once. The colours show the stress build-up in the top of the plate elements.

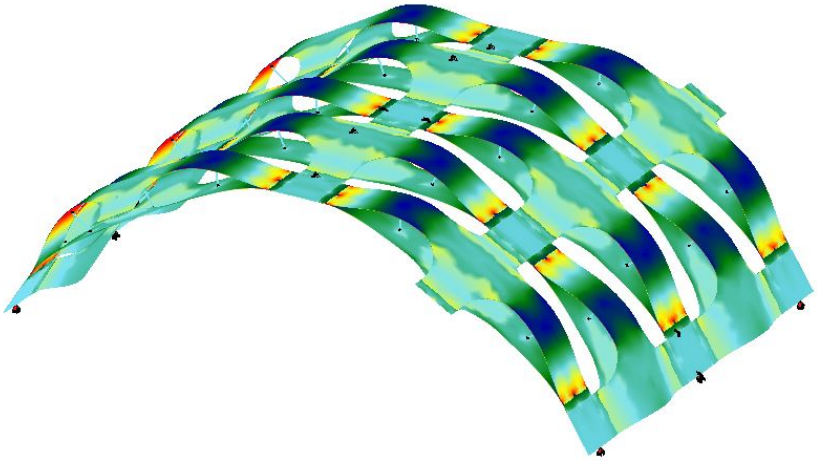

When the form-finding simulation is finished, the plates are connected by setting kinematic constraints to the nodes of the top and bottom plates.

Figure 7.21. Form-finding of the arch with two units linked in the longitudinal direction.

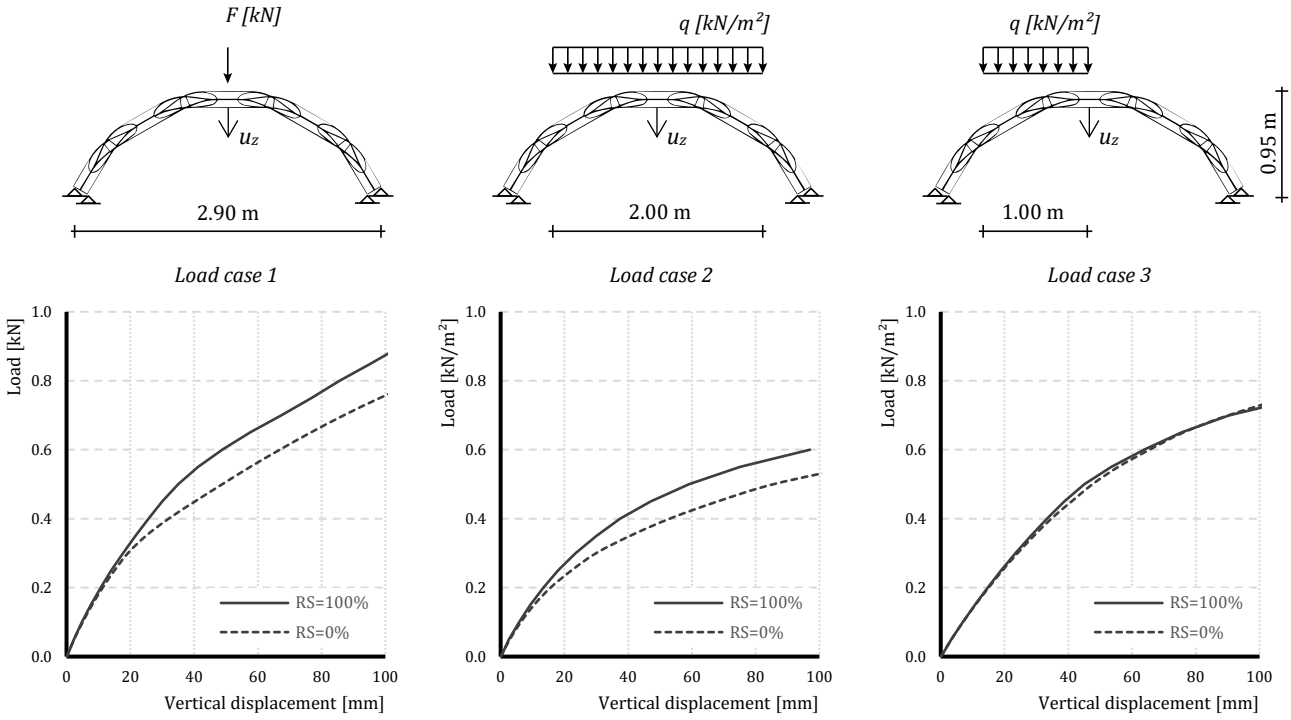

Figure 7.22. Comparing the load carrying behaviour of the form-found arch in the fully stressed condition (RS=100%) with the stress free condition (RS=0%) for three different load cases.

Since the simulations in SOFiSTiK has turned out to give quite an accurate representation of the real structural behaviour, ideally the full geometrical model follows the same modelling approach. A semi-automated parametric model has therefore been developed that uses the form-found mesh as a starting point (see **Annex D)**. Rhino and Grasshopper are used to translate and rotate the unit. From a single mesh, a barrel vault can therefore quickly be modelled an exported to SOFiSTiK for structural analysis. The next chapter discusses a case-study that followed this modelling procedure.

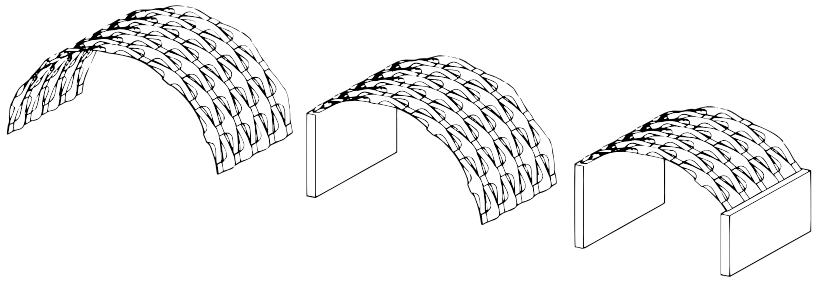

Figure 7.23. Design options

8. STRUCTURAL ANALYSIS AND FURTHER DEVELOPMENT

8.1. INTRODUCTION

For bringing theoretical concepts into the practical and tangible spectrum, prototyping is an important step in all design fields. This chapter explains the development of the modular concept towards a large-scale prototype. This case-study offered the chance to go deeper into the structural behaviour of the system. The structure was on display as part of the Mind the Step exposition during the 2018's Dutch Design Week in Eindhoven (**Figure 8.1**). The exposition offered the possibility to bring attention to bending-active structures and lightweight design to the general public. The prototype shows how structural geometry as a result of bending can be used as the driving factor for the design of load-carrying systems. Furthermore, it aspires to promote the use of wood in construction by presenting a new method of using a thin off-the-shelf plywood sheet. An element that, because of its flexibility, would normally not be used for any structural purpose in load-carrying systems.

Figure 8.1. The prototype was on display during 2018's Dutch Design Week in Eindhoven

8.2. DESIGN PROCESS

The prototype is designed as a free standing system. It does not rely on any other supporting structures or anchoring. A steel strip is used as a tension bar to take the horizontal thrust caused by the dead load. For the purpose of the exhibition, it was important to give the viewers the sensation of being covered by the structure. The prototype is large enough for people to be able to stand beneath it. Efficiency in transportation and construction are also key points for the design. The standardised design elements enable an easy building process. Construction can be done on site with a limited amount of tools and time. The total material is roughly 65 kg and the volume is remarkably small. The elements can easily be transported in the trunk of a small car. Furthermore, bolts are used for the connections, which enables disassembling and rebuilding

at a different site. The design of the units is optimised to limit material wastage. Starting point was a 3.6 mm birch plywood sheet with dimensions of 1.53 × 1.53 m^2. Every sheet nests three cross-shaped plates. The remaining material at the borders is used for the connection elements (**Figure 8.2**). Due to the repetitive design, multiple sheets could be cut simultaneously by a CNC milling machine, which minimised the required machine time.

Figure 8.2. Picture of the plate after the CNC milling process. Material waste was kept to a minimum.

The unit was designed according to the findings of **Chapter 7**. In **Table 8.1**, the parameters that are used for the unit are given. It was important that the stresses remained in the elastic spectrum of the material during construction. At some locations, however, the characteristic value for bending strength perpendicular to the grain is exceeded (**Figure 8.4**). A physical test on a strip indicated that the measured values for the flexural strength are two times higher than the characteristic value (**Table 8.3**). If there are no material defects at the location of these peak stresses, this exceedance should therefore not cause any problems. Furthermore, due to stress-relaxation, these peak stresses fade away rather quickly. No problems regarding these high stresses did occur in the prototype.

Table 8.1. Chosen parameters for the unit design

Input parameters	
t	3.6 mm
E_0	16,471 N/mm^2
E_{90}	1,029 N/mm^2
L_1	1175 mm
L_2	1215 mm
L_3	520 mm
H_1	115 mm
H_2	65 mm
$x_{s,1,2}$	0.4 * L_1/2 = 235 mm
L_2/L_1	1.034
L_3/L_1	0.443
Output parameters	
α	15°
R_A	2618 mm
t_{con}	17 mm

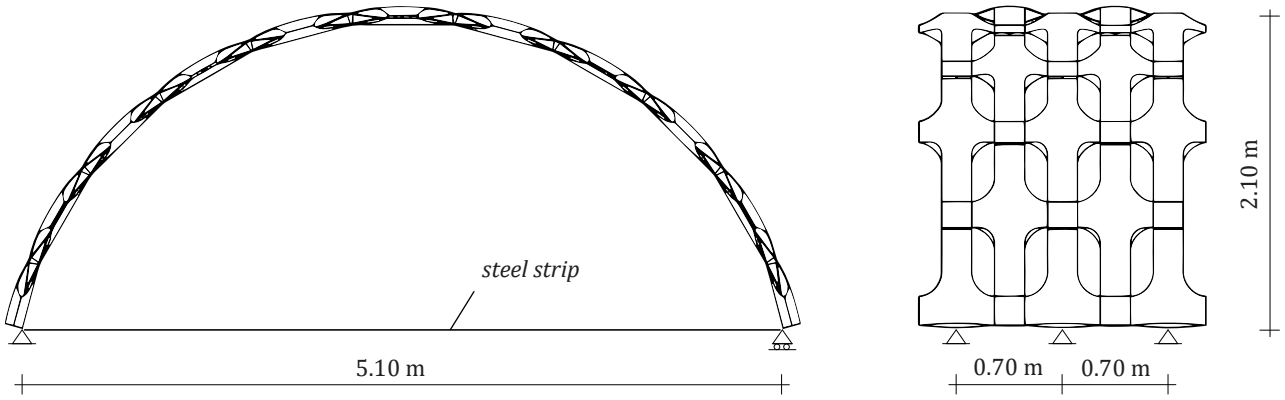

Figure 8.3. Design of the prototype.

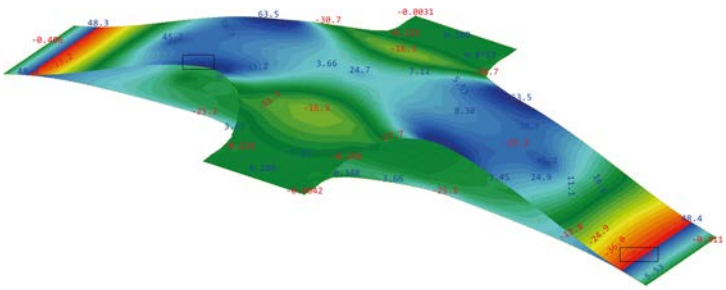

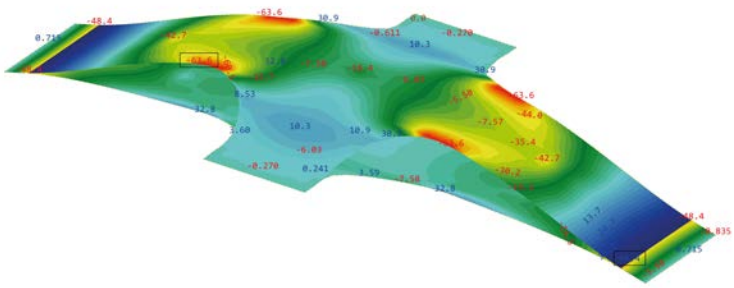

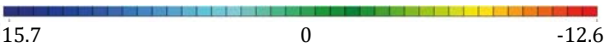

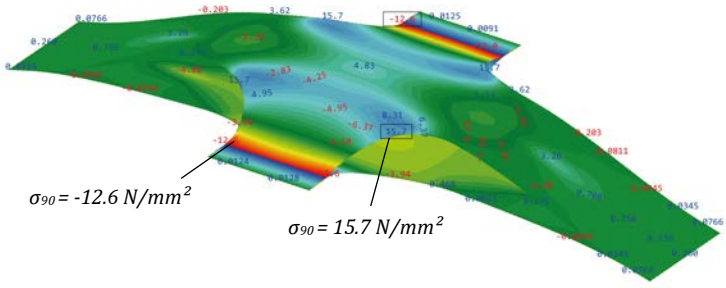

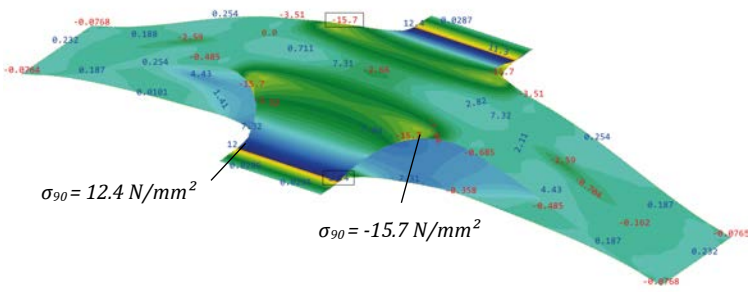

Stresses in the longitudinal direction
$f_{k,m,0}$ = 65.9 N/mm²

σ_0 in the top of the cross-section

Top plate
$\sigma_{0,max}$ = 63.5 N/mm²
$\sigma_{0,min}$ = -47.2 N/mm²

Bottom plate
$\sigma_{0,max}$ = 48.4 N/mm²
$\sigma_{0,min}$ = -25.2 N/mm²

σ_0 in the bottom of the cross-section

Top plate
$\sigma_{0,max}$ = 46.4 N/mm²
$\sigma_{0,min}$ = -63.6 N/mm²

Bottom plate
$\sigma_{0,max}$ = 32.8 N/mm²
$\sigma_{0,min}$ = -48.4 N/mm²

Stresses in the lateral direction
$f_{k,m,90}$ = 10.6 N/mm²

σ_{90} in the top of the cross-section

Top plate
$\sigma_{90,max}$ = 15.7 N/mm²
$\sigma_{90,min}$ = -12.6 N/mm²

Bottom plate
$\sigma_{90,max}$ = 12.3 N/mm²
$\sigma_{90,min}$ = -6.7 N/mm²

σ_{90} in the bottom of the cross-section

Top plate
$\sigma_{90,max}$ = 12.4 N/mm²
$\sigma_{90,min}$ = -15.7 N/mm²

Bottom plate
$\sigma_{90,max}$ = 7.5 N/mm²
$\sigma_{90,min}$ = -12.4 N/mm²

Figure 8.4. Stresses in the unit. The highlighted locations should not possess material defects.
\+ = tension
– = compression

8.3. STRUCTURAL DETAILING

The system is designed taking consideration of a construction process that maximises ease of building. It is essential that the units are closed before they are assembled. The system needs attention to detailing at unit level, for transferring the forces resulting from bending between the top and bottom plate, and at global level, for transferring forces resulting from applied loading.

8.3.1. UNIT LEVEL

At unit level, two different connections can be observed. The forces that have to be transferred by the connections are given in **Table 8.2**. At the longitudinal connection (**Figure 8.5**), the membrane forces in the plates are transferred by a single shear connection. The Yield moment of the bolt and the embedment strength of a plywood plate are calculated conform EN 1995-1-1 by:

$$M_{y,Rk} = 0.3 f_{u,k} d^{2.6} \quad (8.1)$$
$$= 0.3 \times 235 \times 5^{2.6} = 4{,}629\ Nmm$$

In which:
$M_{y,Rk}$ is the characteristic yield moment of the bolt
$f_{u,k}$ is the tensile strength of the bolt = 235 N/mm^2
d is the bolt diameter = 5 mm

$$f_{h,k} = 0.11(1 - 0.01d)\rho_k \quad (8.2)$$
$$= 0.11(1 - 0.01 \times 5) \times 630 = 65.8\ N/mm^2$$

In which:
$f_{h,k}$ is the characteristic value of the embedment strength in N/mm^2
d is the bolt diameter = 5 mm
ρ_k is the characteristic value of the density = 630 kg/m^3

The resistance per bolt can now be computed using the minimal value of equations (8.3 & 8.4) (Jorissen, 2016):

$$F_{v,Rk} = \left(\sqrt{2} - 1\right) f_{h,k} t d \quad (8.3)$$
$$= 0.414 \times 65.8 \times 3.6 \times 5 = 486\ N$$

$$F_{v,Rk} = \sqrt{2 M_y f_h d} \quad (8.4)$$
$$= \sqrt{2 \times 4{,}629 \times 65.8 \times 5} = 1{,}745\ N$$

Two bolts are used at the connection, what makes the total bearing strength:

$$F_{v,Ef,Rk} = n_{ef} F_{v,Rk} = 2 \times 486 = 972\ N \quad (8.5)$$

In the lateral connection (**Figure 8.6**), a tension force is present in the bolt. Due to the curvature in the plate, the washer is pressed into the wood. The tension force is therefore concentrated at the red dot. For a thin plate, this might result in punching shear. It is

Table 8.2. *Forces that are transferred by the connection.*

	Longitudinal connection	Lateral connection
Shear force	337 N	21 N
Axial force	35 N	77 N

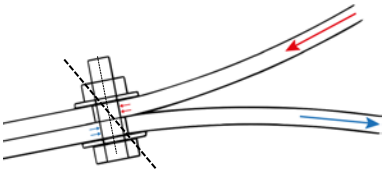

Figure 8.5. Detail and failure mode of the longitudinal plate connection. The membrane forces in the plates are transferred by a single shear connection.

assumed that the shear plane acts under $1/6^{th}$ of the circumference of the washer. The shear strength of this 3-layered panel is not given in literature. For a 5-layered panel, the characteristic strength for shear out of plane perpendicular to the grain $f_{r,90}$ is 1.78 N/mm² (UPM, 2007). A value of 1.5 N/mm² is therefore approximated.

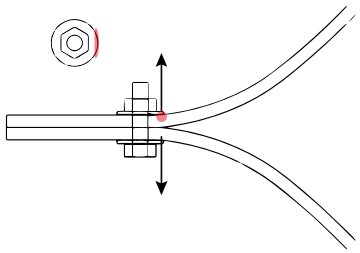

Figure 8.6. Detail of the lateral plate connection. The shear stresses are concentrated at the washer.

The resistance to punching shear in the connection becomes:

$$F_{v,Rk} = \frac{1}{6} A\, f_{r,90} = \frac{1}{6} \times 2\,\pi\, r\, t\, f_{r,90} \qquad (8.6)$$
$$= \frac{1}{6} \times 2\pi \times 7.5 \times 3.6 \times 1.5 = 42\ N$$

In which:

A	is the shear plane
$f_{r,90}$	is the shear strenght out of plane perpendicular to the grain = 1.5 N/mm²
r	is the radius of the washer = 7.5 mm
t	is the thickness of the plate = 3.6 mm

At least two bolts are needed to resist the tension force of 77 N.

8.3.2. UNIT-TO-UNIT CONNECTION

The connection pieces are made from the rest material in the plywood sheets. The nodes are therefore build up from thin plate elements. **Figure 8.8** shows how the different pieces are joined. The units are first joined laterally before they are joined in the longitudinal direction. **Figure 8.9** shows this sequence. There is some eccentricity in the node, because the longitudinal and lateral plate direction do not fall in the same plane. Forcing both directions into the same plane is possible but will affect the arch radius and further stresses the units. Because the elements are already highly stressed, it is chosen to construct the joint with this eccentricity. The joint is schematised in the FE model using beam elements. First an end beam is modelled to the plates to decrease high peak stresses in the model. The beam elements that connect the units are modelled as circular beams with a dimeter that is equivalent to the height of the node. The beams are connected with moment stiff joints (**Figure 8.7**).

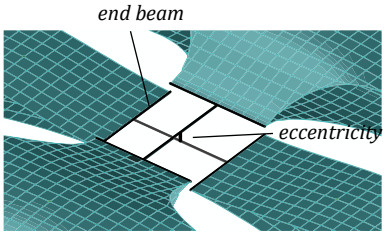

Figure 8.7. Schematisation of the connection in the FE model.

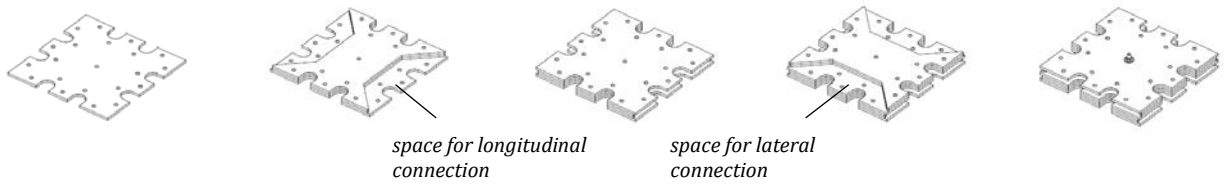

Figure 8.8. The unit-to-unit connection is constructed from multiple thin plates. The places where the units are positioned are indicated in the picture.

1

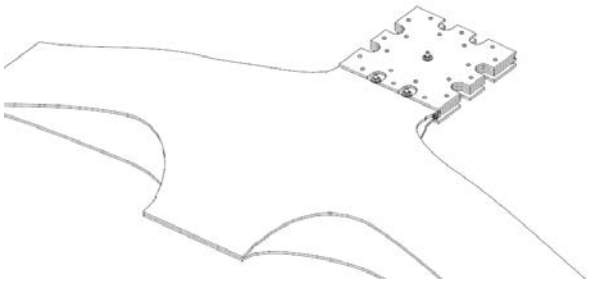

2

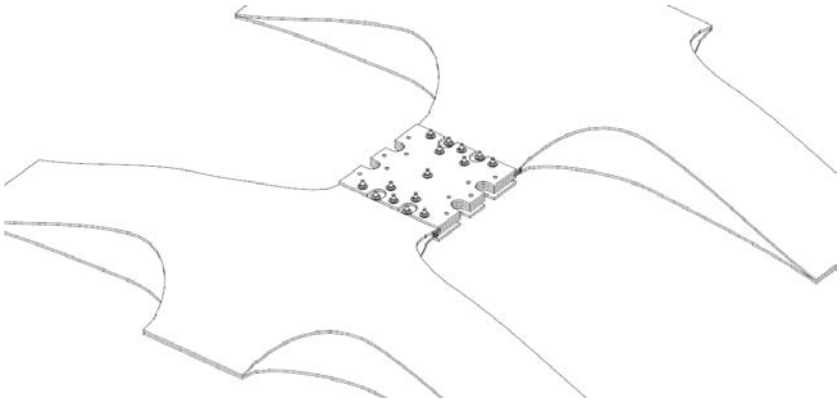

3

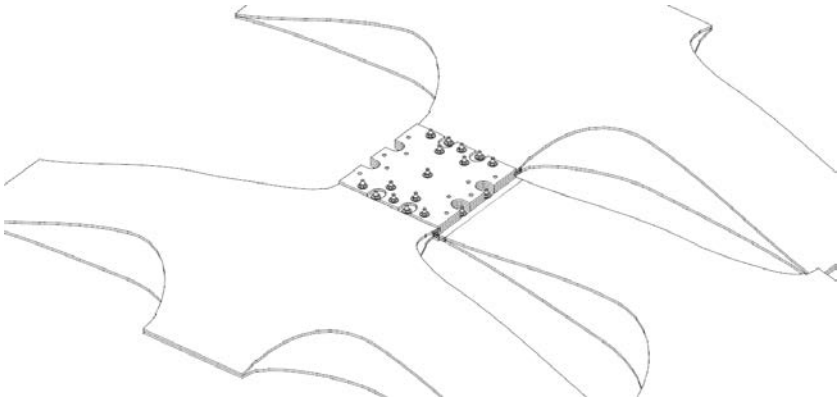

4

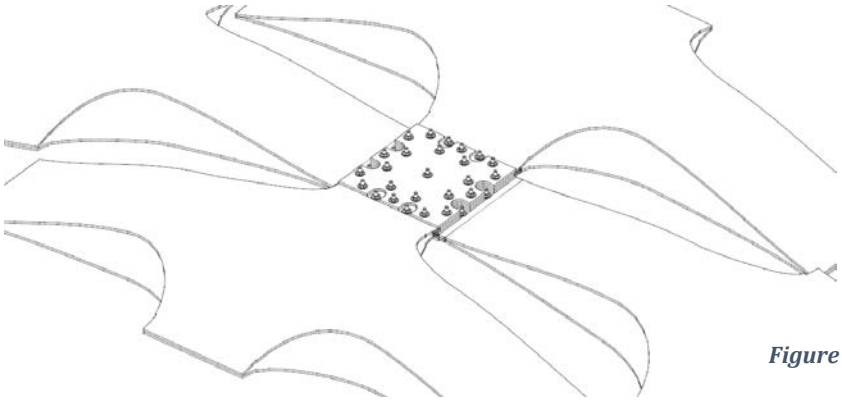

Figure 8.9. Assembly sequence.

8.3.3. *SUPPORTS*

The supporting structure should be able to take a horizontal force due to the horizontal thrust that builds up in the arch. Half a unit is positioned at the ends for a tight connection with the ground plane. This adds the possibility to choose between a single hinged, or a double hinged connection. It should be taken into account that the double hinged connection introduces a bending moment into the supporting structure. For the prototype, a steel strip was used to connect both ends.

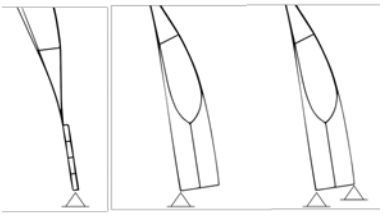

Figure 8.10. Optional boundary conditions

8.4. TESTING THE UNIT

A three point bending test was carried out on a single unit. The unit was loaded multiple times with varying strut lengths to indicate the effects of the strut length on the stiffness. The load tests were carried out directly after bending the unit into shape. It is assumed that no stress-relaxation has taken place prior to the load tests. Because the largest part of the deformation will come from bending, the Young's modulus in bending will be used in the numerical model. $E_{m,0}$ and $E_{m,90}$ were first tested for a flat strip to see if these results coincided with the values from literature (**Table 6.1)**. As shown in **Table 8.3,** these values roughly coincided. The measured values were used in the numerical model.

	Literature values	**Measured values**
t	3.6 mm *(mean value)*	3.8 mm
$E_{m,0}$	16,471 N/mm^2 *(mean value)*	16,000 N/mm^2
$E_{m,90}$	1,029 N/mm^2 *(mean value)*	1,000 N/mm^2
$f_{m,0}$	65.9 N/mm^2 *(characteristic value)*	117 N/mm^2 *(no material defects)*
$f_{m,90}$	10.6 N/mm^2 *(characteristic value)*	21 N/mm^2 *(no material defects)*
G	620 N/mm^2 *(mean value)*	-
G_{90}	620 N/mm^2 *(mean value)*	-
ρ	680 kg/m^3 *(mean value)*	-

Table 8.3. Literature values (UPM, 2007) and measured values of a 4mm birch plywood strip.

The unit was simply supported in the test set-up and had a span of 115 cm. In total, the unit was loaded eight times. The first five tests were loaded to about 0.7 kN. The sixth test was loaded to the critical buckling load. The seventh test was carried out to check if the buckling failure had weakened the material. The eight test was again loaded to the critical buckling load. The deformation of the system during this last test is visible in **Figure 8.11**. The specifications of all the load tests are given in **Table 8.4**. The height of the central strut H_1 and the side struts H_2 was measured from the heart of the plate.

Figure 8.11. Test set-up for system F

System	H_1 [cm]	H_2 [cm]	F [kN]	Type	Test sequence
A	102	57	0.69	Elastic behaviour	1
B	112	57	0.69	Elastic behaviour	2
C	102	67	0.73	Elastic behaviour	4
D	112	67	0.79	Elastic behaviour	3
E	112	77	0.83	Elastic behaviour	5
F	122	67	0.95	Maximum load	8
G	122	77	1.04	Maximum load	6
			0.31	Elastic behaviour	7

Table 8.4. Specifications of the load tests.

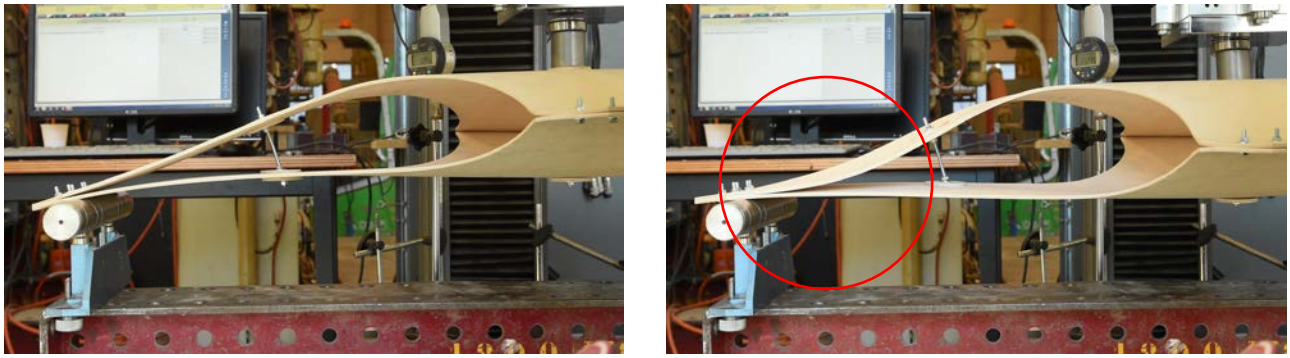

Figure 8.12. System F in the unloaded (left) and loaded (right) state. The buckled region is highlighted in the picture.

Figure 8.13 shows that an increase in structural height has a positive effect on the system's stiffness. The height of the side struts should be chosen in accordance with the height of the centre strut. For systems E and G, it was observed that due to the larger side struts, the stiffness near the supports increased while the stiffness at the centre decreased, resulting in a larger deformation. Furthermore, the load-displacement curve of both tests on system

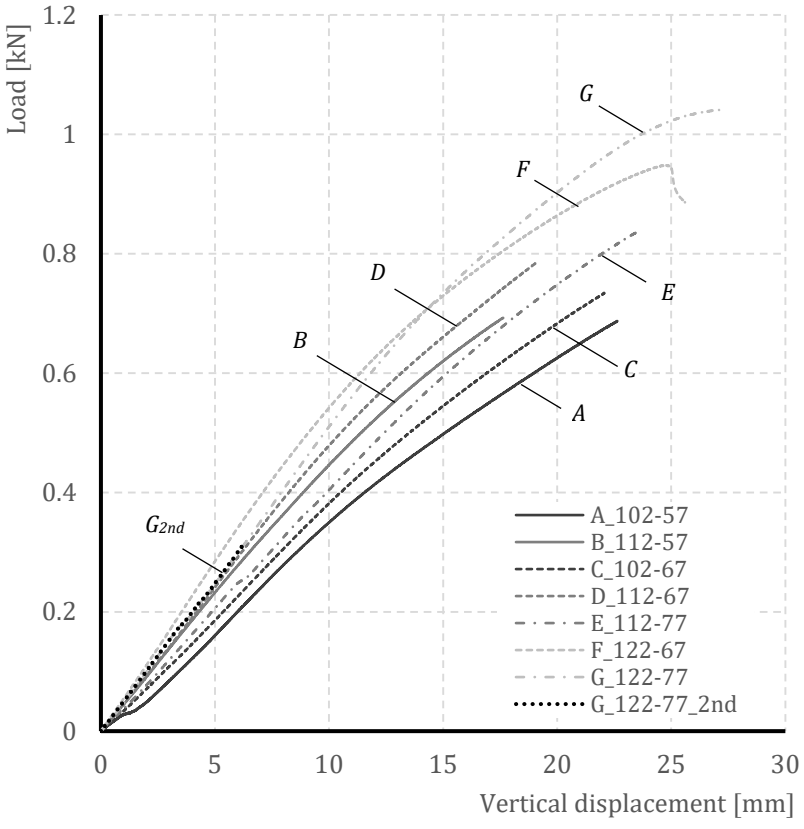

Figure 8.13. Load displacement curves from the load tests. The curves are named by the system's capital letter, followed by the length of the centre strut (H_1) and the length of the side struts (H_2) in accordance with **Table 8.4**. These tests show that increasing the strut lengths, and therefore the structural height, significantly increases the structures load-carrying capacity.

G follow the same elastic behaviour, which indicates that the material was not fractured when the system was loaded to the maximum load.

A numerical model of systems G and F was made in SOFiSTiK. The models assume linear elastic material behaviour and take geometrically nonlinear effects resulting from the residual stress into account. Especially the numerical load-displacement curves of system G show a good correlation with the physical test results (**Figure 8.14**). It is remarkable that where the physical test of system F behaves stiffer than system G, the numerical calculation behaves less stiff. Furthermore, the nonlinear behaviour of the system was not simulated very accurately. In general, however, the numerical simulation gives a fairly accurate representation of the physical behaviour in the linearly elastic spectrum of the system.

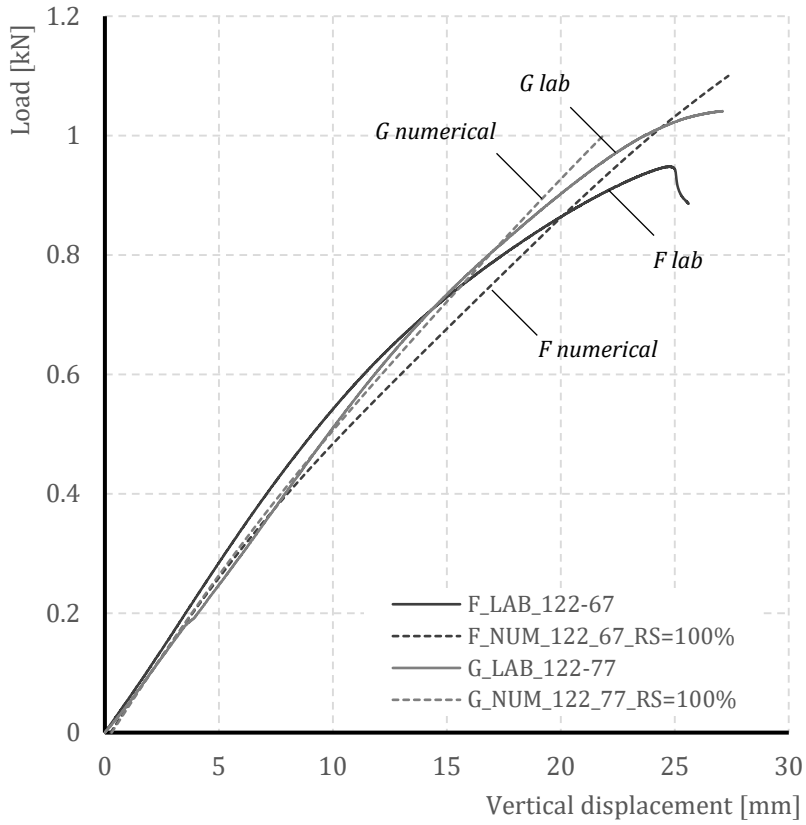

Figure 8.14. Lab and numerical results of systems F and G

The load test on system G was repeated after approximately 1000 hours. The results are shown in **Figure 8.17**. For the numerical model, stress relaxation was calculated following the iterative process described in **Chapter 6**. The process was carried out for a step-size of 5% relaxation in the bottom strip. Taking the relaxation rate in consideration, it was assumed that the relaxation after 1000h is comparable to time-step 5 in the iterative process, where relaxation in the top and bottom plate is 35% and 28% respectively (**Figure 8.15**). **Figure 8.17** shows that the load-carrying behaviour at this time-step has the tendency of diverging from the linear elastic line at about 0.5 kN, what was also observed in the lab results. This figure also shows that the stiffness of the system is decreased when the stresses are fully relaxed.

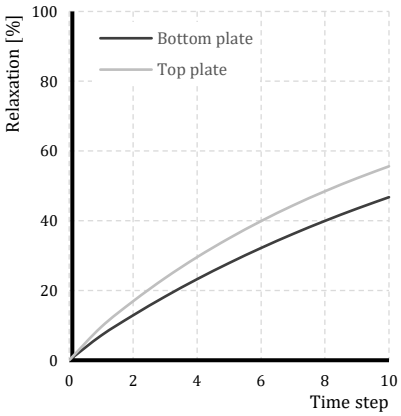

Figure 8.15. Stress-relaxation in the top and bottom plate following the iterative relaxation procedure with a step size of 5% in the bottom plate.

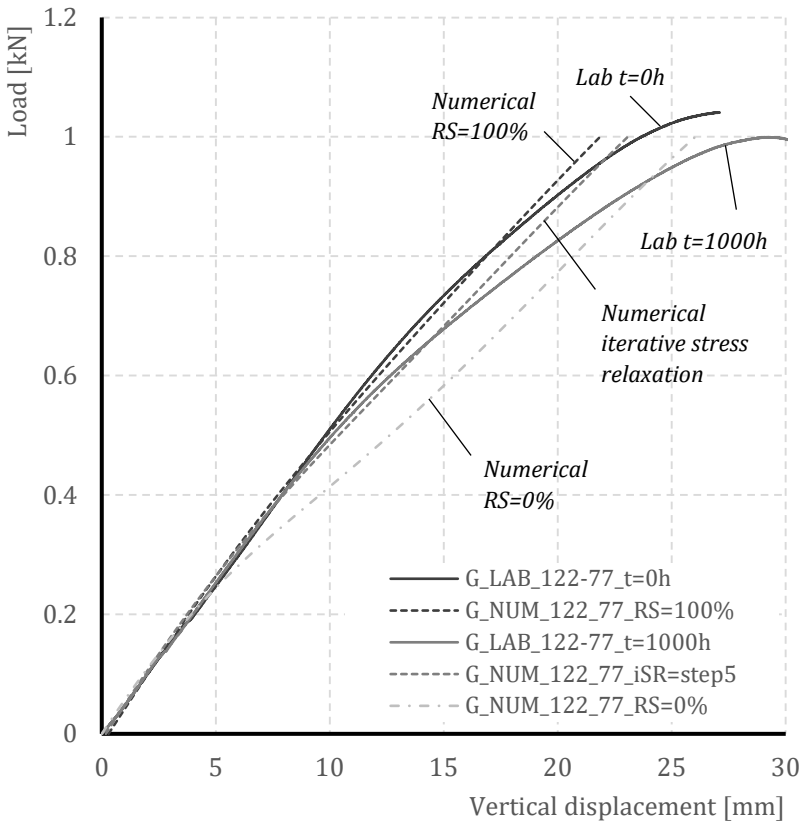

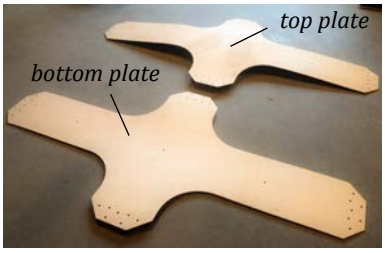

Figure 8.16. Plastic deformations as a result of stress-relaxation were visible after dismantling the unit.

Figure 8.17. Lab and numerical results of system G before and after stress-relaxation. The graph shows both the behaviour in iterative relaxation step 5 and in the completely relaxed state.

8.5. STRUCTURAL ANALYSIS AND FURTHER DEVELOPMENT

8.5.1. ANALYSIS METHOD

Taking the prototype as a starting point for the analysis, this section will discuss the possibilities to further develop the prototype towards a roof system. The analysis and development has been carried out by the following steps:

1) The accuracy of the FE model is verified by comparing the measured deflection in the prototype that was caused by a central point load with the numerical results.
2) Geometrical enhancements that increase the stiffness of the arch will be discussed and tested for two different load cases.
3) A proposition is made for a large-span roof design, following one of the enhanced models.
4) The design is tested for three different plate thicknesses.

8.5.2. ANALYSIS OF THE PROTOTYPE

The prototype was loaded by a central point load, applied by the weight of the author (**Figure 8.18**). The vertical displacement at the edge of the arch could be measured from the picture and is 58 mm under a weight of 0.78 kN. In the numerical model, this same location showed a displacement of 47 mm when the same load was applied to the system. This test indicates that the numerical models behaves 23% stiffer than the prototype. This deviation might be explained by the stiffness of the connection, that is modelled as infinitely stiff. Although the connection in the physical model are sufficiently stiff, a completely moment stiff connection can hardly be made with mechanical fasteners in timber structures. The connection will always have some ability to rotate because the connection loses some stiffness after the washers are pressed into the wood.

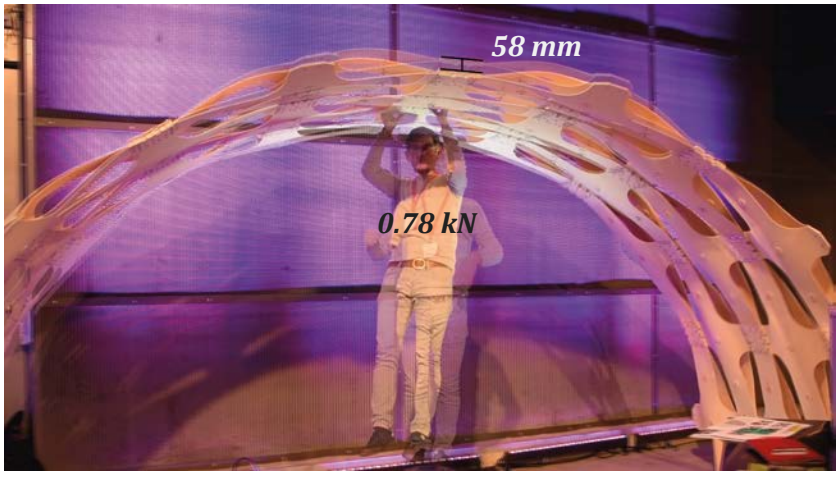

Figure 8.18. *The l*oad test on prototype was performed at the expo site by hanging underneath it. The weight was applied to the centre of the arch.

Although the prototype shows some interesting structural and architectonical qualities, in the current form, the structure is still too flexible to be used in a real structure. There are, however, still multiple ways to improve the structural qualities from a

geometrical point of view. The next section explains some improvements that could be made to the system. The enhanced systems were tested for their behaviour in two load cases, i.e. a central point load and an asymmetrical point load. **Figure 8.23** shows the numerical simulations of the behaviour of these systems, compared to the numerical model of the prototype.

8.5.3. GEOMETRICALLY ENHANCED SYSTEMS

The first enhancement is based on a three-unit design where differences in lateral plate length of the top and bottom plates adds curvature in the lateral direction. In this way, double-curved units are constructed that add corrugations to the barrel vaulted structure. (**Figure 8.19**). This corrugation significantly increases the stiffness of the system, resulting in almost twice as stiff response to an asymmetrical point load (**Figure 8.23**).

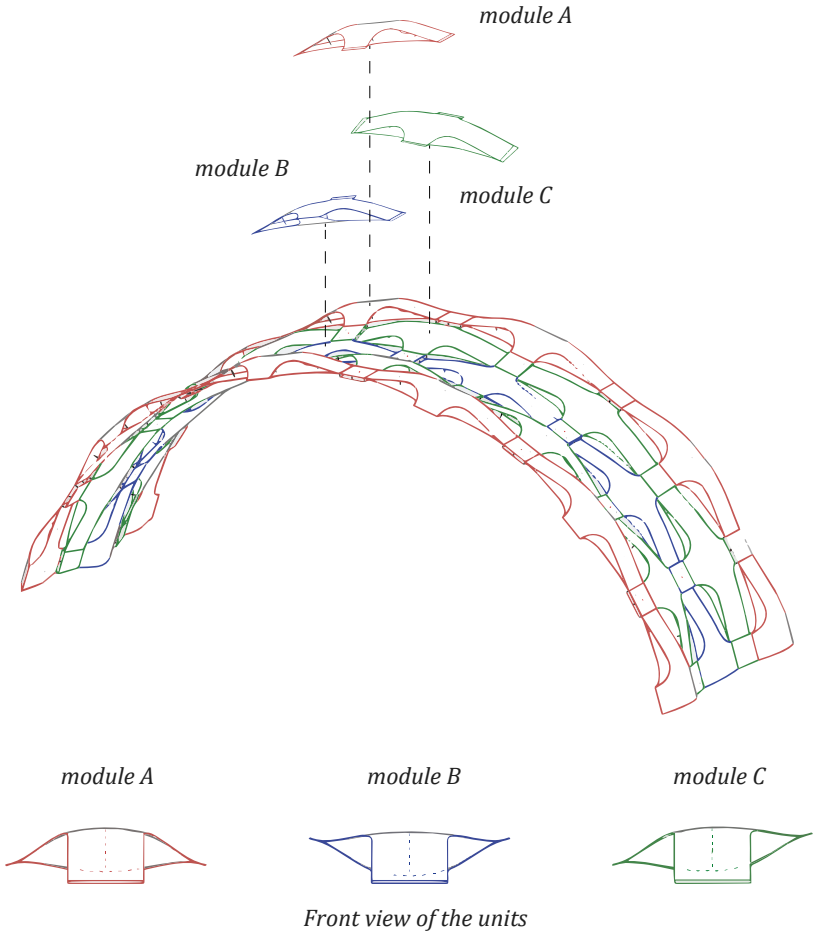

Figure 8.19. The corrugated barrel vault is based on the repetition of three different modules.

Almost no structural height is present where the two plates are joined and the unit is closed. This is by far the weakest location in the structure. The second enhancement increases the stiffness of the system by creating a gap between the plates (**Figure 8.20**). A rigid element should then be added where the units are joined. As a result of this gap, the curvature in the plates is lowered, what decreases the stresses in the elements. The strut lengths can therefore be elongated until the plates reach the same levels of curvature (**Figure 8.21**). For a gap of 30 mm, a stiffness analysis was made for both the model with similar strut lengths as the prototype (115-65mm) as a model with increased strut lengths (150-100mm). In the latter model, the stiffness was more than doubled (**Figure 8.23**). Of course, an adequate structural detail should be designed to transfer the forces in the connection.

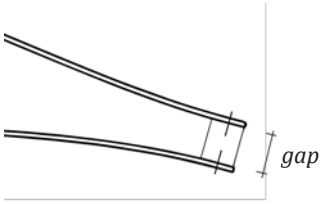

Figure 8.20. The stiffness of the system can be increased by creating a gap between the two plates.

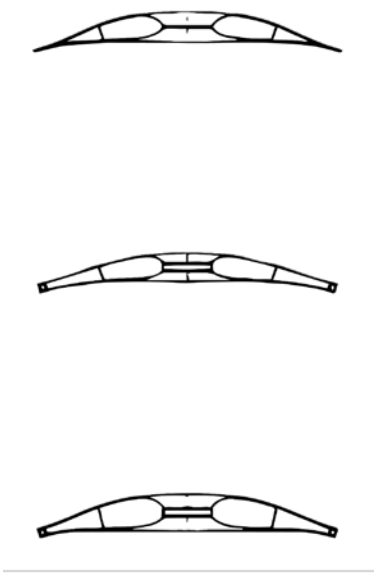

Figure 8.21. The strut length can be increased further to get the same amount of curvature. The strut length is indicated in the figure between parentheses (H_1-H_2).

If both these enhancements are combined, the stiffness of the arch can be increased even further (**Figure 8.22**). It should be noted that this stiffness increase is obtained with almost no additional need for material. Only a little bit of extra timber is required to make up for the larger timber dimensions in the structural nodes. **Figure 8.23** shows the stiffness analysis of all the enhanced systems. The systems have an equal span of 5.10 m. Further increasing the gap or expanding the level of corrugation will of course result in even stiffer systems.

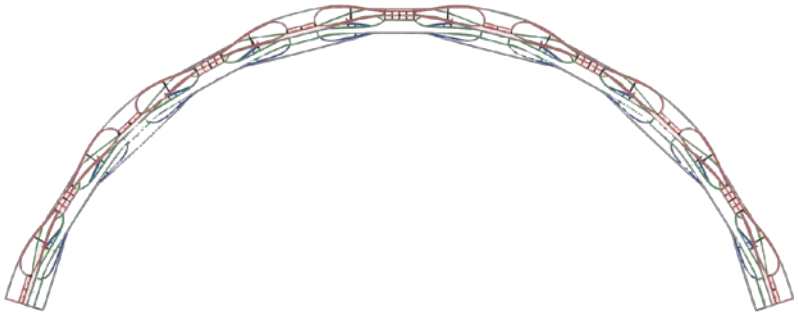

front view

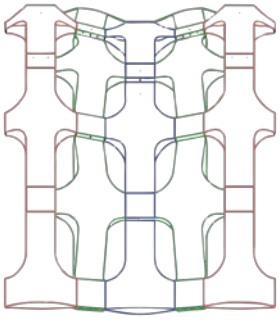

side view

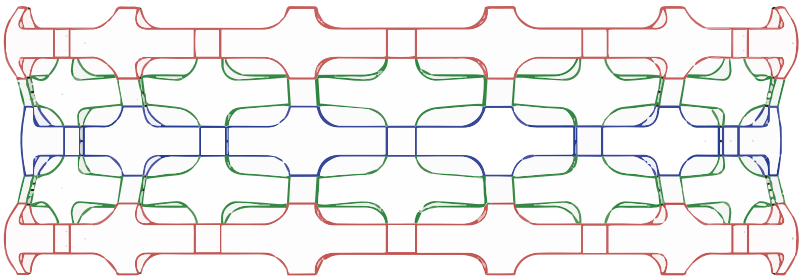

top view

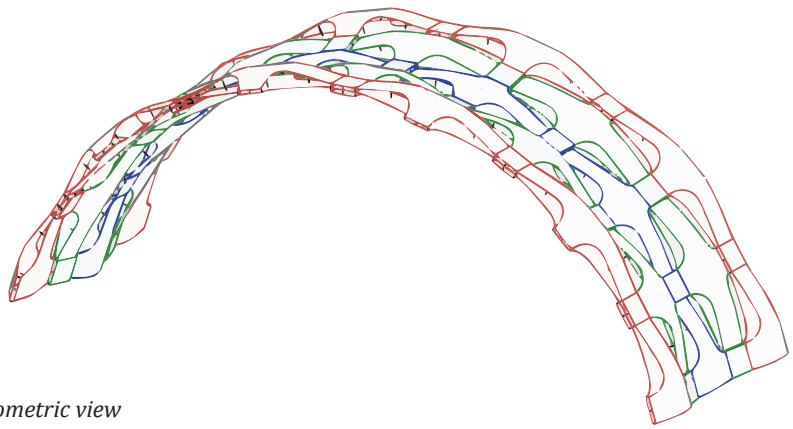

isometric view

Figure 8.22. Gap and corrugation combined

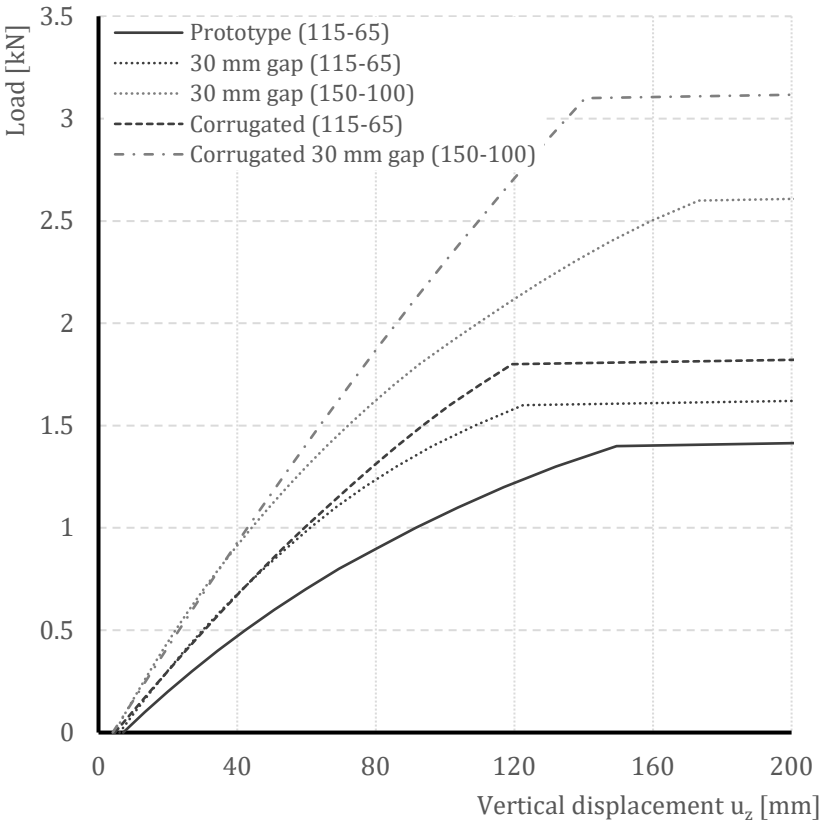

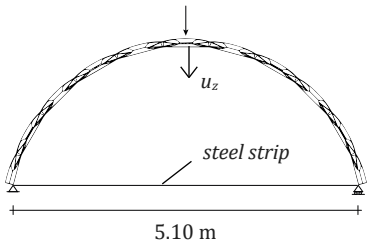

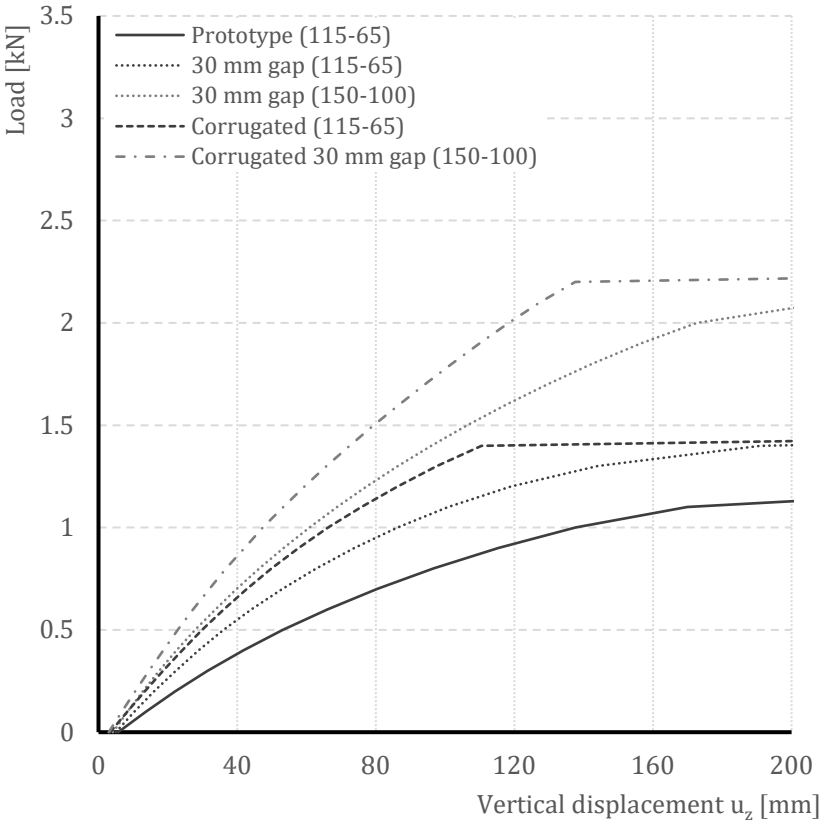

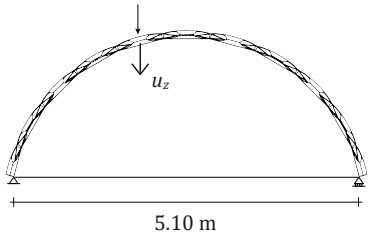

Figure 8.23. Vertical displacement measured at the location of the applied force for a central point load (top) and an asymmetrical point load (bottom). The strut length is indicated in the figure between parentheses (H_1-H_2).

8.5.4. *STRUCTURAL DESIGN OF THE ROOF SYSTEM*

For the sake of comparison, the previous designs all followed a shape that was similar to the prototype. However, a shallow arch would be more promising for a sufficiently stiff roof structure. A roof system where 4 units with gap are joined in the longitudinal direction is chosen for further analysis on different scales. The span is therefore decreased by one unit. The difference in stiffness compared to the 5 unit prototype for load case 1 and 2 is given in **Figure 8.26**. It is assumed that the unit-to-unit connection can be made moment stiff. The connection is modelled by using beam elements according to **Figure 8.24**. The arch is restrained by hinges at the end points of the full and half units (**Figure 8.25**).

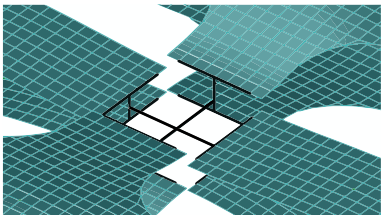

Figure 8.24. FE model of the connection in the model with gap.

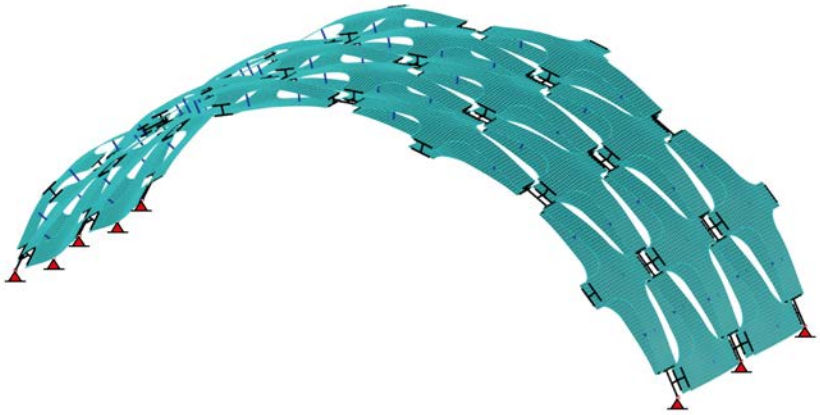

Figure 8.25. FE model of the arch with 4 units and a gap.

For a fair comparison with the small-scale structure, it is assumed that the large-scale models will also be constructed from standard available birch plywood. Upscaling of the structure is done by following the material properties from (UPM, 2007). This means that material properties will change with increasing plate thickness. This is primarily the result of the addition of extra cross-oriented plies, i.e. veneer layers. By increasing the plate thickness, the $E_{m,0}/E_{m,90}$ ratio decreases. This will have an effect on the lateral unit length. Furthermore, the units are restricted in length by the plate dimensions that are available. Creating the gap between the plates would therefore always have been necessary to close the

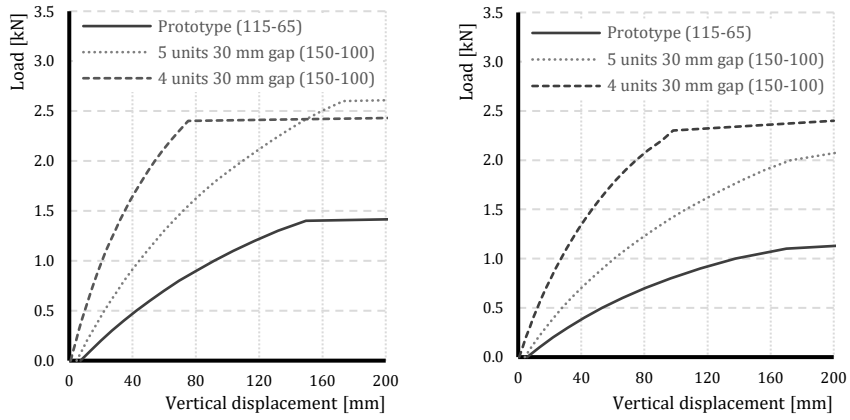

Figure 8.26. 4 unit gap design compared to 5 unit gap design and prototype for LC1 (left) and LC2 (right). The strut length is indicated in the figure between parentheses (H_1-H_2).

unit with sufficient structural height. This section discusses the designs constructed from 3.6, 6.4 and 9.2 mm birch plywood. **Table 8.5** gives flexural moduli and strength for these thicknesses birch plywood plates.

Number of plies	t mean [mm]	$f_{m,0}$ [N/mm^2]	$f_{m,90}$ [N/mm^2]	$E_{m,0}$ [N/mm^2]	$E_{m,90}$ [N/mm^2]	Plate dimensions [cm]
3	3.6	65.9	10.6	16471	1029	153 × 153 250 × 125
5	6.4	50.9	29.0	12737	4763	153 × 153 250 × 125
7	9.2	45.6	32.1	11395	6105	250 × 125

Table 8.5. Material properties for different thicknesses birch plywood (UPM, 2007).

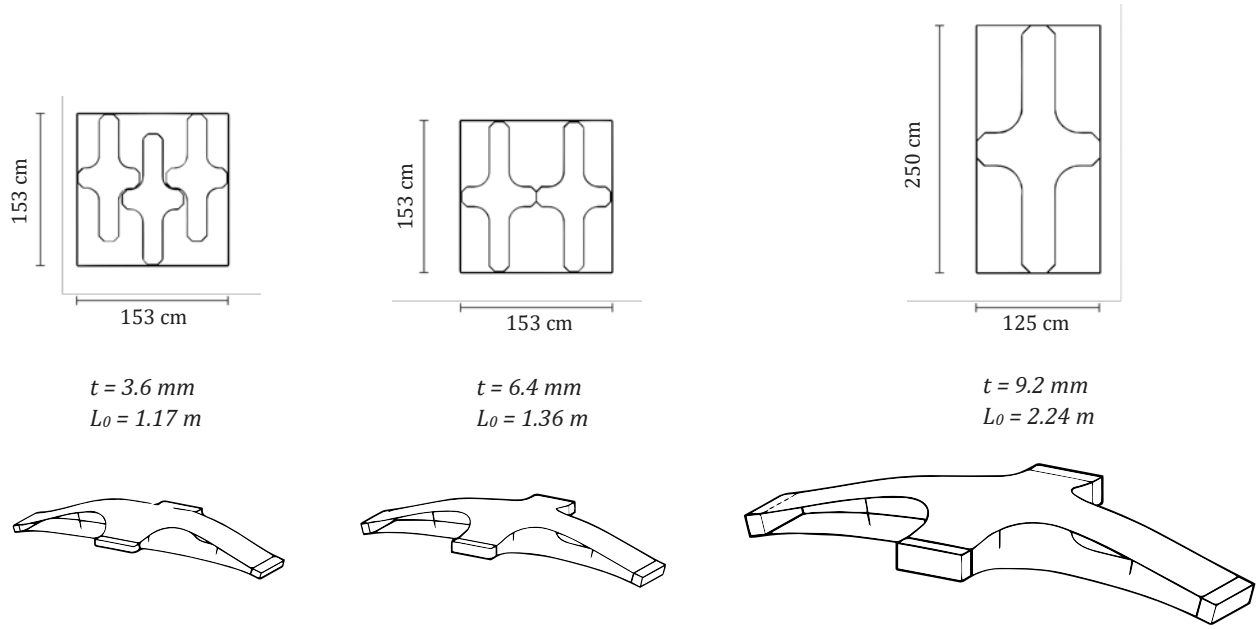

Figure 8.27. Three units constructed from plates with different thicknesses. The cutting patterns are visualised above the units.

Figure 8.27 shows the designs of the units on the three scales. The units were designed with respect to the characteristic flexural material strength (see **Annex E**). The analysis of the arches was carried out for three different load cases, i.e. an equally divided load in vertical direction, an asymmetrically applied load in vertical direction and a load coming from the side (**Figure 8.28**). For each load case, the surface load is translated to a line load applied to the heart of the units. Because there is no specific location or definite design of the structure, the magnitude of the loads will not be computed precisely. However, it is assumed that the structure should be able to take surface loads between 1.0 and 2.0 kN/m^2. These load magnitudes represent permanent loads caused by cladding and secondary structures, and variable loads coming from wind or snow. Self-weight of the main structure is taken into account in every analysis. The values that correspond with a maximum deflection of L/200 are given in **Table 8.6**.

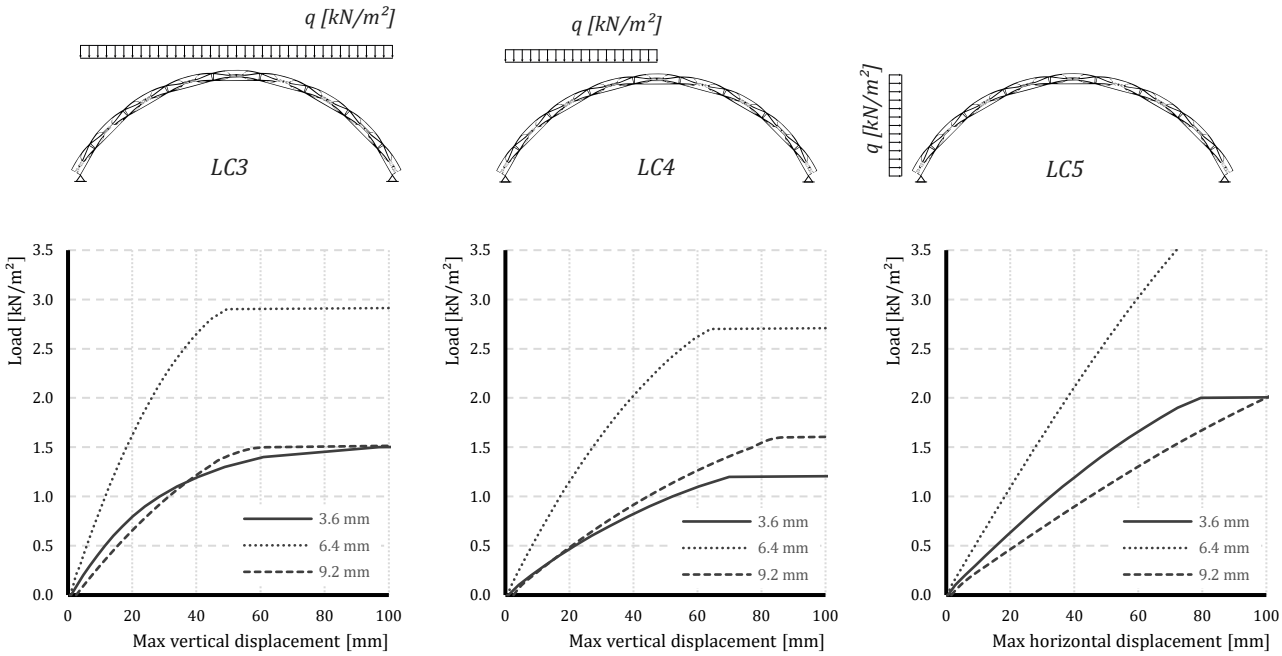

Figure 8.28. Response to LC3-4-5 on three scales. The loads are applied as surface loads translated to line loads over the heart of the units

Table 8.6. Maximum deflection

	t [mm]	L [m]	u_{max} (L/200) [mm]	$LC3_{max}$ [kN/m²]	$LC4_{max}$ [kN/m²]	$LC5_{max}$ [kN/m²]
3-Ply	3.6	4.5	22.5	0.85	0.55	0.70
5-Ply	6.4	5.0	25	1.95	1.40	1.40
7-Ply	9.2	8.5	42.5	1.25	0.95	0.95

Although snap-through buckling is often the governing failure mode for bending-active systems (Lienhard, 2014), a stress check was carried out to investigate if the stresses in the material would not exceed the design values of the material properties. The 6.4 mm and 9.2 mm systems were tested for a variable line load of 1.0 kN/m² conform LC3 and self-weight of the structure multiplied by a factor of 1.5. It is assumed that the structure is designed for standard indoor conditions. Therefore, the values attributed to plywood in climate class 1 can be adopted. The design values of the Young's modulus and the mechanical strength are computed using:

$$E_d = \frac{E_m}{\gamma_m}$$

$$f_d = \frac{f_k}{\gamma_m} k_{mod} k_h k_l$$

In which:

E_d is the design value of the Young's modulus
E_m is the mean value of the Young's modulus
γ_m is the material factor. This is 1.2 for plywood
f_d is the design value of the mechanical strength

f_k is the characteristic value of the mechanical strength
k_{mod} is the load duration factor. This value is assumed 0.90 for short load duration.
k_h; k_l are volume factors. These are 1.0 for plywood.

The design values were only exceeded around the edge beams at the unit-to-unit connection, which can be explained due to modelling errors. An overview of the results is given in **Annex E**. The tests show that stresses in the structure are likely to remain below the ultimate strength upon external loading.

8.5.5. CONCLUDING REMARKS

Considering the maximum deflections under the given loading conditions, the 6.5 mm system with a span of 5.0 m, and the 9.2 mm system with a span of 8.5 m show promise to be used as a roof system. A quick stress test has indicated that the stresses are likely to remain below the design values of the material for these systems. However, it should be noted that these tests were carried out in the stress-free state. Follow-up research should also consider that there are already stresses present from bending the units. Although it can be assumed that a large part of these stresses will relax away rather quickly, it should be checked if the stresses coming from external loading will not exceed the design values when a part of this prestress is added to the system.

Furthermore, this analysis has only considered one design option. The system could still be enhanced by further increasing the gap between the plates or by adding a corrugation to the arch by following the three-module design. Another way forward can be to develop a dome system that spans in two directions (**Figure 8.29**). Also irregularities can be added to the unit that let the system deviate from a circular arrangement and that might increase the load-carrying capacity even further.

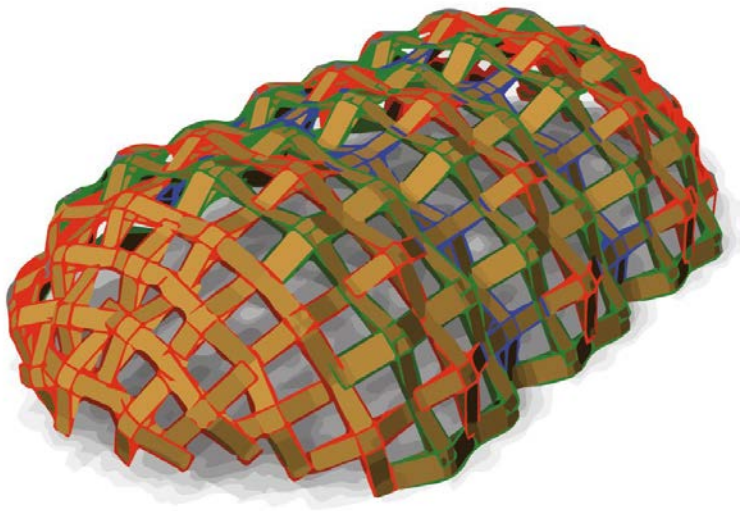

Figure 8.29. Concept of structure spanning in two directions.

9. CONCLUSIONS

9.1. CONCLUDING THE RESEARCH

The research has discussed the possibility of using off-the-shelf plywood sheets to create a spatial roof system. It started from the authors curiosity to the possibility of applying the principle of active-bending to timber plates for developing a system that has sufficient stiffness to be used as a long-lasting load-carrying structure in a large spanning roof system. This led to the necessity of obtaining in-depth knowledge on material specific and method specific behaviour, and the ability to accurately describe and predict this with numerical tools. What followed, was a design exploration where the material and bending behaviour and properties were investigated for numerous bending-active systems. This gave rise to the design of a unit-based actively-bent roof system. The system has been thoroughly tested and researched, both numerically as physically, to come towards an optimised solution in which the material is pushed to its boundaries for a suitable application in a building structure. The stages of this process, together with their findings are briefly discussed below.

MATERIAL, BENDING AND LOAD-CARRYING BEHAVIOUR

It is evident that the highly prestressed parts lose roughly half of their stresses in the first year after construction due to stress-relaxation in the wood. This process is likely to continue throughout the lifetime of the structure, however, the extent of this long-term relaxation has not yet been researched. The investigated systems have shown that these stresses influence the load-carrying behaviour in either a positive or a negative way, depending on either predominant tensile or compressive stresses respectively. It is a safe assumption to say that the structure's strength and stiffness should therefore be sufficient in the stress-free state. Hence, it is not possible to rely on tension stiffening effects caused by the residual tension stresses. Elastic bending is primarily used as a means to develop structural geometries where the main contribution of stiffness comes from the (double) curved elements and efficient couplings.

NUMERICAL COMPUTATION

The exploration of the material and behaviour goes hand in hand with developing the necessary skill-set to accurately simulate and predict the bending and load-carrying behaviour. The structure's geometry is always a direct result of internal force equilibrium. Finding the right computation method was therefore necessary to accurately describe the structure's shape. From three different approaches that were studied, the method based on finite element analysis was found most suiting. A constant exchange between numerical and physical results has built the confidence that the

predictive models for both the form-finding and the structural analysis as well as the simulation of stress-relaxation were sufficiently accurate. This gave enough knowledge for the design and analysis of an actively-bent timber plate structure.

THE SYSTEM

A system was developed that is based on a repeating module. This enables pre-bending of the units. The system harnesses the qualities that timber, and bending-active structures in general, have to offer. The geometric design of the units is led by the properties of the material. The orthotropic nature of the plywood panels was a leading factor for this design. It gave the preference to a primary, main, and secondary, supportive, load-carrying direction. The material properties are exhausted by stressing the plywood to its limits to find geometrically efficient shapes. Small dimensional alterations to the flat plate configurations affect the final geometry significantly. These relations have been thoroughly researched. Using numerical form-finding, the bent shape of the module is accurately predicted. The most important shape parameter is the angle with the horizontal axis. Together with the unit length, this angle determines the arch radius.

Snap-through buckling seems to be the governing failure mode for both the unit and the arch. Resistance to buckling is increased by choosing optimal dimensional parameters and strut locations. When designing this system, a trade-of between two parameters has to be made. On one end, the plate thickness should be thin enough to allow for large curvatures and gain in structural height, on the other hand, the plates should be thick enough to prevent the plates from buckling locally and increase the stiffness of the system. It was shown that choosing a thicker plate is usually the better option when more stiffness is desired.

Numerical form-finding was combined with a semi-parametric geometrical modelling script that translates the form-found geometry to a structural model of the combined units. This allowed for a relatively quick way of generating a variety of models for comparison of the structural qualities, however information on stress-levels in the elements gets lost. Tests have shown that the arch behaves less stiff when the stress-free geometry is analysed. This method therefore gives a lower bound stiffness analysis that has a relation to the completely relaxed state.

PROTOTYPE AND ENHANCEMENTS

Developing the prototype was invaluable for testing the construction process and structural behaviour in the physical world. It has shown that the building method works without resulting in fractures or formability issues. On unit level, the numerical model describes the load-carrying behaviour very accurately. Also the somewhat lower stiffness after stress-relaxation was in line with the simulations. It was shown that the

model could be pressed in its buckled shape without resulting in fractures. Load calculations on the arch were made in the stress-free state, this calculation was expected to be on the safe side. The numerical model of the prototype, however, behaved somewhat stiffer then the physical model. The joints were modelled as continuous plates, where in reality, they were clamped with bolts. These bolts had loosened prior to loading and were therefore able to rotate a little.

The prototype did show that the system has potential, especially when the joint and geometrical design would be further optimised. By further increasing the geometrical aspects of the system, a design was made that would more than double the stiffness and critical buckling load of this prototype. Moving forward from these findings, a design that showed potential for an application in a real structure was made and analysed for three different scales and plate thicknesses.

The method finds its beauty in its simplicity for creating complex forms through a modular approach. During the exposition, it was noticed that the structure was found appealing by a lot of people. This was also expressed in the appreciation of the lightness of the structure, the natural material and curvatures and the interesting shadow play and possibilities for daylighting. When looking for a solution to cover the structure and make it weather tight, these qualities should ideally be preserved.

APPLICABILITY TO LARGE SCALE DESIGNS

The proposed building method and system show some qualities that could be of interest while being adopted for developing spatial building structures. When complex shapes are desired, this often results in expensive structures. A building method that relies on standardised flat elements for developing these (double) curved shapes, therefore shows a lot of promise. Due to the limited volume and weight of the structural elements, bending-active systems could be ideal for temporary structures or structures at remote locations, but also as long-lasting roof systems where low self-weight is desired. The research has shown that the system has potential to be used in roof systems of at least 8.5 metres span. The structure was tested for load cases with load magnitudes that can be expected for roof structures. It was shown that deformations and stress-levels could be kept below acceptable values.

9.2. DISCUSSION

The research from this report was divided into two main parts. The first part (**Chapters 1-6**) has discussed the general behaviour of bending-active systems and has shown how these systems should be approached when using timber for the design of an actively bent roof structure. The second part (**Chapters 7-8**) has shown the development and optimisation of a design concept, where the author has given his personal twist to the way how bending-

activity should be approached in timber engineering. A large part of the research has been a search for a system that shows potential for large-scale designs. Where this search would eventually lead to could not have been clear from the start of the project. The report has discussed the process of the study and emphasises on some parts that were deemed most important for the current stage of development. During the design process, the author has made several side steps from the red thread. Not all of them had the possibility to be explained with the same amount of detail and it was inevitable that the research would be finished leaving some gaps open. However, the report is intended as a framework which can be followed for a bending-active design and as a means to bring enthusiasm to and show the potential of this interesting building method. It was therefore deemed important to highlight as much as was said. Some of the topics that were left undiscussed and would be necessary for further development from the authors point of view are briefly pointed out in the following section.

9.3. RECOMMENDATIONS

Looking at possibilities for further research, this can be approached in three ways, i.e. additional research to bending-active timber systems in general, additional research to the current system and research to new ways of combining elements and form systems. For every area, a short elaboration is given below.

RESEARCH TO BENDING-ACTIVE TIMBER

Thin plates tend to buckle easily. It could be beneficial to use a timber species with a lower Young's modulus to achieve thicker sections. In-depth research to applicable timber species should therefore be carried out. Apart from material specific alterations, the relation between curved configurations and their critical buckling load could shine light on new ways of using bending and twisting to develop more efficient shapes from flat plate configurations. This research should take into account the structural behaviour with respect to the prestress resulting from bending and the effects of stress-relaxation.

Stress-relaxation can result in movements and shape alterations. A predictive simulation can be programmed that bases the amount of relaxation on the stress-levels in the elements. Following the iterative procedure, and by adding local stress differences to this procedure, the relaxation process can be accurately predicted. This asks for the necessity of an automated process. For a better simulation of the process, additional research to the relaxation rate with respect to the stress levels in the elements is necessary.

ADDITIONAL RESEARCH TO THE MODULAR SYSTEM

For developing the system using thicker plates, experimental tests should be carried out to verify the formability of these plates. The necessary force to bend these thicker plates becomes higher as well. Consequently, tools should be used for bending and the

mechanical connection is stressed to a larger extent. These implications should be studied when designing for large-span structures. Furthermore, the joint design could be improved for a more optimised construction process and a stiffer connection. This raises questions to the applicability of bolts. However, when the structure does not need the possibility to be easily dismantled, an alternative to bolts can be proposed. Also a connection detail for the design where the gap is included between the plates should be developed.

Additional research is still needed to guarantee the safety of the structure conform building regulations in the ultimate limit state (ULS) and the serviceability limit state (SLS) design. Although it was demonstrated that the absence of residual stresses lowers the stiffness and buckling load, it should be checked if stress levels are not exceeded when the residual stress is (partly) taken into account. Furthermore, it is questionable if these systems can be constructed fire safe. Using fire retardant adhesives with a high environmental impact goes against the vision of developing of a sustainable lightweight timber system. Therefore, it can be argued that the system could only be used for functions where there are no special requirements regarding fire safety. On the other hand, sprinkler systems could also be used to guarantee fire safety.

The qualities of the current system could still be improved by increasing the gap between the plates or by increasing the level of corrugation. Furthermore, from an architects and an engineering point of view it is interesting to deviate from the imposed circular form. The three-unit design of the corrugated barrel vault already showed one design possibility that can be made by slightly altering parameters in the flat plate configuration. However, ideally a free-form geometry could be approached with the construction system. A possible design solution is briefly presented below.

Every unit has a certain base length, width and angle. In the report, these are indicated with L_0, L_{90} and α. These parameters are also clearly visible when a rectangular mesh is used to approach a double-curved surface. In such a mesh, every rectangle has a certain length, width and an angle with its neighbouring rectangle. It might be possible to use these parameters as boundary conditions for the design of the bending-active units. In this way, a double-curved surface could be approached by first using a rectangular mesh to approach the surface, and then use bending-active units with varying parameters to fill the rectangular planes. The parameter relations that were discussed in **Chapter 7** could be used for forming the modules.

RESEARCH TO NEW SYSTEMS

Following the more general research of **Chapters 1-6**, other bending systems could be developed. The main challenge for these structures is how to achieve stiff configurations from flexible

sheets and how to approach free-form geometries with bent elements that acquire their shape from internal force equilibrium.

New ways could be found that create double curvature from single curved bent elements. A field which is less highlighted in this report is twisting of members. However, it is a question if twisting is favourable in timber systems, because these systems lose a lot of stiffness due to stress-relaxation. On the other hand, twisting, could also greatly increase the second moment of area of a cross-section and therefore might have potential for bending-active timber systems.

IMAGE INDEX

Figure 1.1: Image retrieved from: https://inspiration.detail.de/centre-pompidou-metz-103525.html?lang=en Photograph by Frank Kaltenbach
Figure 1.2: Image retrieved from: https://www.designtoproduction.com/
Figure 1.3: Image retrieved from: https://nl.pinterest.com/pin/507429082992788739/?lp=true Photograph by Domiciano Pereira
Figure 1.4: Image retrieved from: https://temoore.net/fifties/plywood-dome/
Figure 1.5: Image taken from: (Lienhard, 2014)
Figure 1.6: Image retrieved from: http://architectuul.com/architecture/view_image/mannheim-multihalle/10247
Figure 1.7: Image taken from: (Fleischmann and Menges, 2011)
Figure 1.8: Image taken from: (Wienand and Hudert, 2010)
Figure 1.9: Image taken from: (Schleicher and La Magna, 2016)
Figure 2.1: Own image
Figure 2.2: Image taken from: (Lienhard, 2014)
Figure 2.3: Own image
Figure 2.4-9: Image taken from: (Lienhard, 2014)
Figure 2.9a: Photograph by Pierluigi D'Acunto
Figure 2.10: Image taken from: (Lienhard, 2014)
Figure 2.11: Own image
Figure 3.1: Image taken from: (Green *et al.,* 1999)
Figure 3.2: Own image
Figure 3.3: Image taken from: (Bechert *et al.,* 2016)
Figure 3.4: Image taken from: (D'Acunto and Kotnik, 2013)
Figure 3.5: Image taken from: (Lienhard, 2014)
Figure 3.6: Image taken from: (Wienand and Hudert, 2010)
Figure 3.7: Image taken from: (Hudert, 2014)
Figure 3.8: Image taken from: (Schönbrunner *et al.,* 2015)
Figure 3.9: Image taken from: (Fleischmann and Menges, 2011)
Figure 3.10: Image taken from: (Brütting *et al.,* 2017)
Figure 3.11: Image taken from: (Schleicher and La Magna, 2016)
Figure 3.12: Image taken from: (Bechert *et al.,* 2016)
Figure 3.13-14: Image taken from: (Schleicher and La Magna, 2016)
Figure 3.15: Image taken from: (D'Acunto and Kotnik, 2013)
Figure 4.1: Image taken from: (La Magna, 2017)
Figure 4.2: Image taken from: (Lienhard, 2014)
Figure 4.3: Image taken from: (Längst, Michalski and Lienhard, 2016)
Figure 4.4: Image taken from: (Bauer *et al.,* 2017)
Figure 4.5: Image taken from: (Adriaenssens and Barnes, 2001)
Figure 4.6: Own image
Figure 5.1: Own image
Figure 6.1-15: Own image
Figure 7.1-23: Own image
Figure 8.1-29: Own image

BIBLIOGRAPHY

Adriaenssens, S. M. L. and Barnes, M. R. (2001) 'Tensegrity spline beam and grid shell structures', *Engineering Structures*, 23(1), pp. 29–36. doi: 10.1016/S0141-0296(00)00019-5.

Bauer, A. M. *et al.* (2017) 'Embedded structural entities in NURBS-based isogeometric analysis', *Computer Methods in Applied Mechanics and Engineering*. Elsevier B.V., 325, pp. 198–218a. doi: 10.1016/j.cma.2017.07.010.

Bauer, A. M. *et al.* (2017) 'Isogeometric Analysis for Modeling and Simulation of Building Processes', (October), pp. 1–10.

Bauer, A. M. *et al.* (2018) 'Exploring Software Approaches for the Design and Simulation of Bending Active Systems', *Proceedings of athe IASS Symposium 2018*, (July), pp. 1–8.

Bechert, S. *et al.* (2016) 'Textile Fabrication Techniques for Timber Shells', in Adriaenssens, S. et al. (eds) *Advances in Architectural Geometry 2016*, pp. 204–221. doi: 10.3218/3778-4.

Brütting, J. *et al.* (2017) 'Bending-Active Segmented Shells', in *Proceedings of the IASS Annual Symposium 2017 'Interfaces: architecture.engineering.science'*. International Association for Shell and Spatial Structures (IASS), pp. 1–10.

Crisfield, M. A. (1997) *Non-linear Finite Element Analysis of Solids and Structures*. Chichester: Wiley.

D'Acunto, P. and Kotnik, T. (2013) 'AA/ETH-Pavilion', in *Proceedings of the TENSINET Symposium 2013*. Istanbul, pp. 99–108.

EN 1995-1-1. *Eurocode 5: design and calculation of wood constructions – part 1-1: general – common rules and rules for buildings.* Dutch Standardization Institute, Delft, 2007.

Gerrard, C. (1987) 'The equivalent orthotropic elastic properties of plywood', *Wood Science and Technology*, 21(4), pp. 335–348. doi: 10.1007/BF00380201.

Green, D. W., Winandy, J. E. and Kretschmann, D. E. (1999) *Mechanical properties of wood*, *Wood Handbook - Wood as an engineering material*. U.S. Department of Agriculture.

Happold, E. and Liddell, W. I. (1975) 'Timber Lattice Roof for the Mannheim Bundesgartenschau.', *Structural Engineer*, 53(3), pp. 99–135.

Hudert, M. (2013) *Timberfabric: Applying Textile Assembly Principles for Wood Construction in Architecture*. École Polytechnique Fédérale de Lausanne. doi: 10.5075/epfl-thesis-5553.

Jorissen, A. (2016) 'Introduction to Timber Structures', in *7KP5MO – Advanced Timber and Lightweight Structures*. Eindhoven University of Technology, pp. 1–52.

Jorissen, A. (2016) 'Introduction into Timber Connections, in *7KP5MO – Advanced Timber and Lightweight Structures*. Eindhoven University of Technology, pp. 1–45.

Kotelnikova-Weiler, N. *et al.* (2013) 'Materials for Actively-Bent Structures', *International Journal of Space Structures*, 28(3–4), pp. 229–240. doi: 10.1260/0266-3511.28.3-4.229.

Längst, P., Michalski, A. and Lienhard, J. (2016) 'Integrated Design Approach for Shell Structures Using Isogeometric Analysis', *Nexus Network Journal*. Springer International Publishing. doi: 10.1007/s00004-016-0320-x.

Lienhard, J. (2014) *Bending-Active Structures : form-finding strategies using elastic deformation in static and kinetic systems and the structural potentials therein*. Universität Stuttgart.

Lienhard, J. and Knippers, J. (2013) 'Considerations on the Scaling of Bending-Active Structures', *International Journal of Space Structures*, 28(3), pp. 137–148. doi: 10.1260/0266-3511.28.3-4.137.

La Magna, R. (2017) *Bending-Active Plates*. Universität Stuttgart.

La Magna, R. and Knippers, J. (2017) 'On the behaviour of bending-active plate structures', in *Proceedings of the IASS Annual Symposium 2017 'Interfaces: architecture . engineering . science'*. Hamburg.

Nabaei, S. (2014) *Mechanical form-finding of timber fabric structures*. École Polytechnique Fédérale de Lausanne. doi: 10.5075/epfl-thesis-6436.

Nicholas, P. and Tamke, M. (2013) 'Computational Strategies for the Architectural Design of Bending Active Structures', *International Journal of Space Structures*, 28(3–4), pp. 215–228. doi: 10.1260/0266-3511.28.3-4.215.

Panagoulia, E. and Schleicher, S. (2016) 'Bending-active Structures A Case study for an Office Chaise Lounge', in *Complexity & Simplicity - Proceedings of the 34th eCAADe Conference*, pp. 621–630.

Schleicher, S. and Magna, R. La (2016) 'Bending-active Plates : Form-finding and Form-conversion Bending-Active Plates', (October), pp. 260–269.

Schleicher, S., Magna, R. La and Zabel, J. (2017) 'Bending-active Sandwich Shells : Studio One Research Pavilion 2017', (November), pp. 544–551.

Schönbrunner, A. *et al.* (2015) 'Design strategies for bending-active plate structures out of multiple cross-connected layers', *Proceedings of the International Association for Shell and Spatial Structures (IASS) Symposium 2015*, (Future Visions).

Schreurer, F. (2011) 'Lost in Parameter Space or Digital Craftsmanship – From Thinking to Modeling to Building', in *Lecture Series – Spring 2011: 'Models of Design in the Age of Computation' - Organized by Axel Kilian*. Princeton University School of Architecture. Available at: https://vimeo.com/69024741.

Slabbinck, E. L. M. *et al.* (2017) 'Conceptual framework for analyzing and designing bending-active tensile hybrid structures', *Proceedings of the IASS Annual Symposium 2017 'Interfaces: architecture.engineering.science'*.

Slabbinck, E. L. M., Körner, A. and Knippers, J. (2017) 'TORSION AS A DESIGN DRIVER IN BENDING-ACTIVE TENSILE STRUCTURES - An Assembly-based Approach for Torsion in Plate-hybrid Structures', *Proceedings of the IASS Annual Symposium 2017 'Interfaces: architecture.engineering.science'*.

Tachi, T. (2013) 'Interactive Form-Finding of Elastic Origami', *Proceedings of the International Association for Shell and Spatial Structures (IASS) Symposium 2013*, (5), pp. 7–10.

Takahashi, K. *et al.* (2016) 'Scale effect in bending-active plates and a novel concept for elastic kinetic roof systems', in *Proceedings of the IASS Annual Symposium 2016*. International Association for Shell and Spatial Structures (IASS).

Weinand, Y. and Hudert, M. (2010) 'Timberfabric: Applying textile principles on a building scale', *Architectural Design*, 80(4), pp. 102–107.

ANNEXES

ANNEX A – CASE STUDY PROJECTS

CONTENTS

I. PLYDOME – 1957

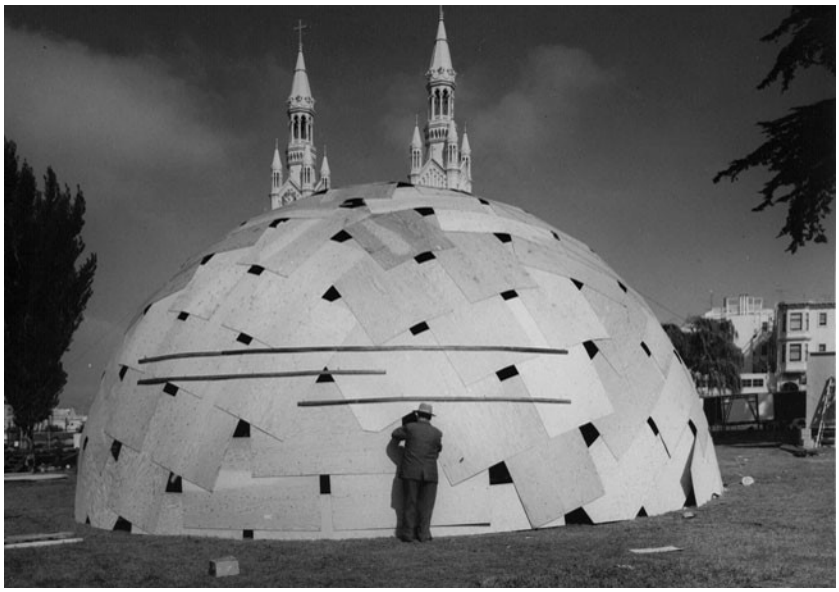

Figure I.2. Plydome by Buckminster Fuller constructed in des Moines, Iowa in 1957.

Figure I.1. Plywood dome constructed by Thomas Moore in 1957 at Washington Square in San Francisco.

In his research to geodesic domes, Buckminster Fuller has developed a principle of using flat plywood sheets, that had only found their way into the industry by the 20th century, for creating a double-curved dome structure. These so-called plydomes (**Figure I.1**) were the first structures on record that actively used the flexibility of the plates to construct a spatial structure from off-the-shelf timber plate elements. **Figure I.2** shows a large dome as constructed by Thomas R. Moore to Fuller's patent.

Figure I.3. The structure is supported by a central pole during construction.

SYSTEM'S PRINCIPLE

The structure uses standard plywood sheets. The plates are most easily bent at the corner points of the plates. Every other plate is used in the system to restrain the plates into their curved shape, resulting in a closed system that finds its equilibrium globally.

ASSEMBLY METHOD

The plates are assembled one-by-one, starting from the centre point of the dome. A pole was used as a temporary supporting structure (**Figure I.3**). With the addition of every sheet, the dome shape is further approached (**Figure I.4**).

Figure I.4. With the addition of every plywood sheet, the final shape is further approached.

ARCHITECTURAL EXPRESSION

The construction results in a dome that can achieve full coverage of the roof. Some holes are still present for possibilities of daylighting. Optionally, these openings could be enlarged. The sheets are still clearly visible in the final design, giving a close relation in the final structure to the standard plate element.

II. MULTIHALLE MANNHEIM – 1975

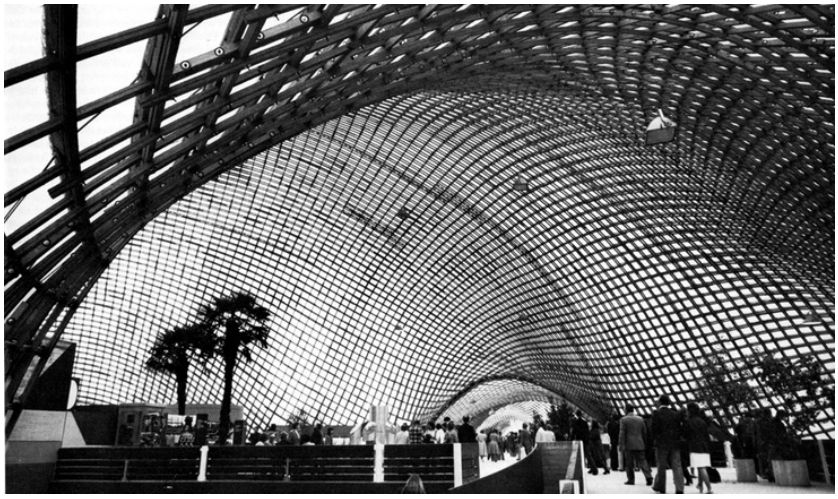

Figure II.1. Photograph of the interior of the Multihalle in Mannheim.

The first, and still only one of the few, large-scale bending-active timber structure that has been build is the Multihalle in Mannheim, designed by Frei Otto (**Figure II.1**). Construction was finished in 1975. Although currently propped, the building is still standing today.

SYSTEM'S PRINCIPLE

Contrary to the other discussed projects, this structure uses a grid of one-dimensional laths the form a shell. The system is commonly referred to as a gridshell structure. However, since this structure is one of the few bending-active systems that has been built on a large-scale, a lot can be learned from this example that can be adopted in timber plate systems.

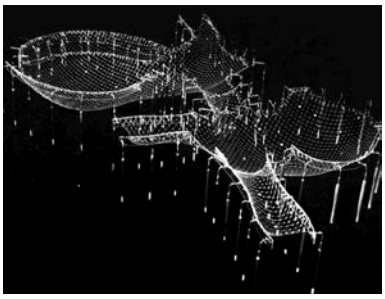

Figure II.2. A hanging chain model was used for the form-finding.

STRUCTURAL QUALITY

Physical form-finding models have been used to design a funicular shell where double-curvature is added to resist buckling (**Figure II.2**). Cables were added to resist in-plane deformations. Multiple layers are used to overcome the curvature limitations of thicker cross-sections; Also the effects of creep and relaxation were noted, but were mainly seen as positive, since it would lower the stress where a large curvature is present over time, increasing the ultimate strength (Happold and Liddell, 1975).

ASSEMBLY METHOD

The structure is built by erecting a rectangular mesh of flexible timber rods and fixing it to the foundation. he connection allows for some sliding to occur between the layers during construction.

ARCHITECTURAL EXPRESSION

The construction method offers the possibility to develop a large variety of double-curved free-formed shapes from one-dimensional laths. This gives the possibility to develop numerous designs using the same construction method. Furthermore, grid pattern gives a very characteristic identity to the structure.

III. ICD/ITKE RESEARCH PAVILION – 2010

Figure III.2. Photograph of the pavilion in Stuttgart.

Every year, the Institute for Computational Design (ICD) and the Institute of Building Structures and Structural Design (ITKE) at the University of Stuttgart collaborate on the design and construction of a research pavilion to showcase research carried out at both faculties. The pavilion is build up from 80 unique strips of 6.5mm birch plywood that are robotically manufactured. The strips are elastically bent and restrained into a torus shape with an approximate span of 4 meters.

Figure III.1. The plate intersections are varied over the width of the structure.

SYSTEM'S PRINCIPLE

The pavilion is built from a sequence of elastically bent strips that keep each other into place. The curved segments are constrained by the straight parts of each of the neighbouring strips. Consequently, a two-dimensional system appears in which the curved parts are in bending and compression and the straight parts are in tension. At the intersections hinges occur. The different strips are positioned following a radial grid.

Figure III.3. Plywood strips are added one-by-one.

STRUCTURAL QUALITY

On their own, a cross-section is not very stable to resist external loads because a mechanism would form due to the weak intersections. This is prevented, however, by changing the location of the hinges in each successive element. Also, the radial orientation of the two-dimensional elements further increases the structure's stiffness and stability (**Figure III.2**).

ASSEMBLY METHOD

The structure was assembled fairly easy by hand with the help of numerous workers. The strips were bent and interlocked at the construction site one by one (**Figure III.3**).

Figure III.4. Architectural expression

ARCHITECTURAL EXPRESSION

The form and interplay of the strips give a very interesting display of light inside the structure. The curves that result from force equilibrium follow a shape that seems very natural. Aesthetically pleasing structure for the eye (**Figure III.4**).

IV. TIMBERFABRIC MODULE – 2010

Research to Timberfabric at IBOIS EPFL comes from the idea to incorporate qualities of fabric, such as friction in a weaving pattern, to timber structures. In textiles multiple elements work together to create one coherent structure. This 'social behaviour' can be compared to yarn in fabric (Hudert, 2014).

SYSTEM'S PRINCIPLE

A single timberfabric module is constructed by entwining two identical planar strips (**Figure IV.2**). The helical order in which the plates are rearranged is similar to twisting of yarn. What follows is a closed module that can be extended into a barrel vault by forming an array in the axial and tangential direction (**Figure IV.4**). Changing the strip dimensions and the properties of the connection alters the curvature of the arch.

STRUCTURAL QUALITY

A multi-layered system can be made to improve the structure's rigidity. Several rigid connecter pieces has been developed for joining the extra layer to the base layer. By analysing a freely supported timber fabric module with a central vertical force acting on it, an interesting self-stabilising effect can be observed. While the span increases in length, the total width of the cross-section decreases. This results in an increase in cross-sectional height of the central triangular cross-section.

ASSEMBLY METHOD

The system is based on closed modules. Connector pieces are used to facilitate joints with additional layers (**Figure IV.3**).

Figure IV.1. Prototype of the Timberfabric system.

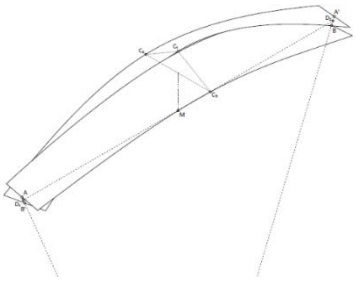

Figure IV.2. A single Timberfabric module.

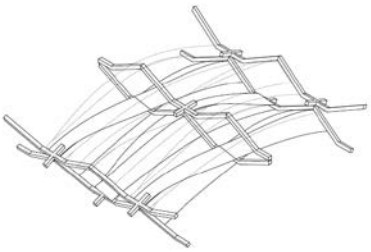

Figure IV.4. Connection elements are used to form a multi-layered system.

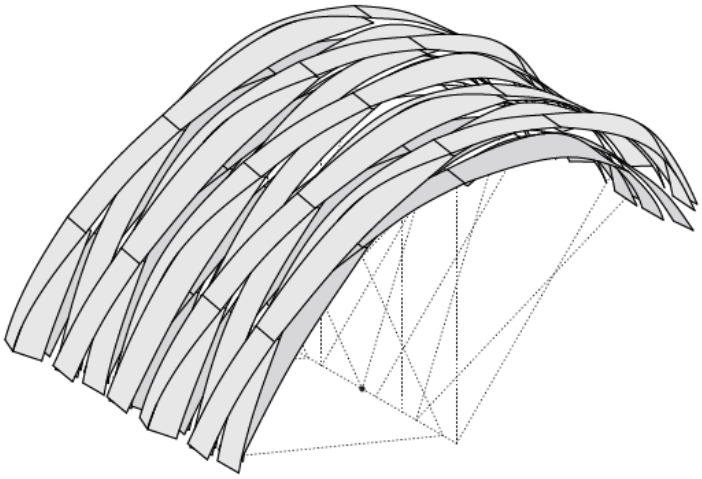

Figure IV.3. The system follows a circular arrangement.

V. AA/ETH PAVILION – 2011

Figure IV.1. Photograph of the pavilion.

The AA/ETH pavilion has been made as a collaboration between the EmTech Programme at the AA School in London and the DARCH Chair of Structural Design at ETH Zurich. The project had the goal to build a short-term lightweight sun-shading plywood pavilion, which evolved into a meeting place. The used panels have a thickness of 18mm and are build-up from six layers of spruce veneer, from which four layers are oriented with the fibres in longitudinal direction and two in lateral direction. Spruce has been favoured over the frequently used birch, which has superior mechanical qualities and is often used in similar projects, because of the lower Young's modulus that spruce possesses. The structure is constructed from of three bent panels with dimension up to 2.3m in width and 10.3m in length and facilitates a maximum span of 8.5m (D'Acunto and Kotnik, 2013).

Figure V.2. The plates are connected by prestressed cables.

SYSTEM'S PRINCIPLE

The triangular shape of the panels and the parabola shaped cuts alter the bending stiffness over the longitudinal axis and thus control the shape which the plates take when bent. The stiffness distribution is designed to let the plates bent into their funicular shape. The three panels are connected together by pre-stressed steel cables that stabilise the overall structure and evenly transfer external forces though the system.

Figure V.3. The large plate elements are first bend and then restrained.

STRUCTURAL QUALITY

The pre-stressed cables sustain stability under external loads (**Figure V.2**). The flexible lamellas that are a result of the cuts not only facilitate the bending, but also dissipate a portion of the wind loads through vibration. Although no test were performed on the time dependent material behaviour, the plywood elements did show significant deformations after demolishing the structure. Furthermore, the steel cables had to be tensioned a few times over the year the pavilion was standing due to the loss of pre-stress.

VI. BERKELEY WEAVE – 2014

Figure VI.1. The Berkeley Weave prototype

Double curved surfaces can normally not be approached with planar elements. The Berkeley Weave follows from research that describes a method to create double curved surfaces from an assembly of single curved elements (Schleicher and La Magna, 2016). This method is referred to as form-conversion. The prototype follows a weaving pattern of four layers of 3mm birch plywood. In total, 480 different parts were used.

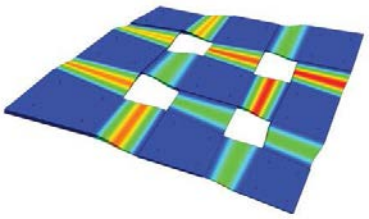

Figure VI.2. The curvature is taken by twisting and bending the intermediate parts, annotated by a red colour to describe the level of curvature.

SYSTEM'S PRINCIPLE

The structure is designed by approximating a free-form double curved geometry with a quadrilateral mesh. From this mesh a weaving pattern is derived. The intersections contain the stiffer parts of the structure. The Gaussian curvature of these parts is therefore set to zero. The more flexible intermediate parts will still have a small Gaussian curvature, but, this can be taken by twisting the strip (**Figure VI.2**). The structure that follows, essentially is a meshed shell structure that is built up from two layers of unique plywood elements each direction.

STRUCTURAL QUALITY

Double curved shells have superb structural qualities. For wood, funicular shells can be desired to counter creep deformations. The form-conversion method allows for the generation of these kind of double curved geometries. Also, structural rigidity can simply be improved by adding an additional layer to the system.

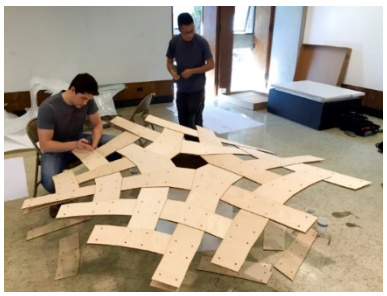

Figure VI.3. The system is assembled by connecting plates to the system one-by-one.

ASSEMBLY METHOD

Mass customisation techniques have been used to fabricate the massive variety of unique parts. During assembly, the elements are connected one by one, bending itself into shape (**Figure VI.3**). The layers are bolted together at the intersections.

ARCHITECTURAL EXPRESSION

The designer takes charge and can therefore impose his will upon a structure. This prototype shows that the possibilities are endless. As a nice touch, all the joints has been hidden in the mid layers, making it look like a seamlessly woven structure.

VII. BEND9 – 2014

Figure VI.1. Bend9 prototype

The Bend9 pavilion follows from the same research as the Berkeley Weave. Again, 3mm birch plywood has been used for construction. In total, 196 unique parts have been used to construct the pavilion.

SYSTEM'S PRINCIPLE

Also in the Bend9 project, the form-conversion method has been used to approach a user defined free-form geometry. Contrary to the previous project, a triangulated mesh has been used to form the base element grid (**Figure VII.2**). By offsetting the triangles inward, and connecting their edges, rectangles are formed that account for most of the bending.

Figure VII.2. A triangular mesh is used to approach the curvature of the system.

STRUCTURAL QUALITY

Again, the double curved shape greatly improves the stiffness of the flexible panels. Additional rigidity has been acquired by adding an extra layer (**Figure VII.3**). Where in the Berkeley Weave additional layers where placed directly onto the previous one, the Bend9 pavilion uses connector pieces between the layers. This increases the overall bending resistance of the pavilion.

Figure VII.3. Connection pieces are used to create a double-layered structure.

ASSEMBLY METHOD

The triangular orientation of elements causes a decrease in the amount of parts compared to the rectangular grid of the Berkeley Weave. The unique elements were constructed though mass customisation techniques and were connected one by one to approach the double-curved geometry.

VIII. SCHONENBRUNNER – 2015

Figure VII.1. Picture of the prototype.

This project demonstrates a way to develop a rather complex double curved geometry from triangularly oriented planar elements that fit on a hexagonal grid.

SYSTEM'S PRINCIPLE

Closed modules are formed by connecting two plates to each other. These modules have a hexagonal layout and can therefore be mapped on a freeform geometry that has a hexagonal penalisation (**Figure VIII.2**). The final shape is determined by an extra layer that bends the

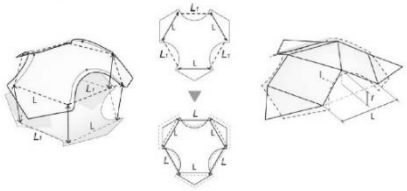

Figure VIII.2. The modules follow a hexagonal arrangement.

STRUCTURAL QUALITY

The coupled system remained quite flexible because of the hinges around the modules. An additional layer was added to prevent these hinges axis from reducing the structural capacity (**Figure VIII.3**). In a two-dimensional abstraction of the system, it can be explained that the two initial layers work as a hinged chain that can be deformed and locked by a third layer. Additional layers could be added to further increase the structure's rigidity.

ASSEMBLY METHOD

Unique elements are manufactured and put together to create the closed modules. These modules can be joined together to form the first two layers of the free-from structure. When the third layer is connected, the structure is locked in its final shape.

Figure VIII.3. The three-layered arrangement rigidifies the system.

IX. ICD/ITKE RESEARCH PAVILION – 2015

Figure IX.1. Picture taken from the inside of the pavilion.

SYSTEM'S PRINCIPLE

Custom lamination is used to control the curvature of the elements (**Figure IX.4**). Connections between elements are made by finger joints that are tied together using laces (**Figure IX.2**). This connection is similar to the fibrous connection that can be found in the exoskeleton of sea urchins (Bechert *et al.,* 2016). The connection allows for some tolerance due to its flexibility. Due to the fact that the elastic bending behaviour of wood cannot be modelled with great precision, the flexibility in the connection lets the elements be rearranged in the shape that is desired by the material.

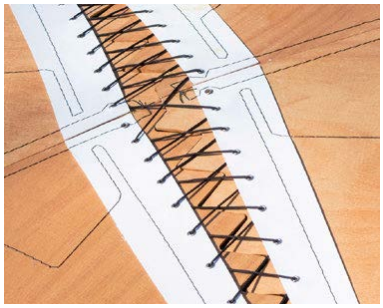

Figure IX.2. The fibrous connection refers to nature.

STRUCTURAL QUALITY

Especially where a connection is needed between thin sheets, this fibrous connection is favourable for its quality. The continuous connection facilitates an even distribution of stress over the cross-section. Furthermore, a relatively large structural height is present in the units.

Figure IX.3. The modules are first closed before they are connected to each other.

ASSEMBLY METHOD

The bending-active modules are first closed and then connected to each other (**Figure IX.3**). The different modules are connected using laces.

ARCHITECTURAL EXPRESSION

The bending-active system follows a cellular structure that has a close relation to forms and principles that can be found in nature.

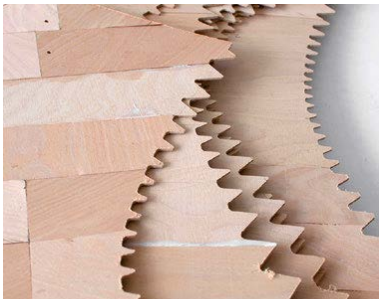

Figure IX.4. Custom lamination of plates results in varying stiffness over the length of the elements.

X. BENDING-ACTIVE SEGMENTED SHELL – 2017

Figure X.1. Bending-active segmented shell model.

SYSTEM'S PRINCIPLE

A double curved geometry is approximated by a sequence of single curved strips (Brütting *et al.,* 2017). By unrolling these single curved strips, the shape of each flat strips is found. Once bent into shaped, the strips are connected laterally to form a coherent shell. The shapes of the bent strips are controlled by altering the stiffness over the longitudinal axis and are therefore not limited to the elastica curve.

STRUCTURAL QUALITY

This method for constructing bending-active structures results in closed thin shells that can be assembled fairly easily from planar strips. The thin shell has structurally superb qualities because it can transfer forces through membrane action. Although this method shows potential, it has not yet been tested in a project using timber panels. When used in a real project, questions about the structural capacity and also about its detailing should be further elaborated on.

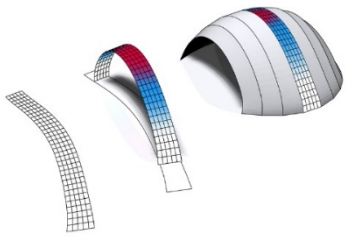

Figure X.2. Stirps are bent separately

ASSEMBLY METHOD

The panels are bent by moving the endpoints of the elements inward and joining them to the foundation. The strips are connected to its neighbour, one strip at the time.

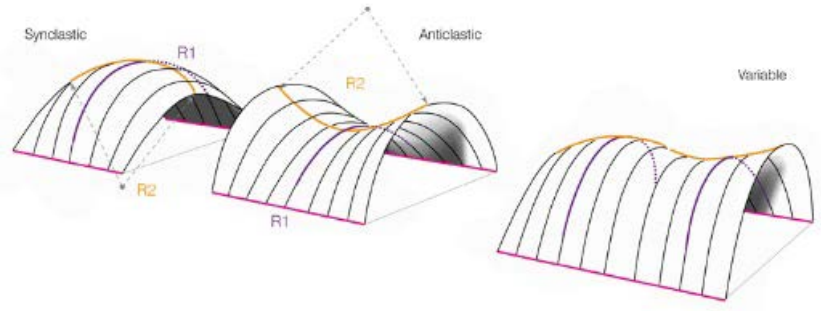

Figure X.3. This method allows for different orientations of the shell.

XI. STUDIO ONE RESEARCH PAVILION – 2017

Figure XI.1. Impression of the Studio One research pavilion.

The design of the Studio One Research Pavilion is part of research at UC Berkeley into bending-active structures (Schleicher and La Magna, 2017). The pavilion will be constructed from 18 unique panels of fibreglass and raisin composite material. Although not yet been built, proof of concept was delivered by the team by constructing and bending the most challenging panel into the desired shape.

Figure XI.2. The pavilion follows a segmented arrangements of bending-active sandwich panels.

SYSTEM'S PRINCIPLE

The principle of the system is quite similar to the bending-active segmented shell, however, in this structure an extra sheet layer and a corrugated layer in-between are added to form a sandwich panel (**Figure XI.3**). The corrugated layer is designed to still allow bending of the panel.

Figure XI.3. The multi-layer arrangement increases the stiffness but still allows the bending.

STRUCTURAL QUALITY

Independently, the flat sheets still behave very flexible, however, when cross connected to form a sandwich panel, structural rigidity is won. When these strips are laterally connected, one coherent shell is formed that has good structural qualities.

ASSEMBLY METHOD

The panels are bent by moving the endpoints of the elements inward and joining them to the foundation. The strips are connected to its neighbour, one strip at the time.

Figure XI.4. Bending the most curved element was tested.

LIST OF FIGURES

ANNEX B – SCRIPT FOR NUMERICAL FORM-FINDING

```
!+!CHAPTER: Model preparation
-PROG AQUA
HEAD 'Materials & sections'

$Materials
TIMB  NO 1  TYPE PLY EP 11500 G 620 E90 1000 G90 170  GAM 6.7   TITL 'PLY'
MATE  NO 2  E 210000 MUE 0.3  GAM 78.5                          TITL 'STEEL'

$Sections
TUBE  NO 1  D 5   MNO 2                                         TITL 'CABL'
END
$_____________________________________________________________________________


$_____________________________________________________________________________
-PROG SOFIMSHC
HEAD 'System definition'
 SYST SPAC GDIV 1000 GDIR NEGZ

 #include $(project)_msh.dat
END
$_____________________________________________________________________________


!+!CHAPTER: STEP 1 Contract 1st set of cables
$ _____________________incremental load/displacement_____________________
$ Brought to you by Dr.-Ing. Riccardo La Magna & Dr.-Ing. Julian Lienhard
$ Attribution and feedback is always appreciated.

-PROG TEMPLATE
HEAD 'Variables definition'
 #define ini = 1         $load/displacement first increment
 #define max = 1         $final value of load/displacement
 sto#l 900               $Reference Loadcase
 sto#lc 1                $Start Loadcase
 sto#x 1000              $maximum iteration loops
 sto#I 50                $optimal number of inner iterations
END
$_____________________________________________________________________________


$_____________________________________________________________________________
-PROG SOFILOAD
HEAD 'Load'
 ECHO val off
 lc no #l

 $Loads definition
 CABL from GRP 5  type ex -0.99*1000.0
END
$_____________________________________________________________________________


$_____________________________________________________________________________
-PROG ASE
HEAD 'Solve'
 ECHO val off

 let#n 0.001       $initial load factor
 let#iter 0        $iteration counter
 let#plc  0        $initial primary load case
 let#s #n

 let#lambda0 0.0   $initial factor for adaptive increments
 let#lambda  0.0
 let#lambdaInc #n  $sum of the increments

 let#tol -0.001

<TEXT,FILE=loadIncrement.txt>
'Iteration / Convergence / Lambda / Lambda increment'

</TEXT>

 loop #x
  let#break 1
   loop
```

```
    SYST  prob th3  iter 500  plc #plc  fmax 0.5  tol #tol
    CTRL iter val 3  v2 1          $ update tangential stiffness by each iteration
    $CTRL iter v4 10
    $CTRL solv 4
    CTRL opt cabl 0
    CTRL opt beam 5

    GRP -
    GRP 6 off
    let#lambda ($(ini)*#n)
    LC  no #lc  dlz  -0.3  titl 'iter #iter, lambda #(#lambda,.3)'
     $LCC  no #l  fact #n
     LCC  no #l  fact #lambdaInc
    end

    @key LC_CTRL #lc
    let#converge @cri1
     if (#converge > 0)
      let#break 0

<TEXT,FILE=+loadIncrement.txt>
#lc       'yes'           #(#lambda,.3)    #(#lambdaInc,.3)
</TEXT>
     else
      let#n (#n-0.5*#s)
      let#s 0.5*#s
      let#lambdaInc #s/(1.0-#n0)

<TEXT,FILE=+loadIncrement.txt>
#lc       'no'            #(#lambda,.3)    #(#lambdaInc,.3)
</TEXT>
     endif

    endloop #break

    $__________options of increasing increments__________
    if #lambda < $(max)
     $let#n   #n+0.01               $ linear increment
     $let#n   #iter*#iter           $ quadratic increment
     $let#n   #n*1.1                $ nonl increment

     @key LC_CTRL #lc               $ adaptive increments
     let#Ik @cri1
     let#s0 #lambda-#lambda0
     let#lambda0 #lambda
     let#s (#s0*(#I/#Ik)^0.2)
     let#n0 #n
     let#lambdaInc #s/(1.0-#n)
     let#n #s+#n
    $_____________________________________________________

     $set exact displacement
     if ($(ini)*#n) > $(max)
      let#n $(max)/$(ini)
      let#lambdaInc 1.0
     endif

     let#plc #lc     $ use previous lc as primary

    elseif ($(ini)*#n) == $(max)
     end
    endif

    let#iter #iter+1
    let#lc #lc+1

  endloop

END
$_____________________________________________________________________________


-sys copy $(projekt).cdb $(projekt)_step1.cdb
```

```
$_____________________________________________________________________________
-PROG TEMPLATE
HEAD 'Variables definition'

 sto#PLC_1 22
END
$_____________________________________________________________________________

$_____________________________________________________________________________
-PROG ASE
HEAD 'System update'
   SYST plc #PLC_1 stor yes
END
$_____________________________________________________________________________

$_____________________________________________________________________________
-PROG SOFIMSHA
HEAD 'Geometry update: connect plates'
   SYST type rest
   CTRL opt rest 2

GRP NO 51
NODE NO 201 NR1 101 FIX KP
NODE NO 202 NR1 102 FIX KP
NODE NO 203 NR1 103 FIX KP

NODE NO 211 NR1 111 FIX KP
NODE NO 212 NR1 112 FIX KP
NODE NO 213 NR1 113 FIX KP
END

!+!CHAPTER: STEP 2 Contract 2nd set of cables
$ _____________________incremental load/displacement_____________________
$ Brought to you by Dr.-Ing. Riccardo La Magna & Dr.-Ing. Julian Lienhard
$ Attribution and feedback is always appreciated.

-PROG TEMPLATE
HEAD 'Variables definition'
 #define ini = 1         $load/displacement first increment
 #define max = 1         $final value of load/displacement
 sto#l 900               $Reference Loadcase
 sto#lc 101              $Start Loadcase
 sto#x 1000              $maximum iteration loops
 sto#I 50                $optimal number of inner iterations
END
$_____________________________________________________________________________


$_____________________________________________________________________________
-PROG SOFILOAD
HEAD 'Load'
 ECHO val off
 lc no #l

 $Loads definition
 CABL from GRP 6  type ex -0.99*1000.0
END
$_____________________________________________________________________________


$_____________________________________________________________________________
-PROG ASE
HEAD 'Solve'
 ECHO val off

 let#n 0.001       $initial load factor
 let#iter 0        $iteration counter
 let#plc  #PLC_1         $initial primary load case
 let#s #n

 let#lambda0 0.0   $initial factor for adaptive increments
 let#lambda  0.0
 let#lambdaInc #n  $sum of the increments

 let#tol -0.001

<TEXT,FILE=loadIncrement.txt>
```

```
'Iteration / Convergence / Lambda / Lambda increment'

</TEXT>

 loop #x
  let#break 1
   loop
    SYST  prob th3  iter 500  plc #plc  fmax 0.5  tol #tol
    CTRL iter val 3  v2 1          $ update tangential stiffness by each iteration
    $CTRL iter v4 10
    $CTRL solv 4
    CTRL opt cabl 0
    CTRL opt beam 5

    GRP -
    GRP 5 off
    let#lambda ($(ini)*#n)
    LC  no #lc  dlz  0.0  titl 'iter #iter, lambda #(#lambda,.3)'
     $LCC  no #l  fact #n
     LCC  no #l  fact #lambdaInc
    end

    @key LC_CTRL #lc
    let#converge @cri1
     if (#converge > 0)
      let#break 0

<TEXT,FILE=+loadIncrement.txt>
#lc       'yes'           #(#lambda,.3)    #(#lambdaInc,.3)
</TEXT>
     else
      let#n (#n-0.5*#s)
      let#s 0.5*#s
      let#lambdaInc #s/(1.0-#n0)

<TEXT,FILE=+loadIncrement.txt>
#lc       'no'            #(#lambda,.3)    #(#lambdaInc,.3)
</TEXT>
     endif

    endloop #break

    $__________options of increasing increments__________
    if #lambda < $(max)
     $let#n   #n+0.01               $ linear increment
     $let#n   #iter*#iter           $ quadratic increment
     $let#n   #n*1.1                $ nonl increment

     @key LC_CTRL #lc               $ adaptive increments
     let#Ik @cri1
     let#s0 #lambda-#lambda0
     let#lambda0 #lambda
     let#s (#s0*(#I/#Ik)^0.2)
     let#n0 #n
     let#lambdaInc #s/(1.0-#n)
     let#n #s+#n
    $_____________________________________________________

     $set exact displacement
     if ($(ini)*#n) > $(max)
      let#n $(max)/$(ini)
      let#lambdaInc 1.0
     endif

     let#plc #lc     $ use previous lc as primary

    elseif ($(ini)*#n) == $(max)
     end
    endif

    let#iter #iter+1
    let#lc #lc+1

  endloop

END
$_____________________________________________________________________
```

```
-sys copy $(projekt).cdb $(projekt)_step2.cdb


$_____________________________________________________________________________
-PROG TEMPLATE
HEAD 'Variables definition'

 sto#PLC_2 134
END
$_____________________________________________________________________________


$_____________________________________________________________________________
-PROG ASE
HEAD 'System update'
   SYST plc #PLC_2 stor yes
END
$_____________________________________________________________________________


$_____________________________________________________________________________
-PROG SOFIMSHA
HEAD 'Geometry update: parallel plate connection'
   SYST type rest
   CTRL opt rest 2

GRP no 52
NODE NO 201 NR1 101 FIX KF
NODE NO 202 NR1 102 FIX KF
NODE NO 203 NR1 103 FIX KF
NODE NO 204 NR1 104 FIX KF
NODE NO 205 NR1 105 FIX KF
NODE NO 206 NR1 106 FIX KF
NODE NO 207 NR1 107 FIX KF
NODE NO 208 NR1 108 FIX KF

NODE NO 211 NR1 111 FIX KF
NODE NO 212 NR1 112 FIX KF
NODE NO 213 NR1 113 FIX KF
NODE NO 214 NR1 114 FIX KF
NODE NO 215 NR1 115 FIX KF
NODE NO 216 NR1 116 FIX KF
NODE NO 217 NR1 117 FIX KF
NODE NO 218 NR1 118 FIX KF
END
$_____________________________________________________________________________

!+!CHAPTER: SYSTEM
$_____________________________________________________________________________
-PROG SOFIMSHA
HEAD 'Geometry update: update BCs'
   SYST type rest
   CTRL opt rest 2

NODE NO (100 300 1) FIX -PPMM
NODE NO 101 FIX PP
NODE NO (102 103 1) FIX PXPZ
NODE NO 111 FIX PYPZ
NODE NO (112 113 1) FIX PZ
END
$_____________________________________________________________________________

$_____________________________________________________________________________
-PROG ASE
HEAD 'Relaxation 40%-50%'
ECHO Full

ctrl iter 3 v2 1
ctrl cabl 0
CTRL WARN 398
SYST PROB TH3  ITER 100  PLC #PLC_s
GRP 5,6,51 off

LC 300
GRP no 1 FACL 0.6
GRP no 2 FACL 0.5
END
```

ANNEX C – RESULTS FROM PARAMETER STUDY

Results for load case 1

A103		S03			S04			S05		
		-20	0	+20	-20	0	+20	-20	0	+20
M0	P_{max} [kN]	0.3	0.3	0.2	0.3	0.3	0.3	0.6	0.5	0.4
	k_1 [N/mm]	16.4	9.8	6.8	10.9	15.1	15.8	15.5	19.7	15.7
M20	P_{max} [kN]	0.4	0.4	0.4	0.4	0.5	0.4	0.3	0.8	0.5
	k_1 [N/mm]	13.5	16.9	20.0	16.9	25.5	26.3	23.7	29.1	24.8
M40	P_{max} [kN]	0.5	0.6	0.6	0.4	0.5	0.6	0.3	0.5	0.7
	k_1 [N/mm]	20.7	25.3	30.2	23.4	33.7	35.4	28.6	36.8	39.2
A105		S03			S04			S05		
		-10	0	+10	-10	0	+10	-10	0	+10
M0	P_{max} [kN]	0.3	0.3	0.3	0.4	0.4	0.4	0.8	0.7	0.6
	k_1 [N/mm]	9.7	10.6	11.3	15.1	16.5	16.9	20.6	21.7	19.7
M20	P_{max} [kN]	0.5	0.5	0.5	0.6	0.6	0.6	1.0	1.0	0.8
	k_1 [N/mm]	16.6	18.9	20.6	26.1	30.1	31.2	32.8	33.3	28.8
M40	P_{max} [kN]	0.7	0.7	0.7	0.6	0.7	0.8	0.6	1.0	1.0
	k_1 [N/mm]	24.8	28.5	32.2	33.6	40.2	40.7	41.5	41.4	40.1

Results for load case 2

A103		S03			S04			S05		
		-20	0	+20	-20	0	+20	-20	0	+20
M0	ql_{max} [kN]	0.6	0.8	0.8	0.4	0.4	0.6	0.2	0.4	0.6
	k_2 [N/mm]	9.2	12.3	16.1	11.1	20.7	27.0	18.4	32.0	27.8
M20	ql_{max} [kN]	0.6	0.8	1.0	0.4	0.4	0.8	0.2	0.4	0.6
	k_2 [N/mm]	14.5	21.7	31.1	16.5	34.2	44.6	23.9	42.6	42.9
M40	ql_{max} [kN]	0.6	0.8	1.2	0.4	0.6	0.8	0.2	0.4	0.6
	k_2 [N/mm]	22.2	33.1	51.2	22.6	44.2	61.5	24.7	51.5	72.9
A105		S03			S04			S05		
		-10	0	+10	-10	0	+10	-10	0	+10
M0	ql_{max} [kN]	1.0	1.0	1.0	0.6	0.8	0.8	0.6	0.6	0.8
	k_2 [N/mm]	12.0	14.3	16.5	20.4	25.8	29.5	31.1	38.3	36.9
M20	ql_{max} [kN]	1.0	1.2	1.4	0.6	0.8	0.8	0.6	0.6	0.8
	k_2 [N/mm]	20.4	26.0	31.4	33.2	46.5	55.2	48.1	54.8	48.3
M40	ql_{max} [kN]	1.0	1.0	1.2	0.6	1.0	1.0	0.6	0.6	0.8
	k_2 [N/mm]	30.1	39.3	51.1	39.0	58.1	68.3	54.2	66.2	72.4

ANNEX D – MODELLING APPROACH

The flat geometry is drawn and meshed in Rhino.

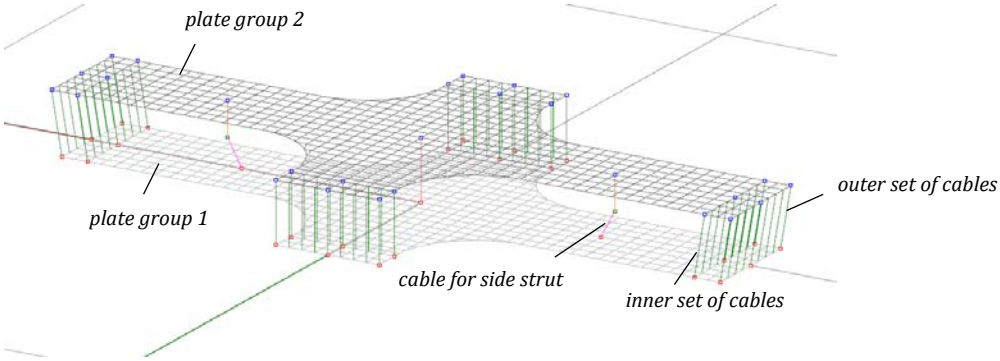

The flat geometry is imported into SOFiSTiK and the cables for the side struts and the outer sets of cables are contracted.

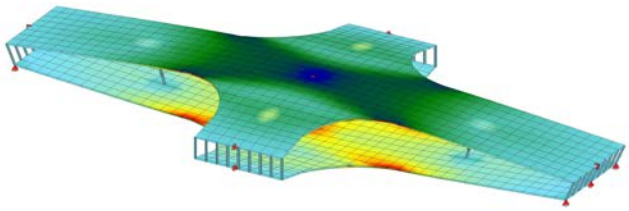

The edges of the plates are connected with hinges and the side struts are connected to the bottom plate.

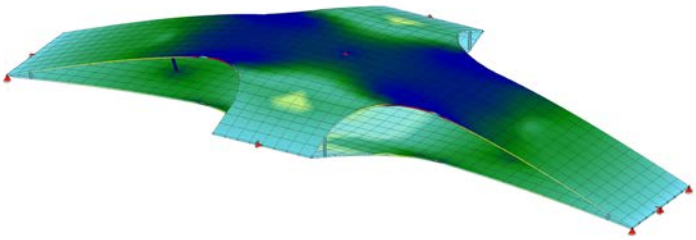

The inner sets of cables are contracted.

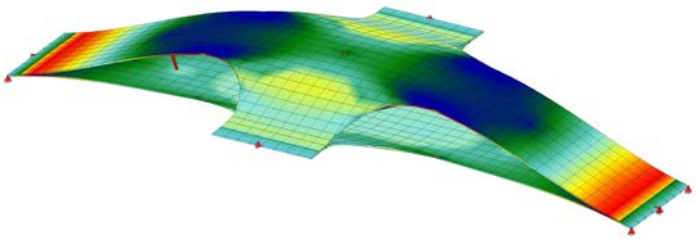

The form-found mesh is imported into Rhino via the STiKbug plug-in for Grasshopper.

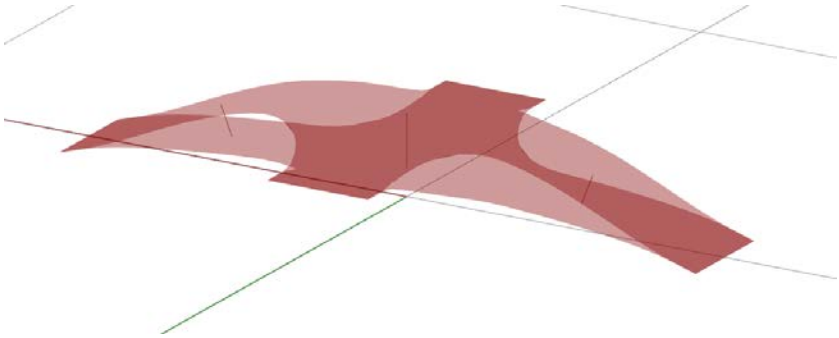

The unit is translated and rotated using a Grasshopper script to form the arch structure.

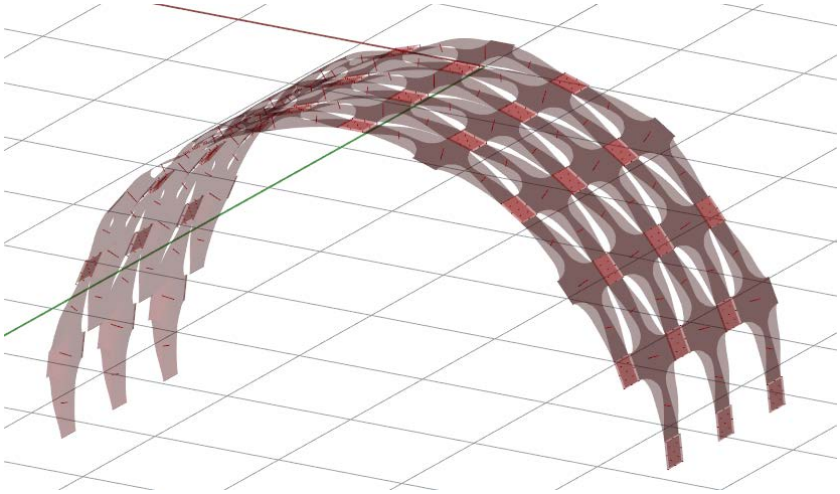

With only little 3D modelling effort, this geometry can be turned into a structural model using the SOFiSTiK interface for Rhino. This model can be imported into SOFiSTiK for structural analysis. During these steps, however, the history of the stresses gets lost.

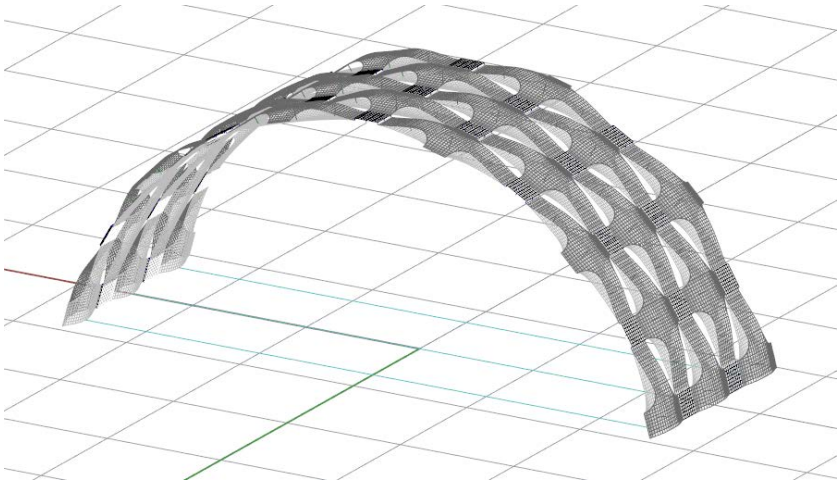

ANNEX E – LARGE-SCALE DESIGN

UNIT DESIGN

DESIGN FOR 6.4 MM PLATE

Mechanical properties of birch plywood with a thickness of 6.4 mm (UPM, 2007)

	Characteristic value	Design value
$f_{m,0}$	50.9	38.2
$f_{m,90}$	29.0	21.8
$f_{t,0}$	42.2	31.7
$f_{t,90}$	32.8	24.6
$f_{c,0}$	29.3	22.0
$f_{c,90}$	22.8	17.1

Stresses in the longitudinal plate direction

Characteristic bending strength $f_{k,m,0}$ = 50.9 N/mm²

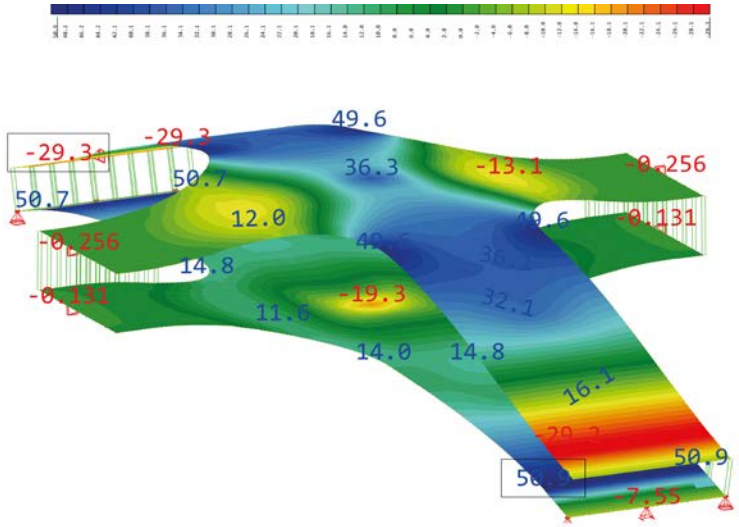

σ_0 in the top of the cross-section

$\sigma_{0,max}$ = 50.9 N/mm²
$\sigma_{0,min}$ = -29.3 N/mm²

***Unity check**:*
Bending strength $\frac{50.9}{50.9} = 1.00$

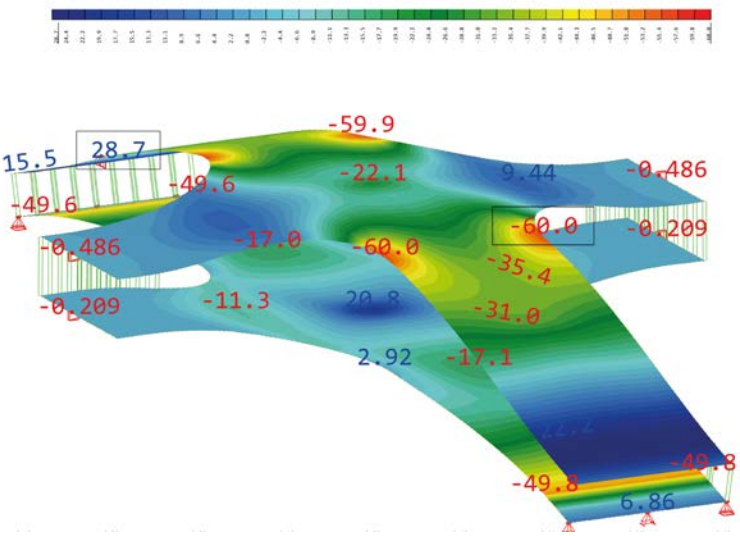

σ_0 in the bottom of the cross-section

$\sigma_{0,max}$ = 28.7 N/mm²
$\sigma_{0,min}$ = -60.0 N/mm²

***Unity check**:*
Bending strength $\frac{60.0}{50.9} = 1.18$

Only exceedence at corners

Stresses in the lateral plate direction

Characteristic bending strength $f_{k,m,90}$ = 29.0 N/mm²

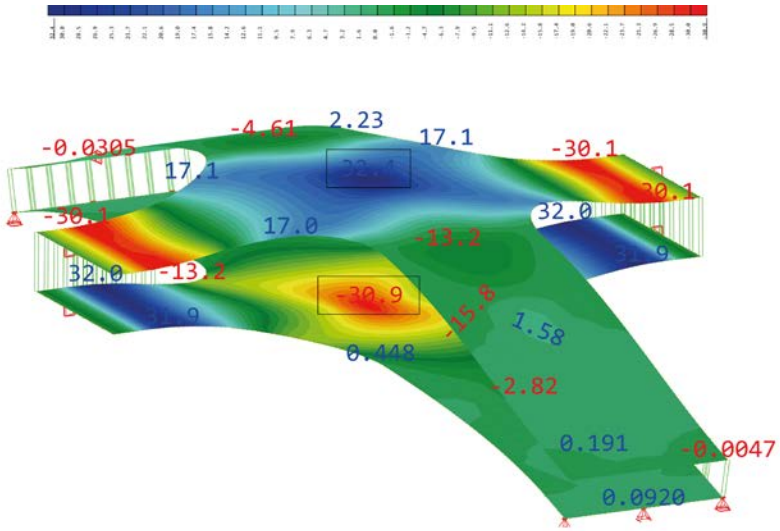

σ_{90} in the top of the cross-section

$\sigma_{90,max}$ = 32.4 N/mm²
$\sigma_{90,min}$ = -30.9 N/mm²

***Unity check**:*
Bending strength $\frac{32.4}{29.0} = 1.12$

Only very small exceedances and due to peak stress at strut connection

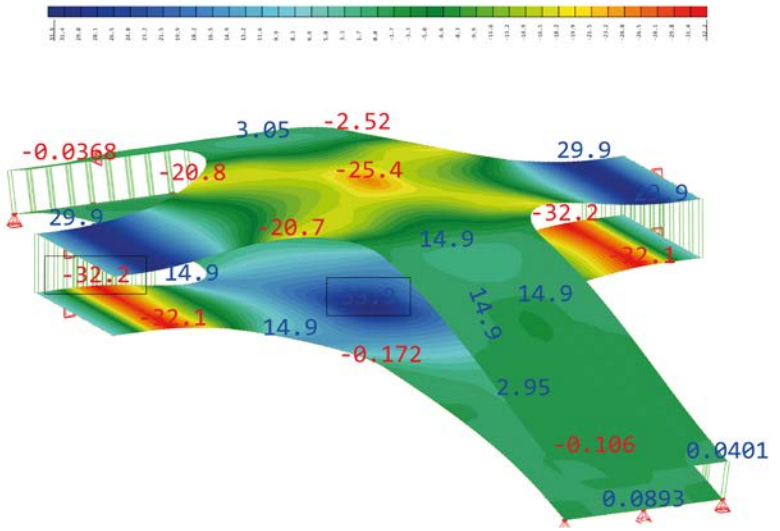

σ_{90} in the bottom of the cross-section

$\sigma_{90,max}$ = 29.9 N/mm²
$\sigma_{90,min}$ = -32.2 N/mm²

***Unity check**:*
Bending strength $\frac{32.2}{29.0} = 1.11$

Only very small exceedances

DESIGN FOR 9.2 MM PLATE

Mechanical properties of birch plywood with a thickness of 9.2 mm (UPM, 2007)

	Characteristic value	Design value
$f_{m,0}$	45.6	34.2
$f_{m,90}$	32.1	24.1
$f_{t,0}$	40.8	30.6
$f_{t,90}$	34.2	25.7
$f_{c,0}$	28.3	21.2
$f_{c,90}$	23.7	17.8

Stresses in the longitudinal plate direction

Characteristic bending strength $f_{k,m,0}$ = 45.6 N/mm²

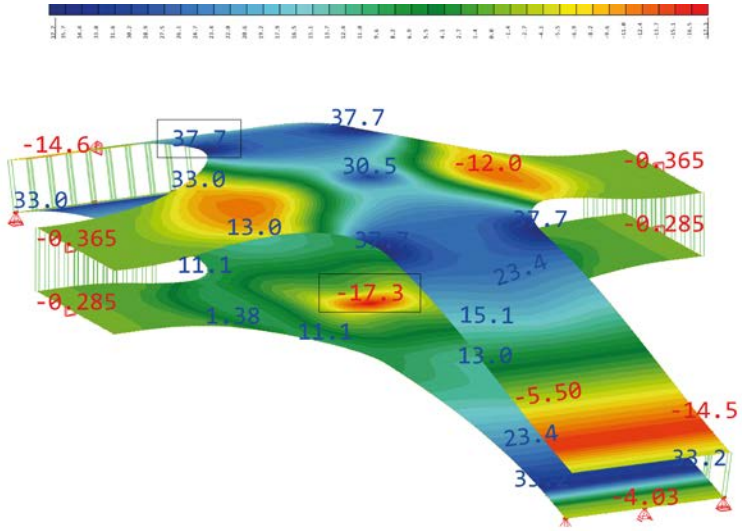

σ_0 in the top of the cross-section

$\sigma_{0,max}$ = 37.7 N/mm²
$\sigma_{0,min}$ = -17.3 N/mm²

***Unity check**:*
Bending strength $\frac{37.7}{45.6} = 0.83$

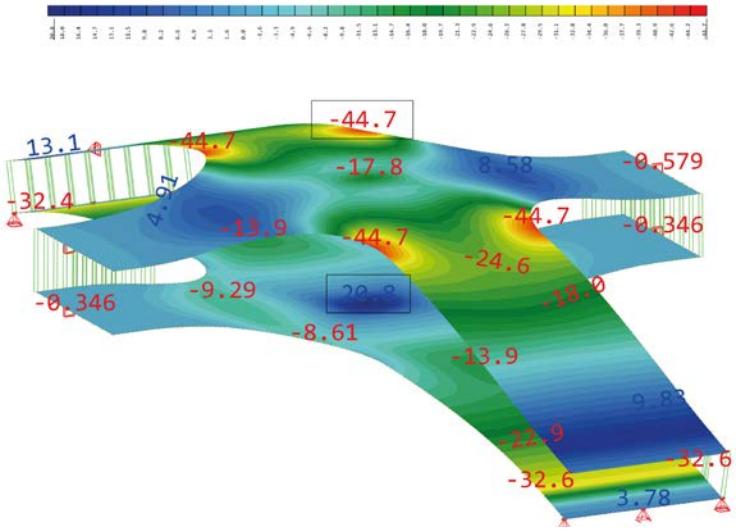

σ_0 in the bottom of the cross-section

$\sigma_{0,max}$ = 20.8 N/mm²
$\sigma_{0,min}$ = -44.7 N/mm²

***Unity check**:*
Bending strength $\frac{44.7}{45.6} = 0.98$

Stresses in the lateral plate direction

Characteristic bending strength $f_{k,m,90}$ = 32.1 N/mm²

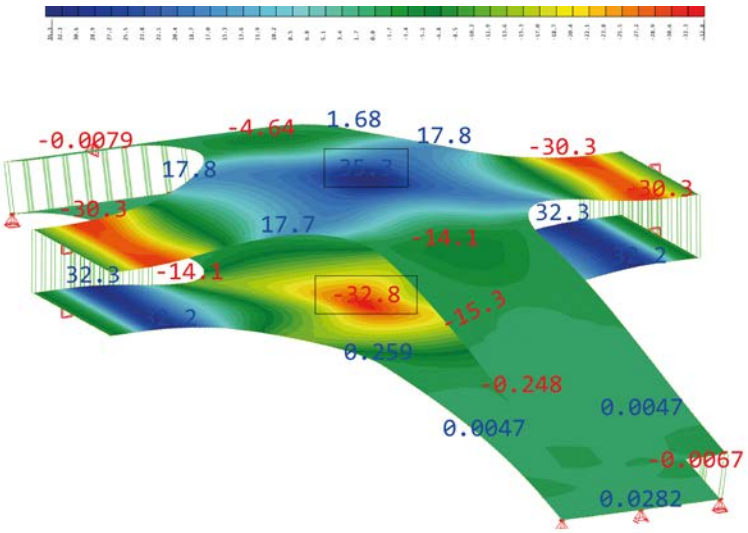

σ_{90} in the top of the cross-section

$\sigma_{90,max}$ = 32.3 N/mm²
$\sigma_{90,min}$ = -30.3 N/mm²

***Unity check**:*
Bending strength $\frac{32.3}{32.1} = 1.01$

Only very small exceedance

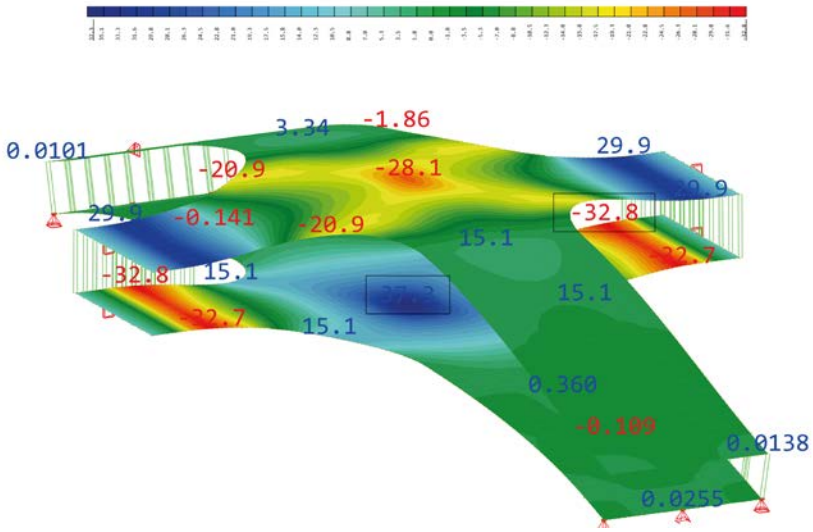

σ_{90} in the bottom of the cross-section

$\sigma_{90,max}$ = 29.9 N/mm²
$\sigma_{90,min}$ = -32.8 N/mm²

***Unity check**:*
Bending strength $\frac{32.8}{32.1} = 1.02$

Only very small exceedance

DESIGN OF THE ARCH

1.5 times dead weight

1.0 kN/m^2 variable load conform LC 3

DESIGN FOR 6.4 MM PLATE

Stresses in the longitudinal plate direction

Design value of the bending strength	$f_{d,m,0}$ = 38.2 N/mm^2
Design value of the tension strength	$f_{d,t,0}$ = 31.7 N/mm^2
Design value of the compression strength	$f_{d,c,0}$ = -22.0 N/mm^2

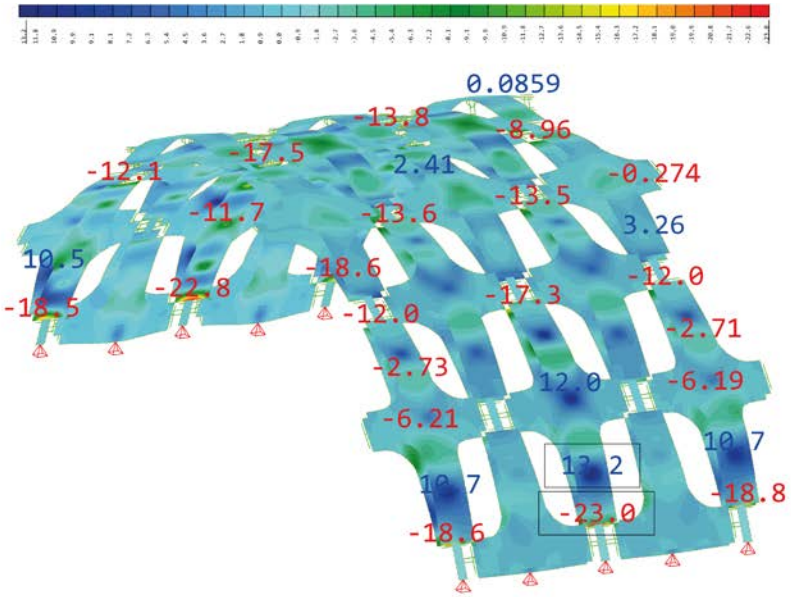

σ_0 in the top of the cross-section

$\sigma_{0,max}$ = 13.2 N/mm^2
$\sigma_{0,min}$ = -23.0 N/mm^2

***Unity check**:*

Bending strength $\frac{23.0}{38.2} = 0.60$

Tension strength: $\frac{13.2}{31.7} = 0.42$

Compression strength: $\frac{-23.0}{-22.0} = 1.05$

Sligth exceedance in compression at peak stress at end beams

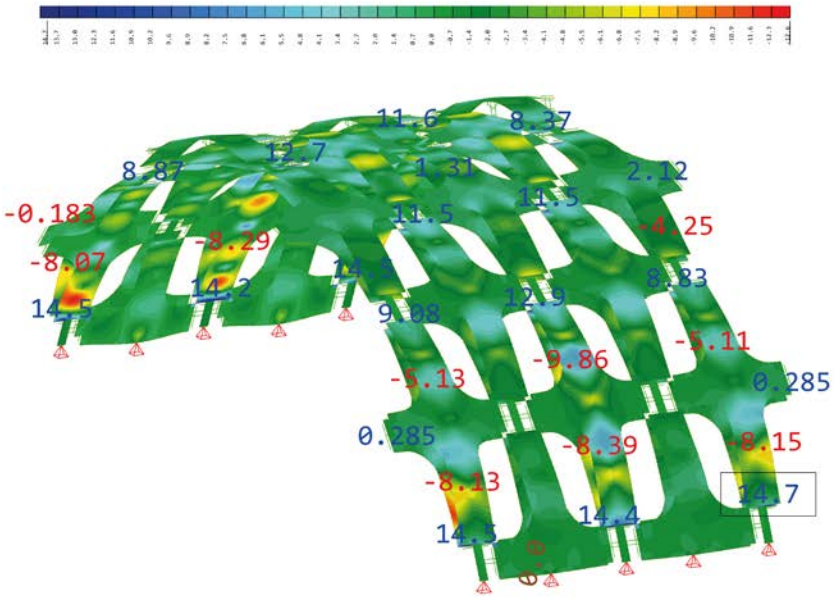

σ_0 in the bottom of the cross-section

$\sigma_{0,max}$ = 14.7 N/mm^2
$\sigma_{0,min}$ = -9.9 N/mm^2

***Unity check**:*

Bending strength $\frac{14.7}{38.2} = 0.38$

Tension strength: $\frac{14.7}{31.7} = 0.46$

Compression strength: $\frac{-9.9}{-22.0} = 0.45$

Stresses in the lateral plate direction

Design value of the bending strength	$f_{d,m,90}$ = 21.8 N/mm²
Design value of the tension strength	$f_{d,t,90}$ = 24.6 N/mm²
Design value of the compression strength	$f_{d,c,90}$ = -17.1 N/mm²

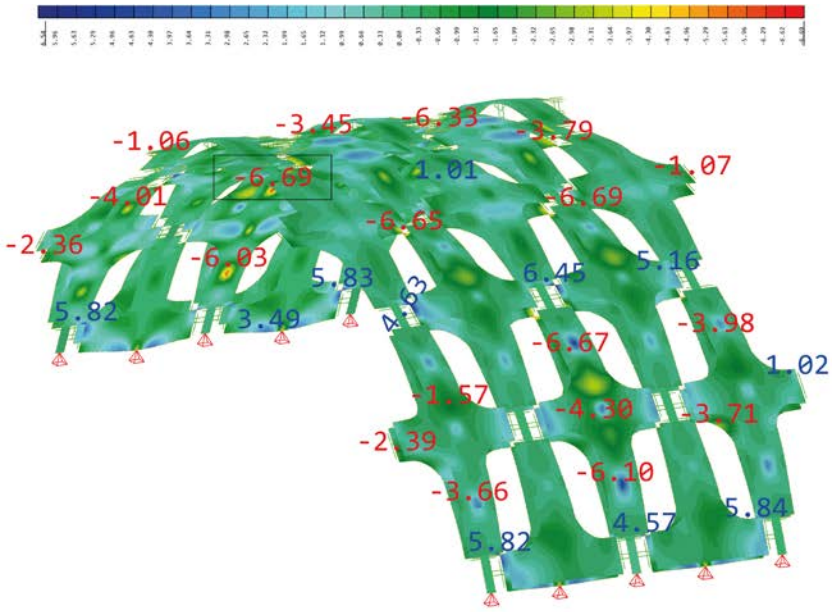

σ_{90} in the top of the cross-section

$\sigma_{90,max}$ = 6.5 N/mm²
$\sigma_{90,min}$ = -6.7 N/mm²

***Unity check**:*

Bending strength $\frac{6.7}{21.8} = 0.31$

Tension strength: $\frac{6.5}{24.6} = 0.26$

Compression strength: $\frac{-6.7}{-17.1} = 0.39$

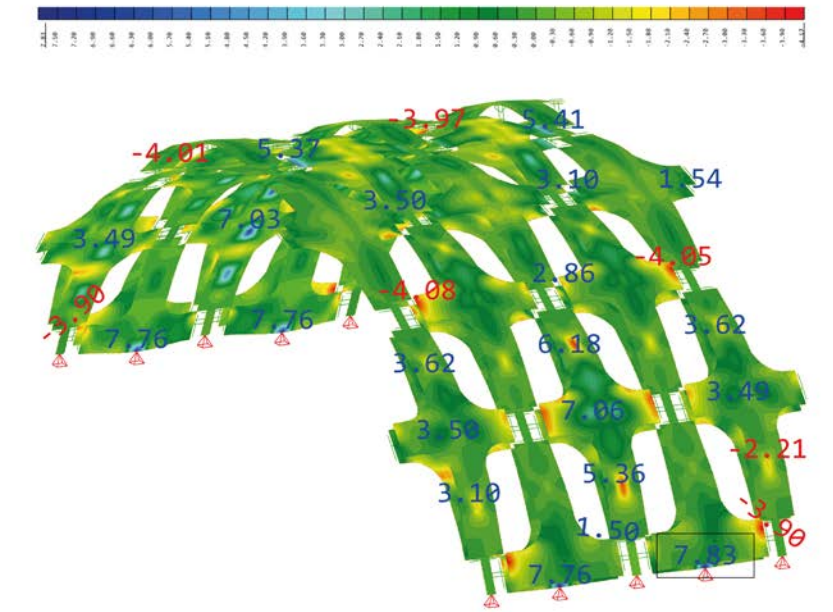

σ_{90} in the bottom of the cross-section

$\sigma_{90,max}$ = 7.8 N/mm²
$\sigma_{90,min}$ = -4.1 N/mm²

***Unity check**:*

Bending strength $\frac{7.8}{21.8} = 0.36$

Tension strength: $\frac{7.8}{24.6} = 0.32$

Compression strength: $\frac{-4.1}{-17.1} = 0.24$

DESIGN FOR 9.2 MM PLATE

Stresses in the longitudinal plate direction

Design value of the bending strength	$f_{d,m,0}$ = 34.2 N/mm²
Design value of the tension strength	$f_{d,t,0}$ = 30.6 N/mm²
Design value of the compression strength	$f_{d,c,0}$ = -21.2 N/mm²

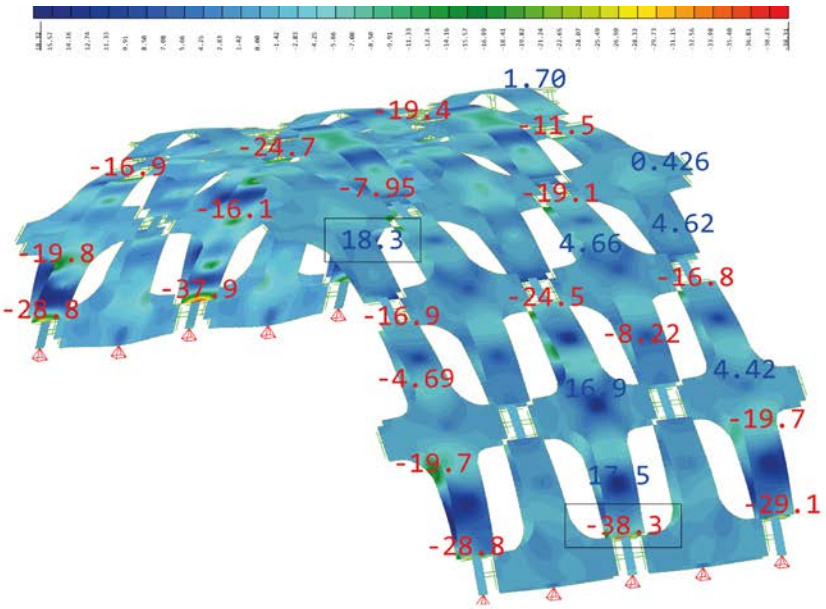

σ_0 in the top of the cross-section

$\sigma_{0,max}$ = 18.3 N/mm²
$\sigma_{0,min}$ = -38.3 N/mm²

***Unity check**:*

Bending strength	$\frac{38.3}{34.2} = 1.12$
Tension strength:	$\frac{18.3}{30.6} = 0.60$
Compression strength:	$\frac{-38.3}{-21.2} = 1.81$

Exceedance in stresses due to large peak stresses at edge beams

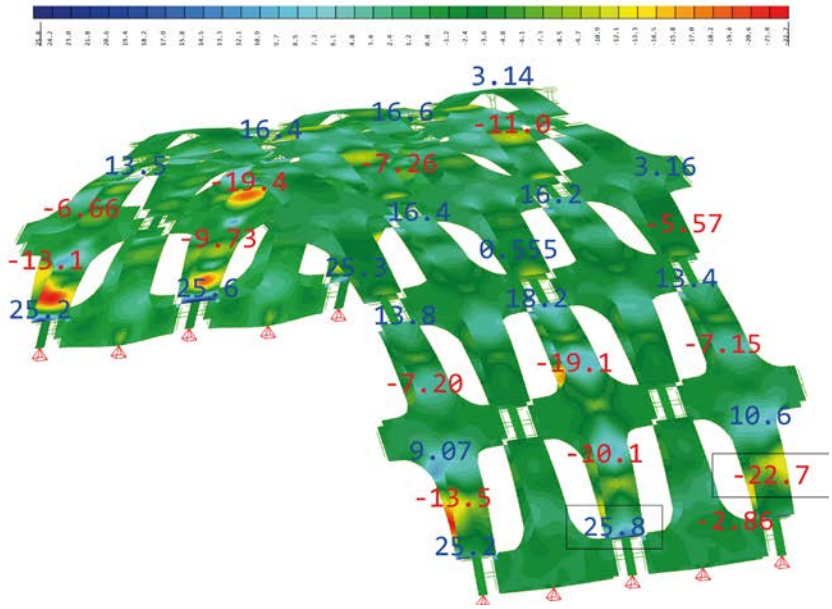

σ_0 in the bottom of the cross-section

$\sigma_{0,max}$ = 25.8 N/mm²
$\sigma_{0,min}$ = -22.7 N/mm²

***Unity check**:*

Bending strength	$\frac{25.8}{34.2} = 0.75$
Tension strength:	$\frac{25.8}{30.6} = 0.84$
Compression strength:	$\frac{-22.7}{-21.2} = 1.07$

Stresses in the lateral plate direction

Design value of the bending strength	$f_{d,m,90}$ = 24.1 N/mm^2
Design value of the tension strength	$f_{d,t,90}$ = 25.7 N/mm^2
Design value of the compression strength	$f_{d,c,90}$ = -17.8 N/mm^2

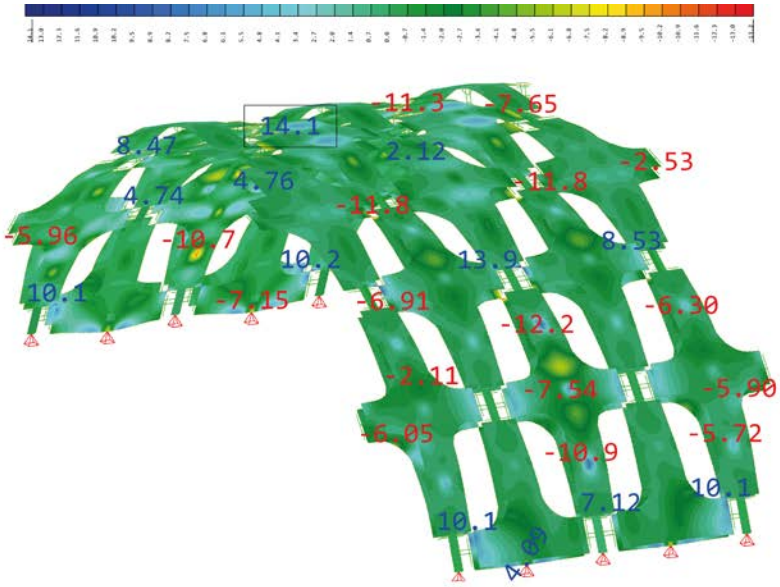

σ_{90} in the top of the cross-section

$\sigma_{90,max}$ = 14.1 N/mm^2
$\sigma_{90,min}$ = -11.8 N/mm^2

***Unity check**:*

Bending strength $\frac{14.1}{24.1} = 0.59$

Tension strength: $\frac{14.1}{25.7} = 0.55$

Compression strength: $\frac{-11.8}{-17.8} = 0.66$

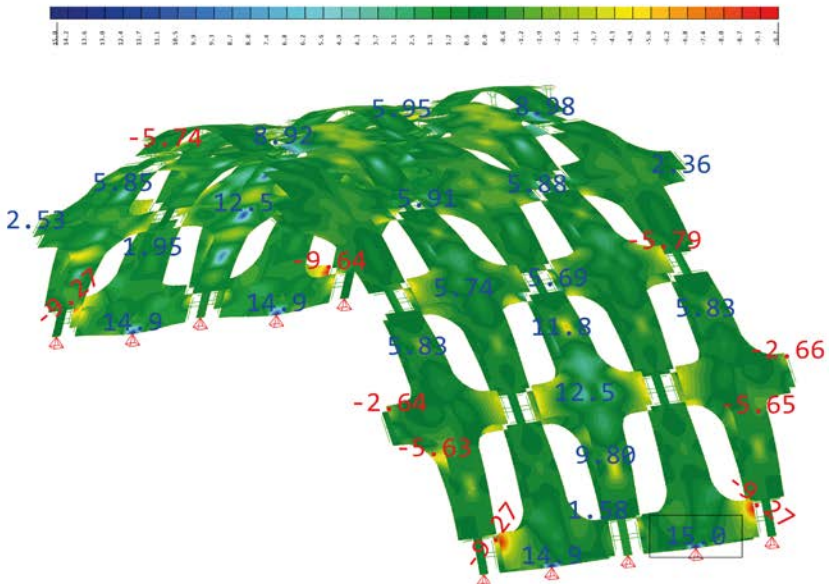

σ_{90} in the bottom of the cross-section

$\sigma_{90,max}$ = 15.0 N/mm^2
$\sigma_{90,min}$ = -9.6 N/mm^2

***Unity check**:*

Bending strength $\frac{15.0}{24.1} = 0.62$

Tension strength: $\frac{15.0}{25.7} = 0.58$

Compression strength: $\frac{-9.6}{-17.8} = 0.54$

ANNEX F – PICTURES OF PHYSICAL EXPLORATIONS

Model constructed from 3 bent plywood strips with the grain direction parallel to the longitudinal direction.

Model constructed from 4 bent plywood strips with the grain direction perpendicular to the longitudinal direction.

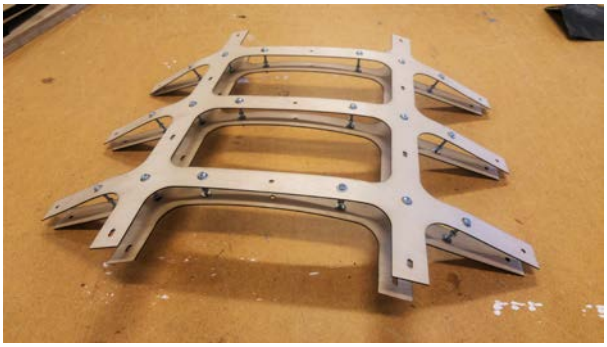

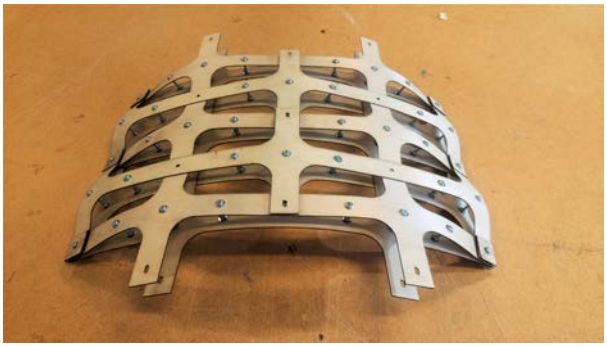

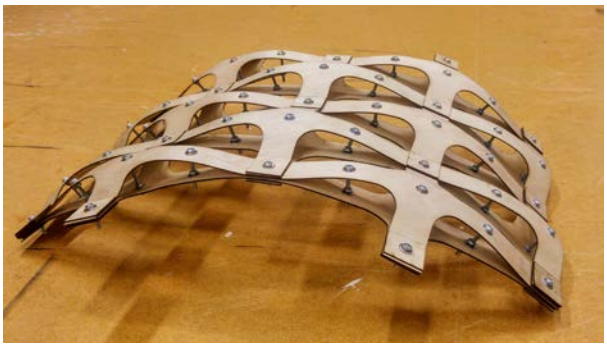

Construction sequence of a scale model of the modular system with 2 units in the longitudinal direction.

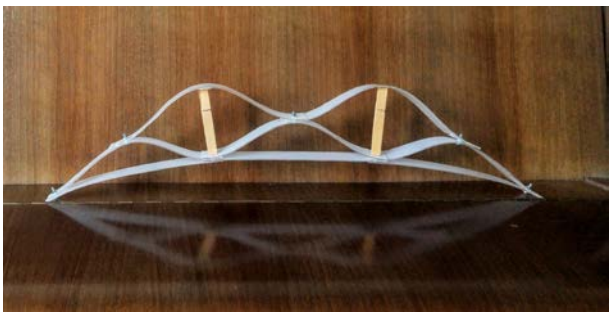

A three layered clamped system with (bottom) and without (top) strut.







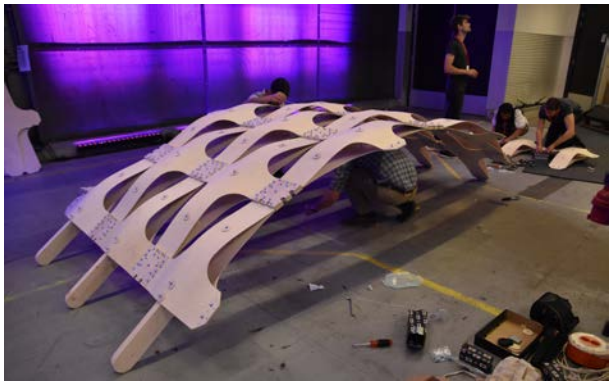


The image sequence shows the construction of the prototype, from milling to bending to assembling.